TECHNICAL REPORT STANDARD TITLE PAGE

1. Report No.	2. Government Accession No.	3. Recipient's Catalog No.
FHWA/TX-82/50+326-1		

4. Title and Subtitle	5. Report Date
Preliminary Analysis of the Behavior of Reinforced Concrete Box Culverts	September 1982
	6. Performing Organization Code
7. Author(s)	8. Performing Organization Report No.
Mark P. Gardner and Jey K. Jeyapalan	Research Report 326-1
9. Performing Organization Name and Address	10. Work Unit No.
Texas Transportation Institute The Texas A&M University System College Station, Texas 77843	11. Contract or Grant No. Study 2-5-82-326
	13. Type of Report and Period Covered Interim - September 1981 September 1982
12. Sponsoring Agency Name and Address	14. Sponsoring Agency Code
Texas State Department of Highways and Public Transportation: Transportation Planning Division P. O. Box 5051 Austin, Texas 78763	

15. Supplementary Notes

Research performed in cooperation with DOT, FHWA.
Research Study Title: Behavior of Reinforced Concrete Box Culverts Under Backfill and Traffic Loads.

16. Abstract

The behavior of Reinforced Concrete Box Culverts under varying backfill, compaction, and traffic loads is not clearly understood. The design rules used at present are mostly empirical and do not allow for the effects of Soil-Culvert interaction. In order to have a better understanding of the field behavior of these culverts, in another research study at the Texas Transportation Institute, an 8' x 8' RC box culvert will be instrumented with earth pressure cells and strain gages. The purpose of the study presented in this report is to perform prediction analyses of the behavior of this 8' x 8' culvert, using the finite element computer program, SSTIPN so that the analytical results can be correlated with field observations whenever these become available.

In this preliminary study, foundation and backfill materials from the culvert site were used to prepare samples in the laboratory at varying compaction conditions and a number of triaxial tests were performed. Using these nonlinear stress-strain data the backfill and foundation soils around the culvert were stimulated in the computer analyses. The culvert was represented in the analyses by a series of beam elements connected at the common nodes. The backfill placement is simulated by an incremental loading analysis procedure.

The earth pressures, stresses and strains at the proposed instrument locations for the test culvert are predicted for a range of backfill conditions. Separate analyses are performed with no-slip and full-slip assumptions for the soil-culvert interface. In addition, the bending moments calculated at various sections of the box culvert are presented in this report. (continued on back)

17. Key Words	18. Distribution Statement
Reinforced Concrete Box Culverts, Soil-Structure Interaction, Backfill, Live Load Conditions.	No restrictions. This document is available to the public through the National Technical Information Service, 5285 Port Royal Road, Springfield, Virginia 22161.

19 Security Classif. (of this report)	20. Security Classif. (of this page)	21. No. of Pages	22. Price
Unclassified	Unclassified	157	

Form DOT F 1700.7 (8-69)

PRELIMINARY ANALYSES OF THE BEHAVIOR OF REINFORCED CONCRETE BOX CULVERTS

by

Mark P. Gardner
Jey K. Jeyapalan

Research Report Number 326-1
Research Project 2-5-82-326

Conducted for
The Texas State Department of Highways
and Public Transportation

In cooperation with the
U.S. Department of Transportation
Federal Highway Administration

by the
TEXAS TRANSPORTATION INSTITUTE
The Texas A&M University System
College Station, Texas

September 1982

DISCLAIMER

The contents of this report reflect the views of the authors who are responsible for the facts and the accuracy of the data presented herein. The contents do not necessarily reflect the official views or policies of the Federal Highway Administration. This report does not constitute a standard, specification or regulation.

ABSTRACT

The behavior of Reinforced Concrete Box Culverts under varying backfill, compaction, and traffic loads is not clearly understood. The design rules used at present are mostly empirical and do not allow for the effects of Soil-Culvert interaction. In order to have a better understanding of the field behavior of these culverts, in another research study at the Texas Transportation Institute, an 8' x 8' RC box culvert will be instrumented with earth pressure cells and strain gages. The purpose of the study presented in this report is to perform prediction analyses of the behavior of this 8' x 8' culvert, using the finite element computer program, SSTIPN so that the analytical results can be correlated with field observations whenever these become available.

In this preliminary study, foundation and backfill materials from the culvert site were used to prepare samples in the laboratory at varying compaction conditions and a number of triaxial tests were performed. Using these nonlinear stress-strain data the backfill and foundation soils around the culvert were simulated in the computer analyses. The culvert was represented in the analyses by a series of beam elements connected at the common nodes. The backfill placement is simulated by an incremental loading analysis procedure.

The earth pressures, stresses and strains at the proposed instrument locations for the test culvert are predicted for a range of backfill conditions. Separate analyses are performed with no-slip and full-slip assumptions for the soil-culvert interface. In addition, the bending moments calculated at various sections of the box culvert are presented in this report. Furthermore, the deflections of the crown of the culvert for varying backfill properties are given in this report.

TABLE OF CONTENTS

LIST OF FIGURES

LIST OF FIGURES (Con't)

LIST OF FIGURES (Con't)

LIST OF FIGURES (Con't)

LIST OF FIGURES (Con't)

LIST OF FIGURES (Con't)

LIST OF FIGURES (Con't)

LIST OF TABLES

CHAPTER I

INTRODUCTION

Increasing number of Reinforced Concrete Box Culverts are being used by several state highway departments to bridge across canals and streams throughout the United States. Over the last two decades the allowable AASHTO permit loads have also increased to a degree for which the behavior of these culverts constructed with shallow backfill covers need to be evaluated accurately. There have been a number of proposals recommending changes in AASHTO specifications to increase the intensity of the design earth pressures applied along the perimeter of the culvert independent of the following parameters:

a) Geometry and Stiffness of the culvert,

b) Properties of the backfill, and

c) Backfill cover depth over the crown of the culvert.

It is expected that the above primary parameters and several other secondary parameters will control the earth pressures exerted on the culvert under varying backfill and live load conditions. In order to study the behavior of Reinforced Concrete Box Culverts, the Texas Transportation Institute is at present involved with the field instrumentation of an 8' x 8' RC box culvert. Earth pressures and strains will be measured on this structure under backfill and live loads. Because of funding limitations, the scope of these field observations will be limited to one box size and one type of backfill, and it will not be possible to consider variations in the factors mentioned previously.

In order to derive the maximum benefit from the ongoing field instrumentation study, a computer research study was initiated so that a series of computer predictions of the behavior of the 8' x 8' box culvert can be made. Later, field observations can be used to verify the computer predictions and further computer analyses of the behavior of other box culverts can be performed by varying the primary controlling parameters. The purpose of this report is to present the preliminary results of the computer analyses of the 8' x 8' box culvert. The analyses of the behavior of the culvert were performed for three types of backfill compaction conditions. Various backfill cover depths were also considered in the analyses. A number of representative soil samples from the culvert site were brought to the laboratory and triaxial stress-strain tests, and other routine soil tests were performed. These test data were used in selecting the hyperbolic stress-strain model parameters for representing the backfill and foundation materials in the computer analyses.

The studies undertaken to achieve the project objectives are described in subsequent chapters:

Chapter 2 contains a discussion of the previous research on culverts and present design procedures for RC box culverts.

Chapter 3 describes the material properties measured in the laboratory and presents the material parameters used in the computer analyses.

Chapter 4 presents the preliminary results on the behavior of the 8' x 8' RC box culvert for three types of backfill conditions.

Chapter 5 contains conclusions and recommendations.

CHAPTER 2

PREVIOUS RESEARCH

2.1 Introduction

In this chapter the results of a literature search on the subject of soil-structure interaction of reinforced concrete box culverts are discussed. The previous research is classified under the following categories and reviewed accordingly:

1) Analytical Solutions,
2) Numerical Solutions, and
3) Empirical Solutions.

2.2 Analytical Solutions

The analytical solutions studied may be divided into two groups: those solutions which do not consider the effects of soil-structure interaction on pressure distribution and those solutions in which these effects are considered.

2.2.1 Solutions Without Soil-Structure Interaction

Early design methods for culverts were developed under the assumption that the dead weight of the fill is distributed uniformly over the full width of the culvert. The weight of this fill was considered equal to the weight of a prism of soil whose height is equal to the width of the structure as given in Polack and DeGroot [13]. This procedure is shown in Fig. 2.1. The lateral pressure on the sides of the culvert was taken as one-fourth the weight of the fill uniformly distributed on the side from top to bottom. The pressure exerted on the bottom of the box culvert was assumed to be the sum of the superimposed loads on the roof, and the dead weight of the roof and sides of the culvert. The pressure was considered uniformly

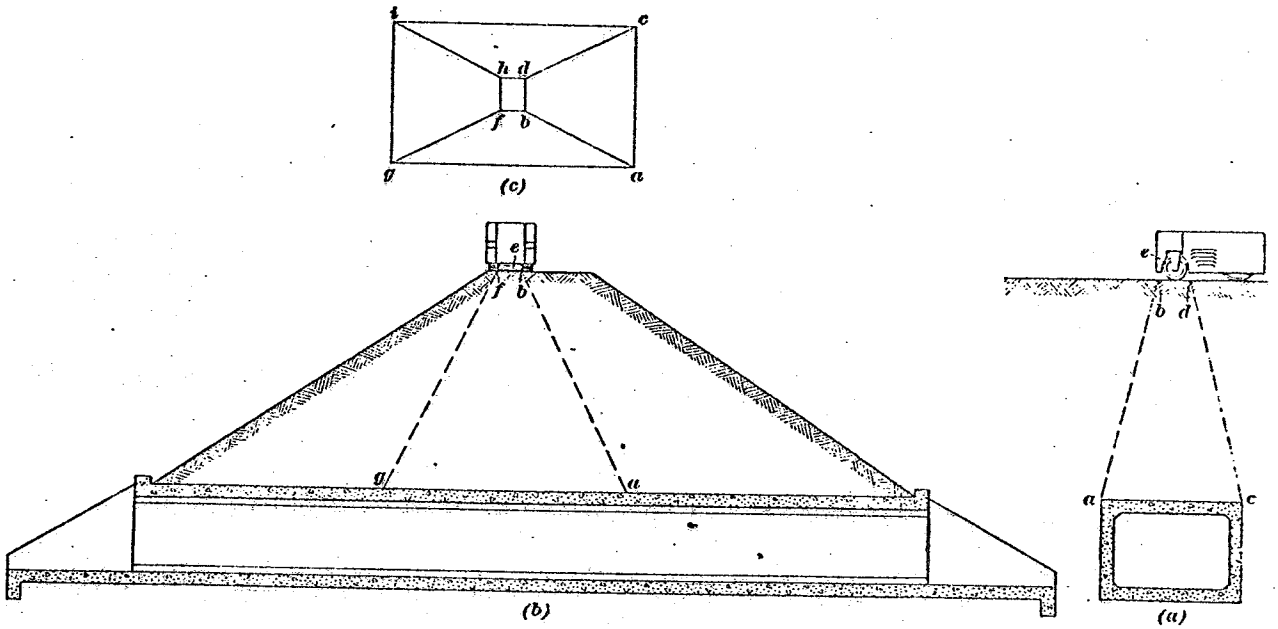

VERTICAL PRESSURE DISTRIBUTION
ON BURIED CONCRETE CULVERTS

FIGURE 2.1

distributed over the base of the culvert. This is the simplest approach, and is used as the basis for most other analysis procedures in box culvert design.

Other studies recognized the effects of "arching" in the soil mass surrounding the culvert, as well as the differences in loads due to various construction techniques. Probably the earliest theory developed which takes these considerations into account was presented by Marston [11].

According to this theory, the resultant vertical load produced by an embankment is made up of two parts: the weight of the column of fill directly over the conduit, and the frictional forces acting either upward or downward on the sides of this column of fill. This frictional force takes into account soil characteristics including angle of internal friction, density, material composition, and moisture content. The frictional effect on the culvert loading is a function of the settlement of the fill adjacent to and directly above the conduit, as shown in Fig. 2.2.

The effects due to frictional forces depend primarily on the relative amounts of settlement between the column of soil above the culvert and the surrounding soil mass. The vertical loads on the culvert are decreased when the fill above the culvert settles downward relative to the adjacent soil, as shown in Fig. 2.2a. However, the embankment load on the culvert may also become greater than the weight of the soil above the culvert, as shown in Fig. 2.2b. Here, the surrounding soil settles downward relative to the column of soil above the culvert. The frictional forces may act to either increase or decrease the total load on the conduit.

It should be noted that the term "conduit" refers to culverts, sewers, water pipes, and other underground structures, of all shapes, materials, degrees of rigidity, and field construction conditions affecting loads or

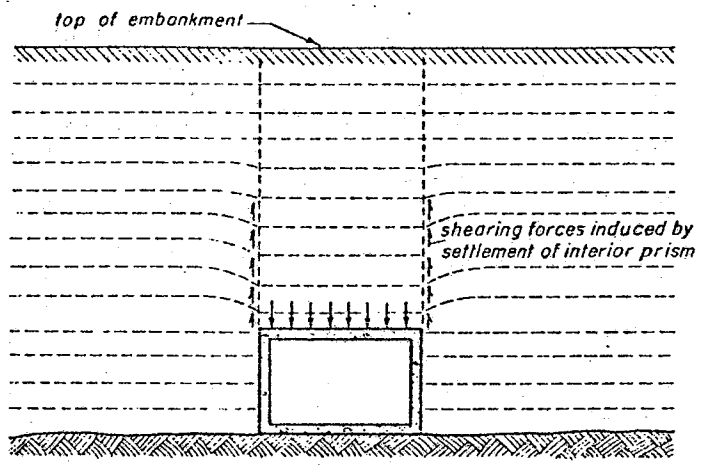

a) FRICTIONAL FORCES, YIELDING FOUNDATION

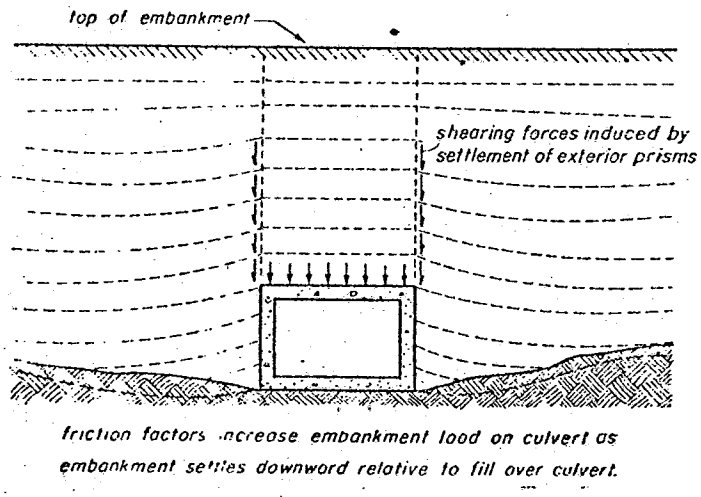

B) FRICTIONAL FORCES, UNYIELDING FOUNDATION

FRICTIONAL EFFECTS ON CULVERT LOADS

FIGURE 2.2

supporting strength.

To account for lateral earth pressures on the conduit, Marston used Rankine's Constant, K. Here, the intensity of the active lateral earth pressure is K times the intensity of the vertical pressure. Rankine's Constant, K, is taken as

$$K = \frac{\sqrt{\mu^2+1} - \mu}{\sqrt{\mu^2+1} + \mu} \qquad [2.1]$$

where μ is the coefficient of internal friction of the material. This coefficient may be expressed as

$$\mu = \tan \phi \qquad [2.2]$$

where ϕ is the angle of internal friction of the material.

Marston's studies also recognized the importance of construction conditions. There were two primary conditions which were considered, which are

a) Culvert in a trench on an unyielding subgrade, or culvert placed on a yielding foundation, and

$$W = PB = wHB \qquad [2.3]$$

b) Culvert placed on an unyielding foundation [such as rock or piles].

for $H > 1.7\ B$

$$W = PB = wB\ [1.92\ H - 0.87\ B] \qquad [2.4]$$

or

for $H < 1.7\ B$

$$W = PB = 2.59w\ B^2\ [e^k - 1] \qquad [2.5]$$

where

W = total load due to earth backfill,

P = unit load due to backfill,

B = external horizontal span of culvert or trench,

width at top of culvert for culverts in trenches,

w = effective weight of fill material,

e = 2.7183,

k = 0.385 $^{H}/_{B}$, and

H = height of earth fill over top of culvert.

Using this analysis, the Portland Cement Association [PCA] [14] developed a set of design charts for culverts. These are presented in Figs. 2.3 - 2.5. Using these figures it is possible to graphically determine the total vertical earth load for culverts of various spans and fill heights. By knowing the height of fill above the conduit, and the span width [or trench width for trenched condition], the vertical load may be obtained directly.

These charts deal only with trench or projecting culverts. Another construction case which must be considered is the imperfect-trench installation procedure. In this case, a layer of compressible material is placed directly over the culvert to allow the shear stresses in the soil to reduce the pressure on the top of the culvert as shown in Fig. 2.6. This installation procedure is only acceptable for high fill situations, so that the fill soil is able to obtain a plane of equal settlement before reaching the top of the embankment.

For the imperfect-trench installation condition, the vertical loads that develop may be calculated using

$$W = C_n W B^2 \qquad [2.6]$$

where

W = total vertical load,

w = density of the fill, and

B = external span of the culvert.

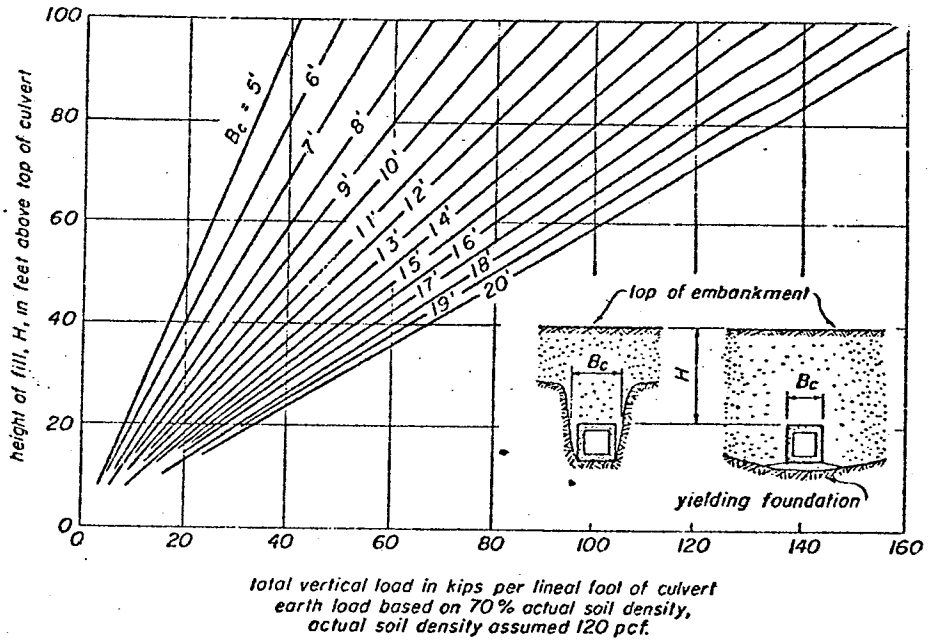

TOTAL EARTH LOAD, TRENCH CONDITION
OR YIELDING FOUNDATION

FIGURE 2.3

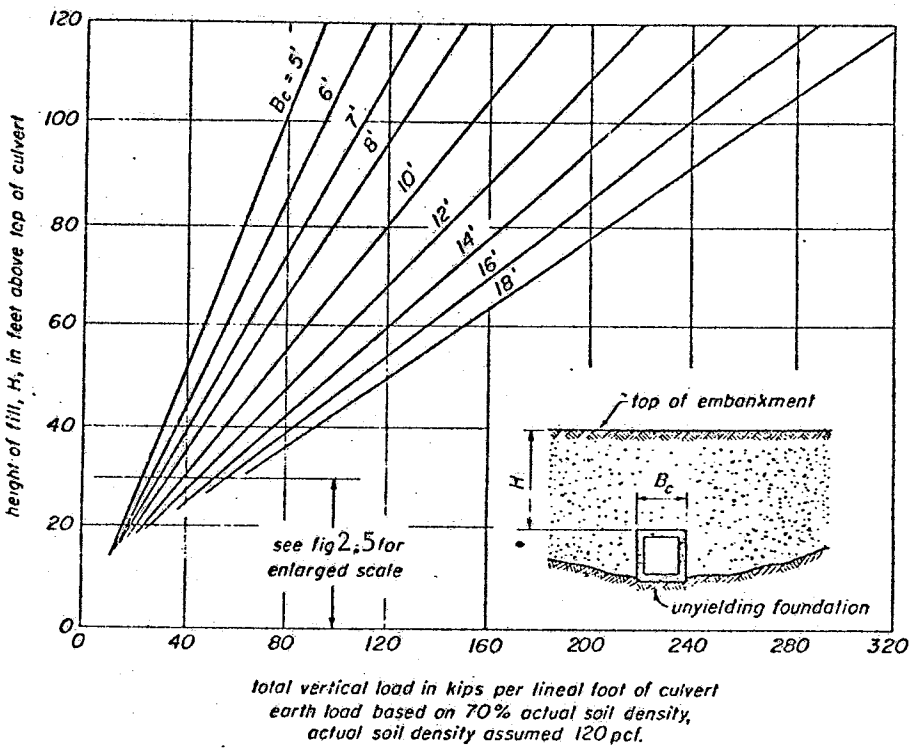

TOTAL EARTH LOAD, UNYIELDING FOUNDATION

FIGURE 2.4

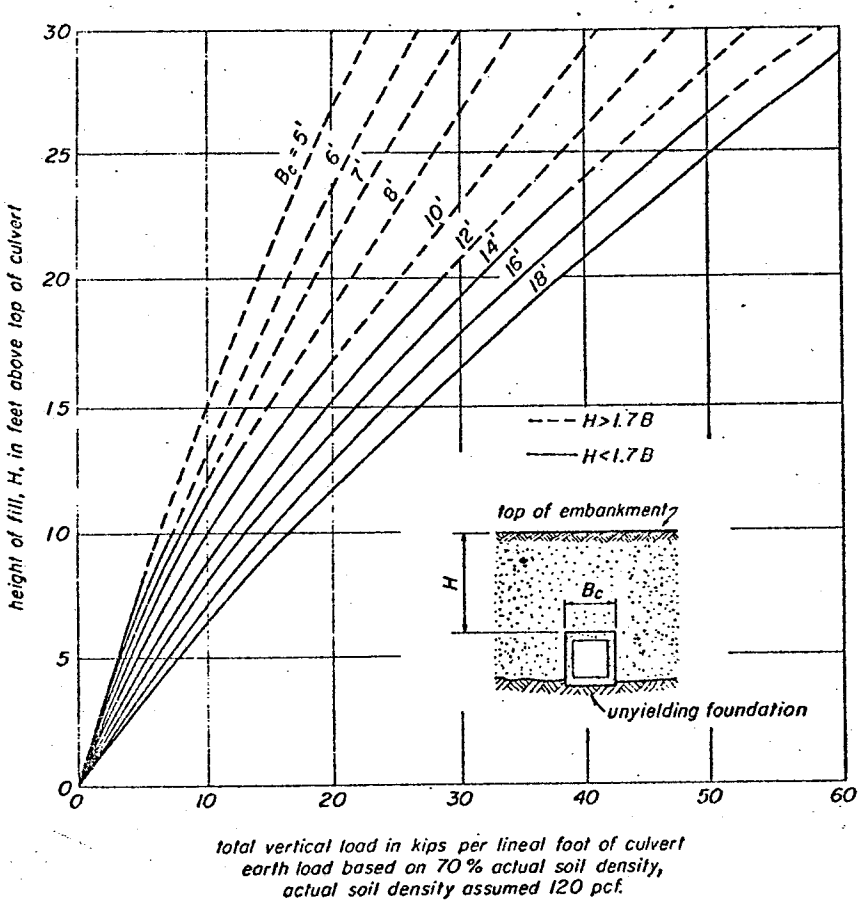

ENLARGED PORTION OF FIGURE 2.4

FIGURE 2.5

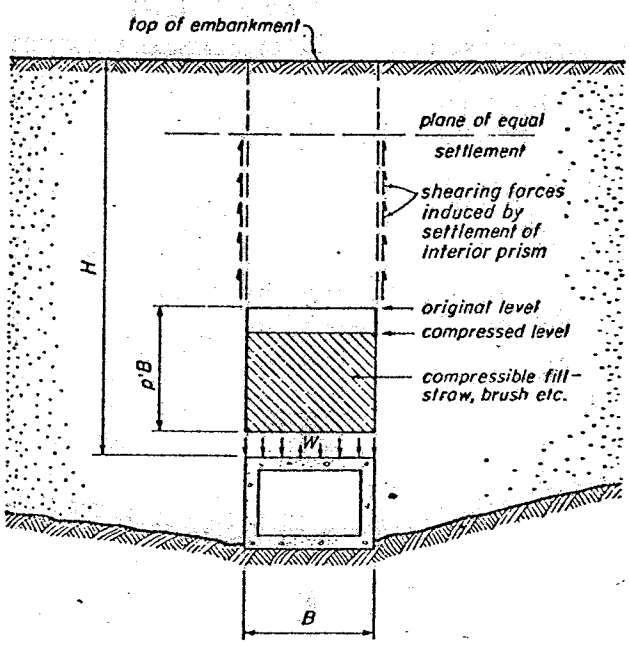

IMPERFECT TRENCH INSTALLATION

FIGURE 2.6

The load coefficient, C_n, may be graphically determined from charts shown in Fig. 2.7 and 2.8. This coefficient is dependent on such factors as the projection ratio, p , and the settlement ratio, r. The projection ratio, p, may have any value, depending on the depth of the trench. Formally, p is the ratio of the imperfect-trench depth to conduit width. Values of the projection ratio are usually taken as 0.5 or 1.0.

The settlement ratio, r, depends on the settlement of the conduit into the foundation, deflection of the conduit, compression of the earth fill, and compression of the loose fill material. Values are normally taken from 0 to -1.0, with -0.5 being considered a reasonable design value for most conditions. Incorporating these the PCA has developed charts to obtain the total earth load for imperfect-trench installation procedures. These are given in Figs. 2.9 and 2.10. By knowing the height of fill above the culvert, as well as the projection and settlement ratios, a value for the total vertical earth load may be obtained.

The PCA has also developed tables for determining design loads such as moments, thrust, and shear at various points around the cross-section of the culvert. A typical table is shown in Table 2.1. The formulae are given in terms of cross-sectional properties for the determination of design moments, axial thrust, and shear.

Karadi and Krizek [10] have presented the method of design used for rigid culverts in the Soviet Union. Culverts are designed for bending moment by the formula

$$M = \nu r^2 (p+q) [1 - \tan^2 (45 - \phi/2)] \qquad [2.7]$$

where

P = vertical pressure due to dead loads

q = vertical pressure due to live loads

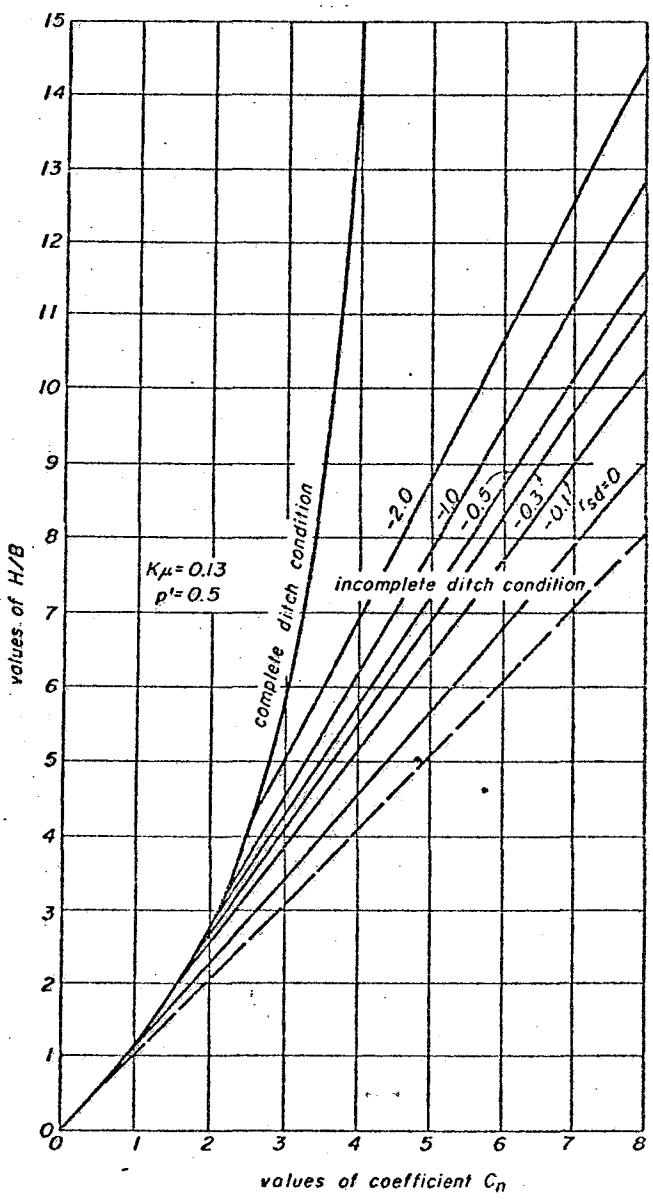

LOAD COEFFICIENT, C_n, FOR IMPERFECT-TRENCH CONDUITS, PROJECTION RATIO p' = 0.5.

FIGURE 2.7

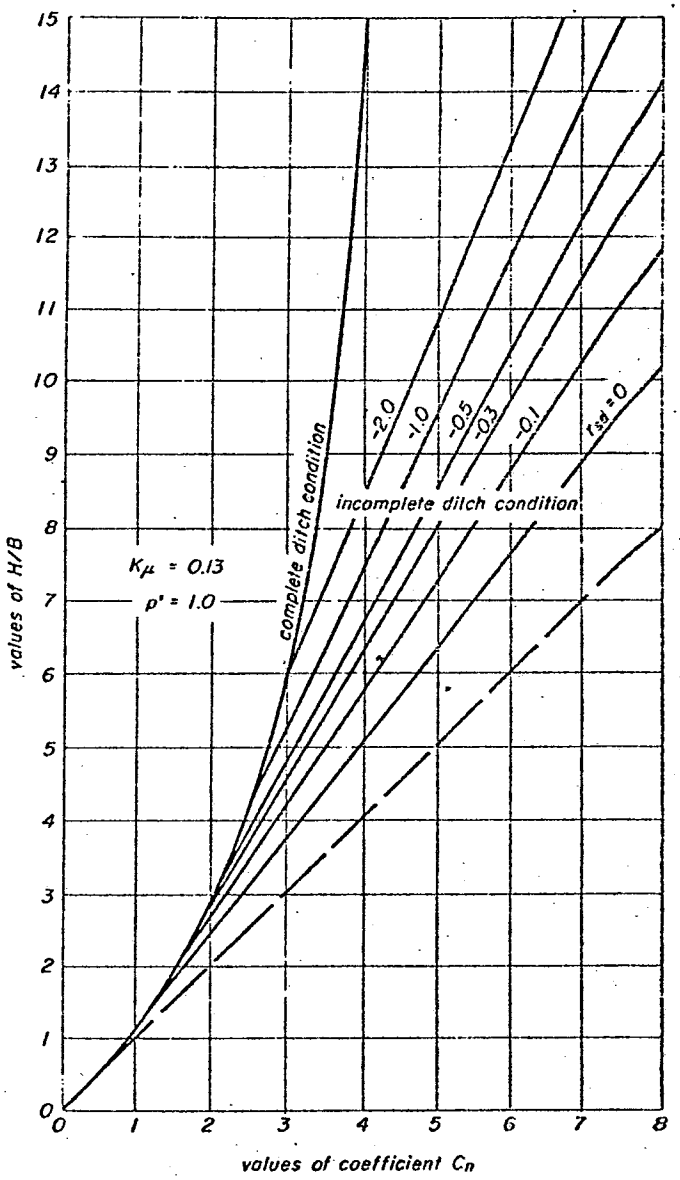

LOAD COEFFICIENT, C_n, FOR IMPERFECT-TRENCH CONDUITS, PROJECTION RATIO p' = 1.0.

FIGURE 2.8

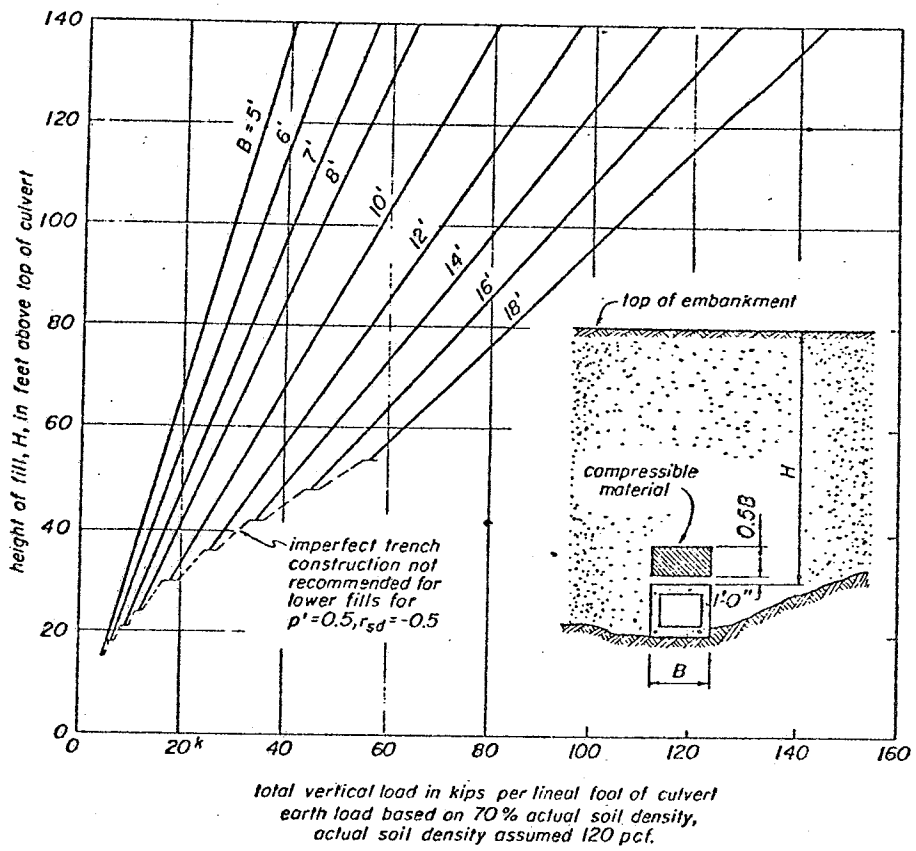

TOTAL EARTH LOAD, IMPERFECT-TRENCH INSTALLATION p' = 0.5

FIGURE 2.9

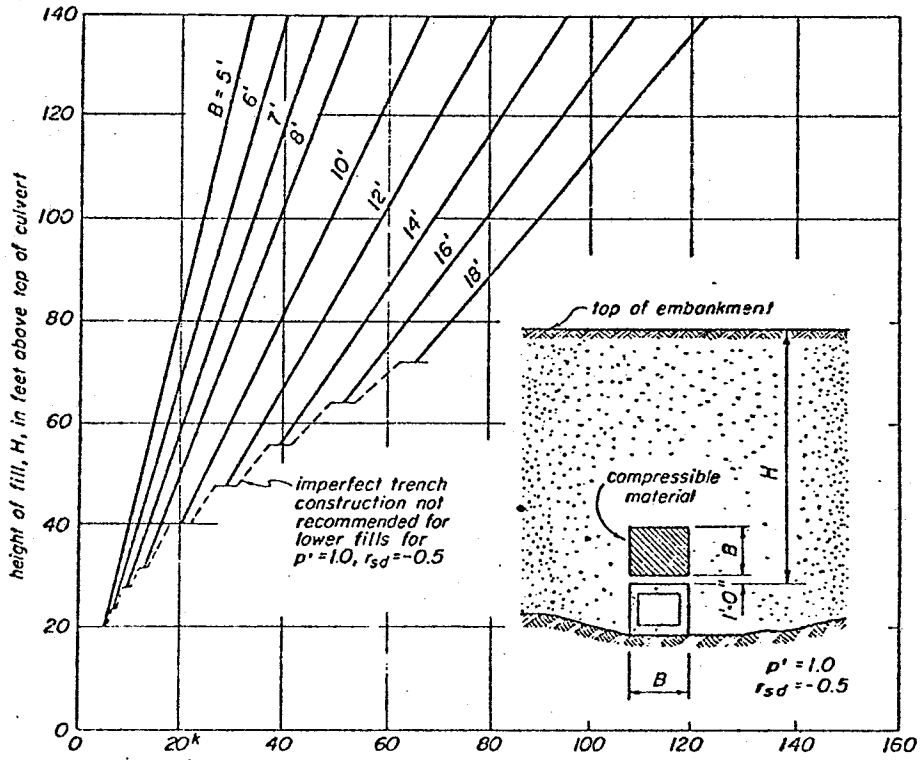

TOTAL EARTH LOAD, IMPERFECT-TRENCH INSTALLATION p' = 1.0

FIGURE 2.10

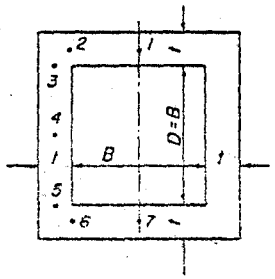

Fig. 53. Transverse section.

SIGNS

+Moment, M, indicates tension on inside face.
+Thrust, N, indicates compression on section.
+Shear, V, indicates that summation of forces at left of section acts outward when viewed from within.

UNITS

M in ft.-lb.; N and V in lb.
(for W, F, and T in lb.; B and t in ft.)

W = total embankment and live load on the culvert, lb. per ft. of culvert length
F = Uniform lateral load on culvert, psf
T = Triangular lateral load on culvert, psf

Section	I			II			III			IV			V		
	Uniform vertical load			Conduit weight			Pressure from contained water			Uniform lateral load			Triangular lateral load		
	M	N	V	M	N	V	M	N	V	M	N	V	M	N	V
	$.0417W(B+t)$	W		$3.13t(B+t)^2$	$t(B+t)$		$1.17B^2(B+t)$	B^2		$.0417F(B+t)^2$	$F(B+t)$		$.0188T(B+t)^3$	$T(B+t)^2$	
1	+2			+ 5			+1	−10.2		−1	+.50		−1	+.16	
2	$-\left[\frac{B-5t}{B+t}\right]$		+.50	$-\left[\frac{B-11t}{B+t}\right]$		+ 75	+1	−10.2		−1	+.50		−1	+.16	
3	−1	+.50		−1	+ 75		$+\left[\frac{B-3.4t}{B+t}\right]$ *		+10.2	$-\left[\frac{B-5t}{B+t}\right]$		−.50	$-\left[\frac{B-3.4t}{B+t}\right]$		−.16
4	−1	+.50		−4	+150		−2.22 *			+2			+2.22		
5	−1	+.50		−7	+225		$+1.22\left[\frac{B-6.3t}{B+t}\right]$		−21.3	$-\left[\frac{B-5t}{B+t}\right]$		+.50	$-1.22\left[\frac{B-6.3t}{B+t}\right]$		+.34
6	$-\left[\frac{B-5t}{B+t}\right]$		−.50	$-7\left[\frac{B-4.1t}{B+t}\right]$		−225	+1.22	−21.3		− 1	+.50		−1.22	+.34	
7	+2			+11			+1.22	−21.3		− 1	+.50		−1.22	+.34	

TABLE 2.1

SQUARE ONE-CELL BOXES: COEFFICIENTS FOR MOMENT M, THRUST, N, AND SHEAR, V.

ν = coefficient determined by type of foundation

The values of p and q are given by

$$p = C \gamma H \qquad [2.8]$$

and

$$q = \frac{19}{H + 3} \quad (H > 1 \text{ meter}) \qquad [2.9]$$

where, in Eq. 2.9, H is expressed in meters and q in metric tons per square meter. In Eq. 2.8,

$$C = 1 + A \tan \phi \tan^2 (45 - \phi/2) \qquad [2.10]$$

and

$$A = m h H^{-3} (2H^2 - m Bh) \qquad [2.11]$$

In this, H is the height of the embankment above the crown of the culvert, h is the distance between the plane of the foundation and the crown of the culvert, B is the external span of the culvert, m is a coefficient determined by soil characteristics, and ϕ and γ are the angle of internal friction and the density of soil, respectively.

2.2.2 Analytical Solutions With Soil-Structure Interaction

Heger [7] presents a method which incorporates a soil-structure interaction factor, F. These analyses were performed on rigid concrete pipes, with the objective of improving the correlation between predicted and actual test strengths.

By this analysis, the total vertical earth load is given by

$$We = F_e w B_c H \qquad [2.12]$$

where

B_c = the outside horizontal projection of the pipe

H = height of cover over the crown of the pipe

and F_e = soil-structure interaction factor.

For the determination of F_e, Heger presents the equation

$$F_e = [1 + 0.2\ {}^{H}/_{B_C}] \qquad [2.13)$$

The maximum specified value of F_e is taken as 1.5 for uncompacted fills and 1.2 for compacted fills.

Heger also presents assumptions for earth pressure distribution in Figs. 2.11 and 2.12. The assumed distribution for the traditionally defined Class C bedding is shown in Fig. 2.11. Two possible assumptions are presented. Earth pressure distribution as given by Olander [12] is shown in Fig. 2.11a, while uniformly distributed pressures are shown in Fig. 2.11.b. Earth pressure assumptions for Class B bedding are shown in Fig. 2.12.

2.3 Numerical Solutions

Numerical Solutions to the problem of soil-structure interaction effects on earth pressure distribution on buried structures have been the result of the availability of high-powered modern computers. A number of computer programs have evolved for this type of study, primarily involving the finite element method.

One of the most popular programs available is CANDE, developed by Katona [9]. CANDE [Culvert ANalysis and DEsign]is a plane strain finite element program used for the analysis of buried structures. Katona first used out-of-ground box tests to verify the CANDE model, then used CANDE to evaluate current standards on box culvert design. The out-of-ground box test set-up is shown in Fig. 2.13. Katona used four-edge bearing on standard box sections, loaded to the point where 0.01 inch cracking occurs, as well as to ultimate shear or flexural failure. He also used the CANDE program to evaluate the culvert for four-edge bearing test procedures.

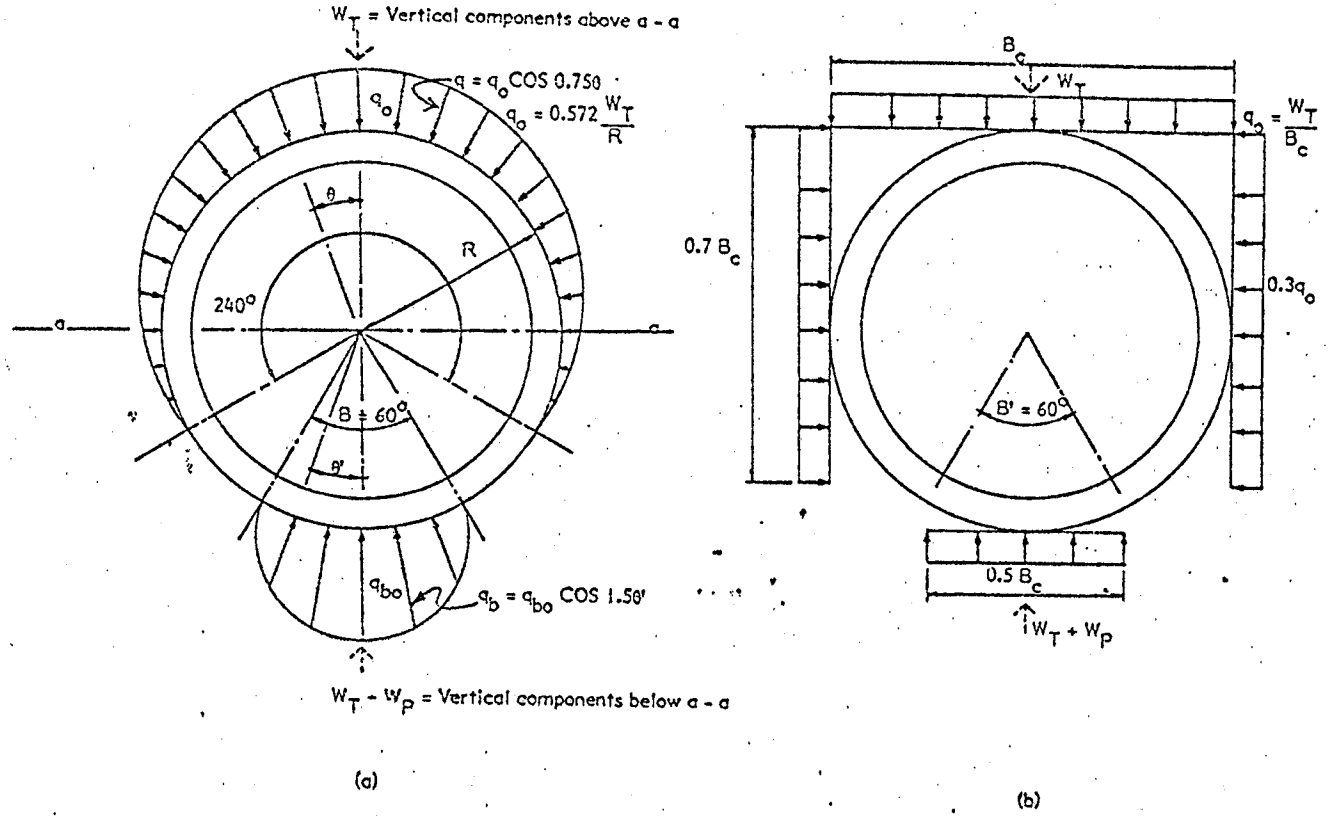

EARTH PRESSURE ASSUMPTIONS FOR EMBANKMENT CLASS C BEDDING

FIGURE 2.11

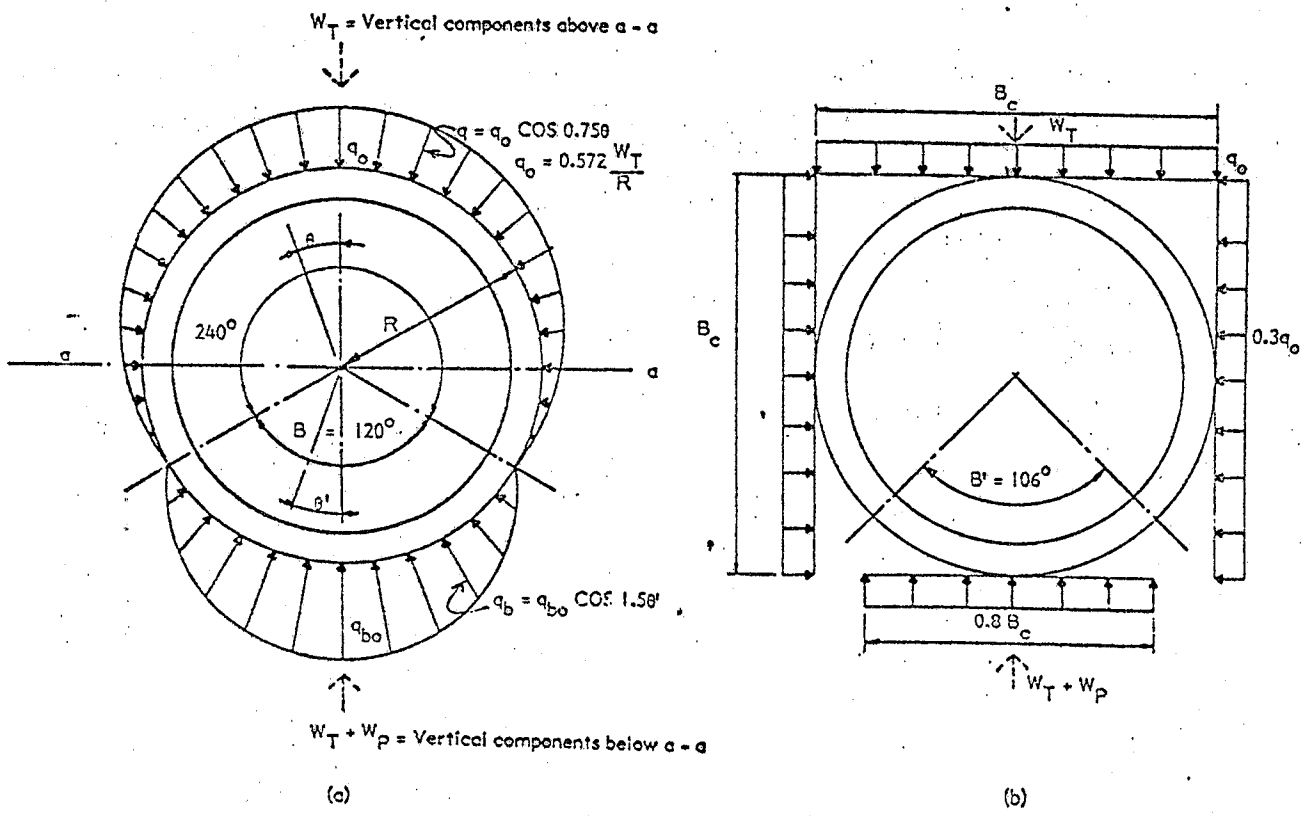

EARTH PRESSURE ASSUMPTIONS FOR EMBANKMENT CLASS B BEDDING

FIGURE 2.12

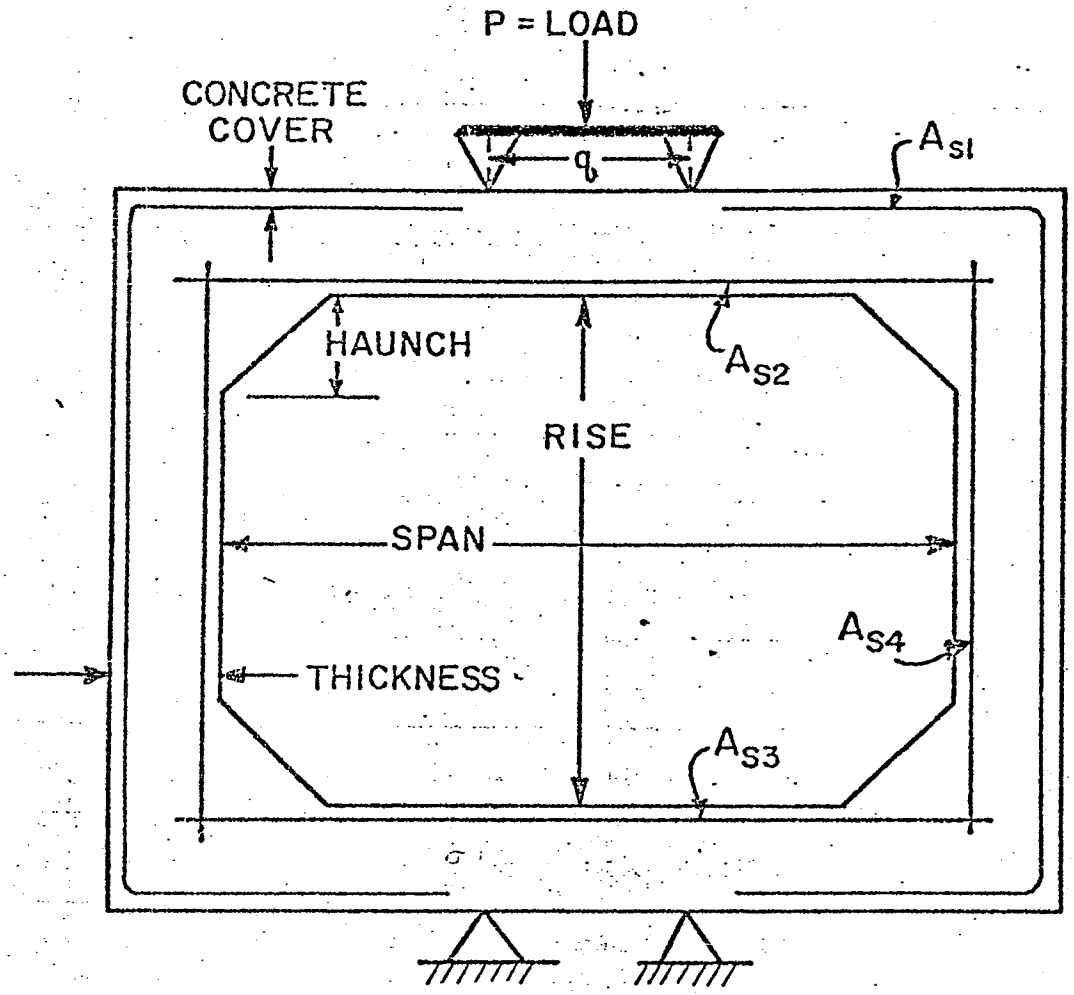

BOX CULVERT IN FOUR-EDGE BEARING

FIGURE 2.13

The CANDE model of the box culvert in four-edge bearing is shown in Fig. 2.14. The correlation between the predicted loads and actual test loads for 0.01 inch cracking to occur is shown in Fig. 2.15. Three standard box sizes were analyzed. Although there is some scatter in the data the correlation is good. A comparison of the predicted and actual ultimate loads for shear and flexural failure is shown in Fig. 2.16. The correlation of these results is very close for the three box sections tested.

Katona also compared data from previously conducted in-ground box culvert tests with his computer predictions. The culvert-soil system used for this analysis is shown in Fig. 2.17. CANDE was used to predict the earth pressures shown by the eight pressure gages located around the perimeter of the culvert. A summary of his test results is shown in Fig. 2.18. The pressures predicted by CANDE and measured by the pressure gages along the top and bottom slabs are not uniformly distributed and this is contrary to what is assumed by most procedures. Also, the correlation of data along the right wall is much closer than the correlation along the left wall of the culvert.

Huang, Gill, and Gnaedinger [8] also used the CANDE program for their analyses. They modeled various combinations of properties in order to evaluate the predicted deflections and earth pressures. The soil-structure system used for this analysis is shown in Fig. 2.19. The primary objective of this study was to determine the effects of different soil and structural properties on predicted earth pressures. Using these results a set of earth pressure charts were established to aid in the design of box culverts.

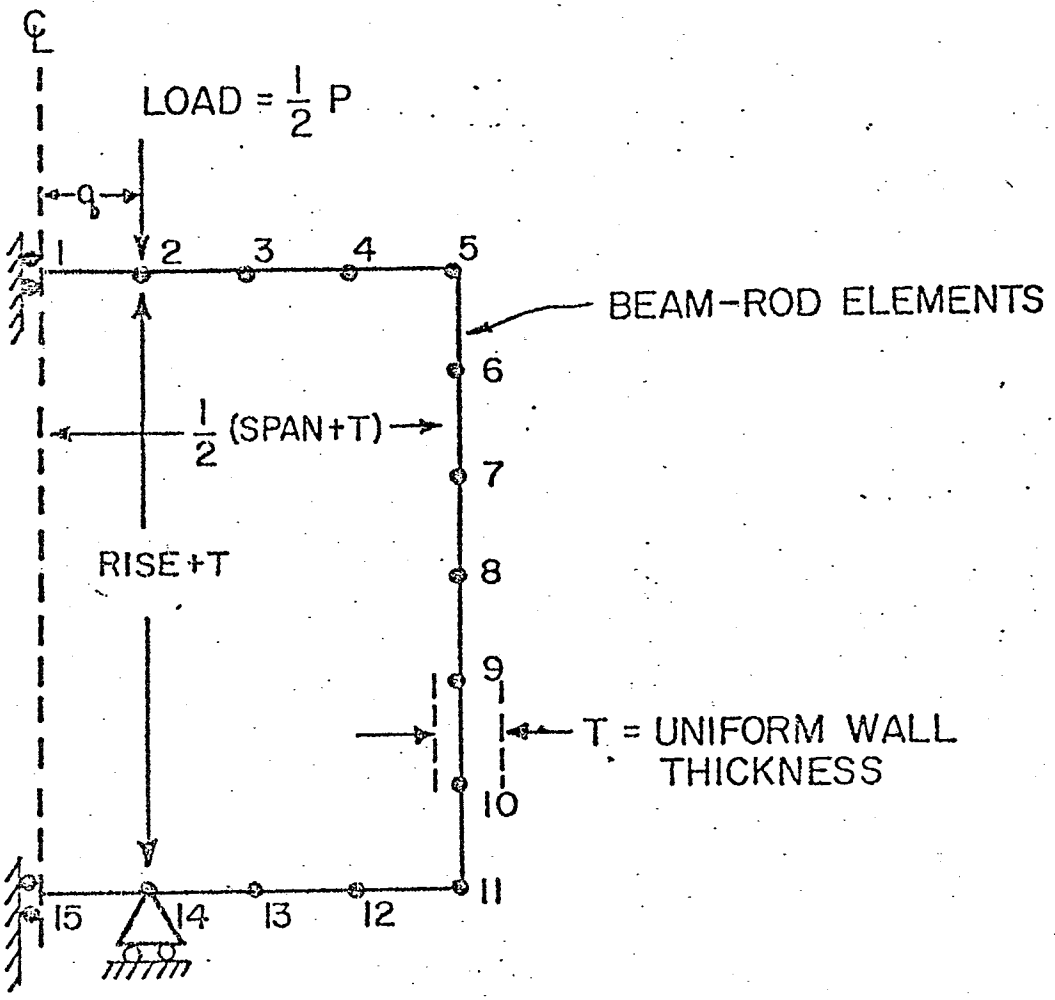

CANDE MODEL OF BOX CULVERT
IN FOUR-EDGE BEARING.

FIGURE 2.14

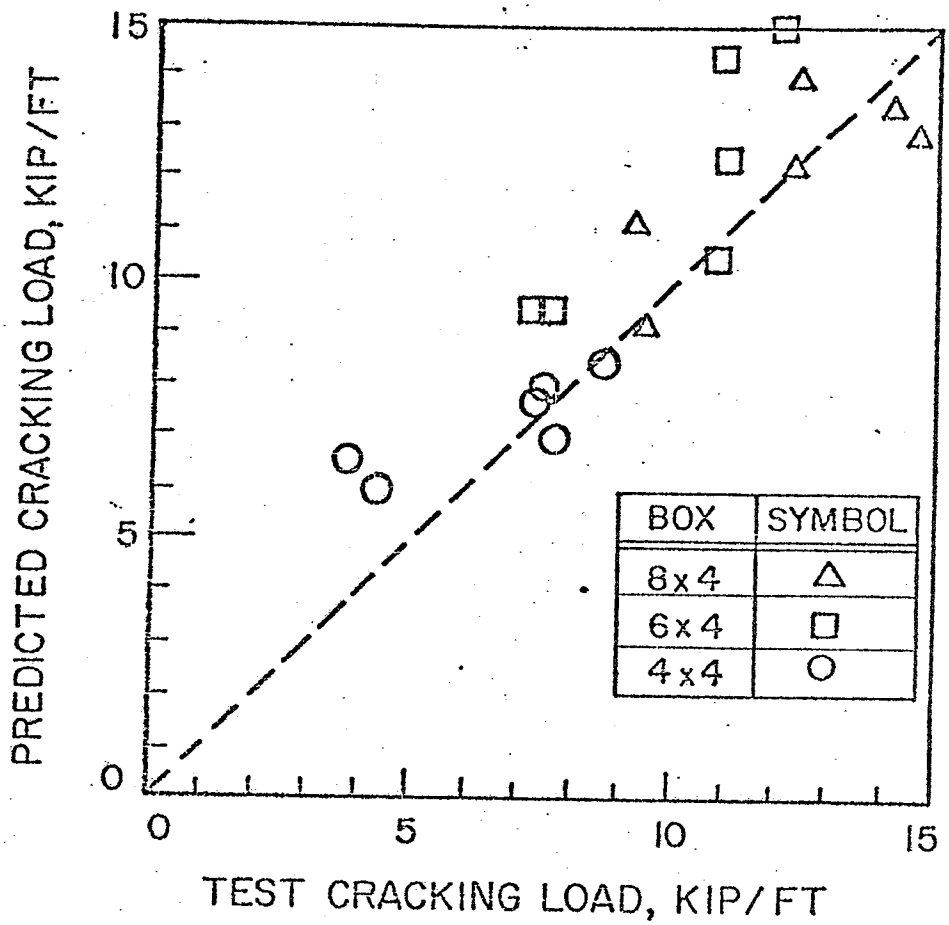

PREDICTION vs. TEST FOR LOAD AT 0.01 INCH CRACKING

FIGURE 2.15

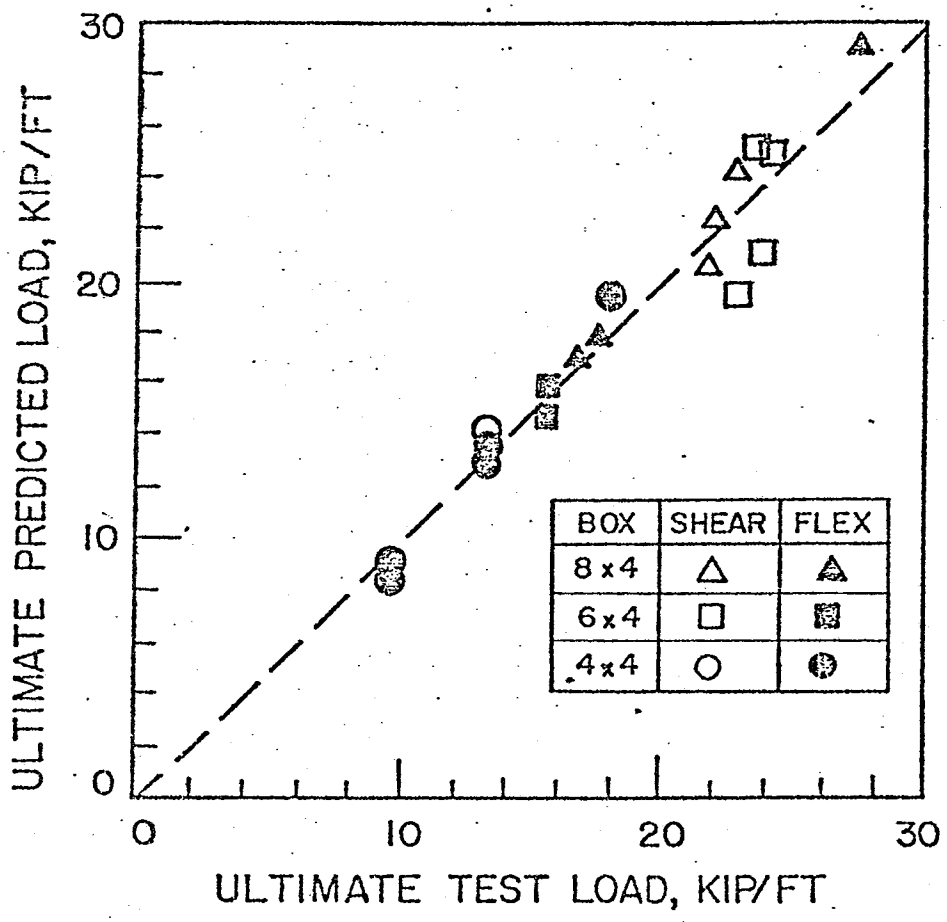

PREDICTIONS vs. TESTS FOR ULTIMATE LOAD

FIGURE 2.16

REINFORCEMENT AND CONCRETE PROPERTIES	f_c' psi	fy ksi	STEEL AREAS IN^2/IN A_{s1}	A_{s2}	A_{s3}	A_{s4}
	4500	60	0.037	0.050	0.050	0.017

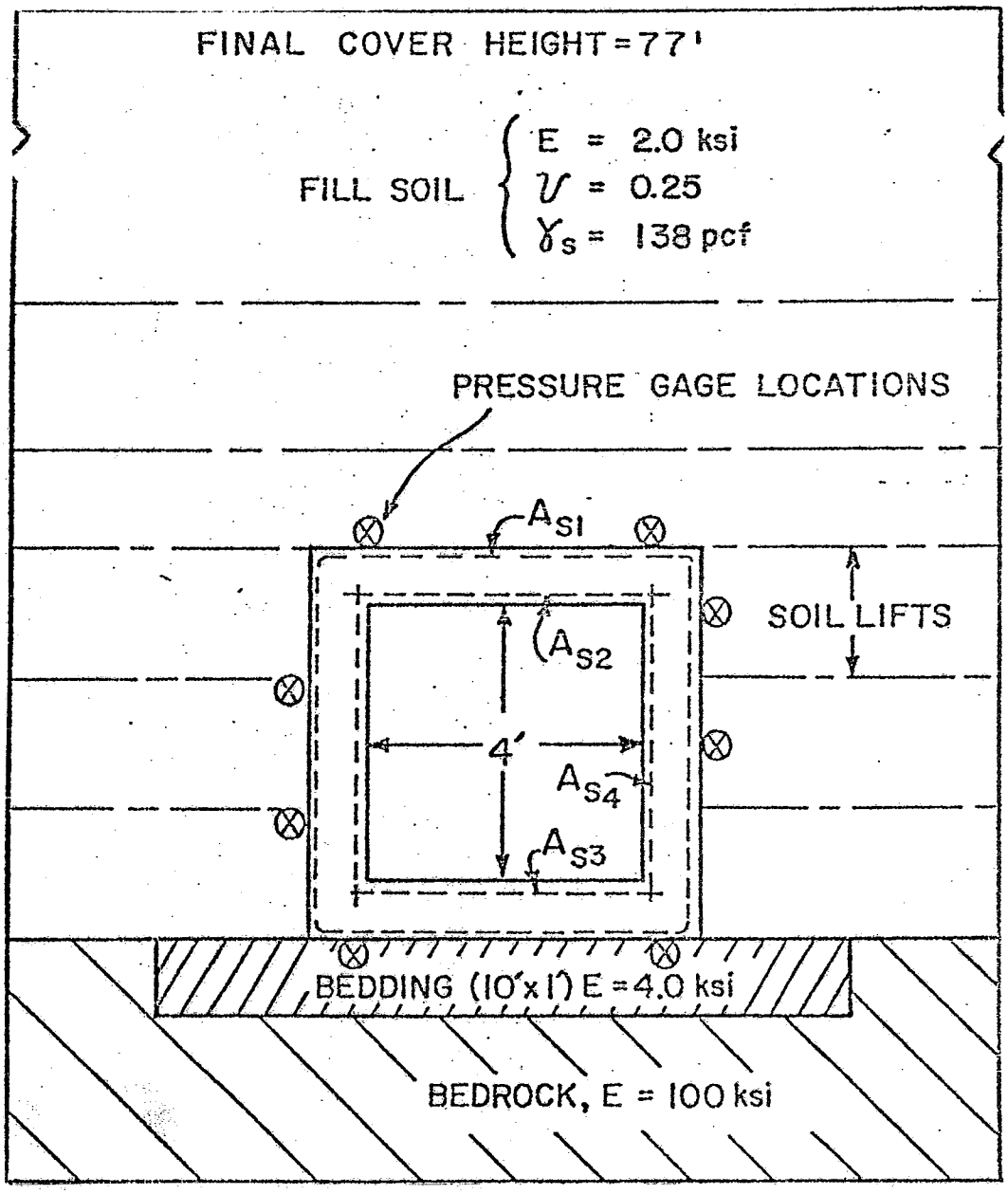

SCHEMATIC VIEW OF BOX-SOIL SYSTEM

FIGURE 2.17

FILL HEIGHT (FT)	LEGEND	
	CANDE	TESTS
21.6	------	o
77.0	———	●

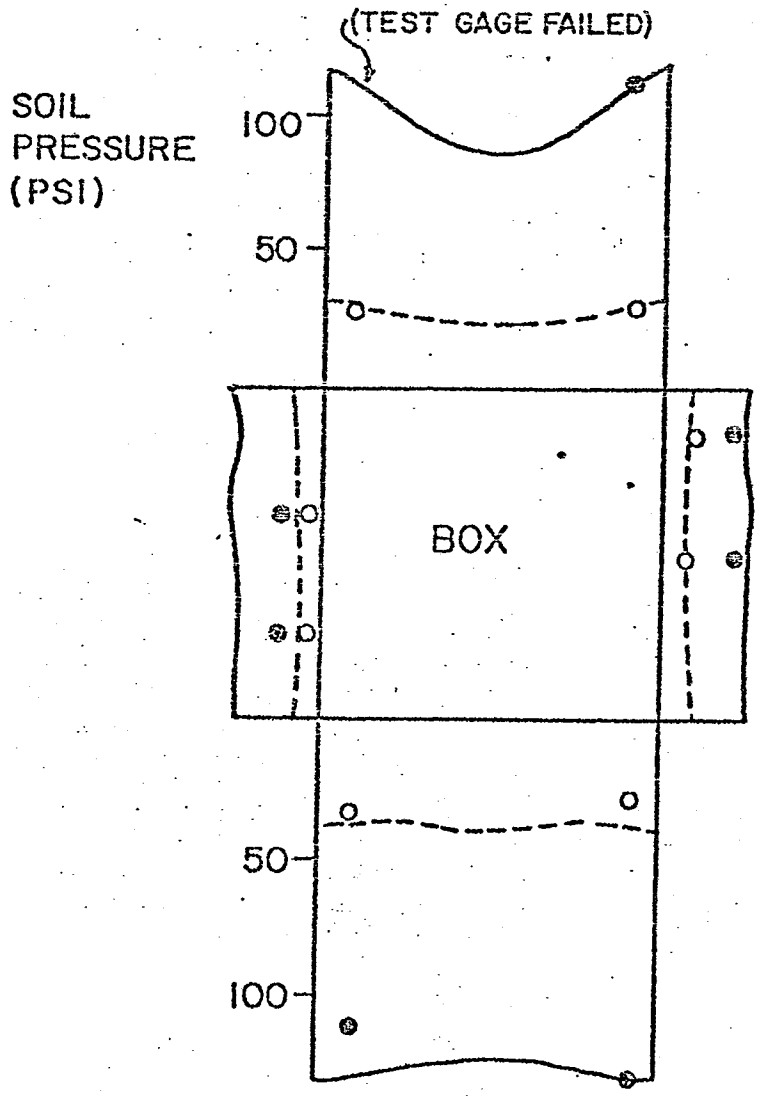

PREDICTION vs. TEST DATA FOR
SOIL PRESSURE AROUND BOX CULVERT.

FIGURE 2.18

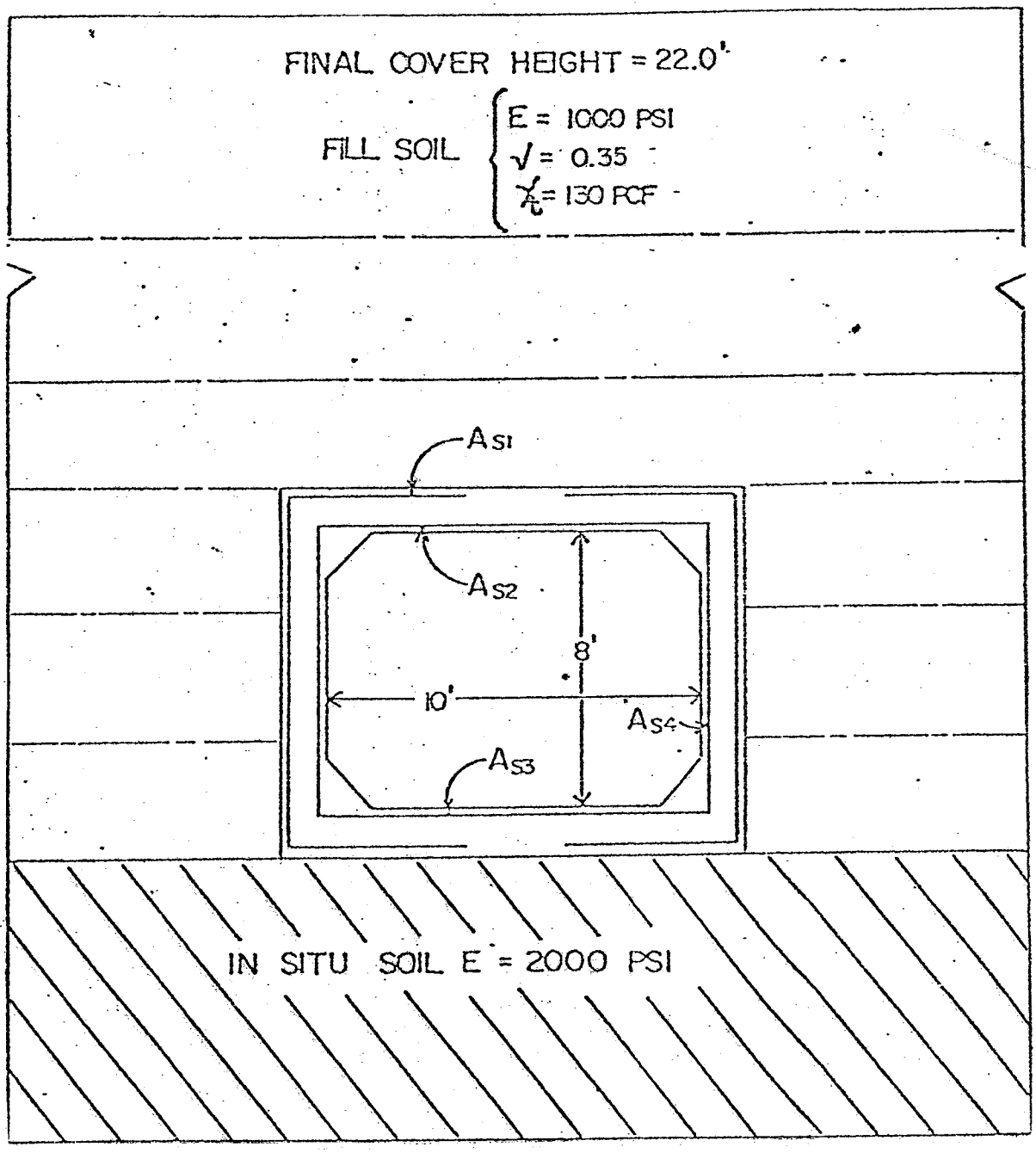

SCHEMATIC VIEW OF SOIL-CULVERT SYSTEM

FIGURE 2.19

The deflections, as predicted by CANDE for 22 feet of soil cover are shown in Fig. 2.20. The inward deflections of both the top and bottom slabs induce an outward deflection of the sides of the culvert. For the same loading conditions, the calculated earth pressures are shown in Fig. 2.21. The pressures increase from the center of the culvert to the outside on the top and bottom slabs. The lateral earth pressure increases with depth, although not linearly as expected.

Furthermore, various foundation and backfill soil properties were used to evaluate their effects on calculated earth pressures. Five different variations of bedding and foundation soil properties were analyzed. The results are shown in Fig. 2.22. The earth pressures on the top and side of the culvert seem to be independent of foundation soil properties. However, the calculated pressures on the bottom slab vary greatly with different foundation soil properties.

Three different variations of backfill soil were analyzed. The calculated earth pressures are shown in Fig. 2.23. The results of all three were very similar, with the sides of the culvert showing the greatest difference in fill pressure.

Huang, Gill, and Gnaedinger also studied the effects of culvert geometry on calculated earth pressures. The CANDE input for this analysis is shown in Fig. 2.24. A total of six box culvert sizes were used, with the properties of the foundation and fill soils held constant. The calculated vertical earth pressures were converted to dimensionless ratios and plotted against depth-span ratios and culvert height-span ratios. This conversion was accomplished by

$$\frac{W}{W_S} = \frac{\text{Calculated Total Earth Load}}{\text{Weight of Soil above the Culvert}} \qquad [2.14]$$

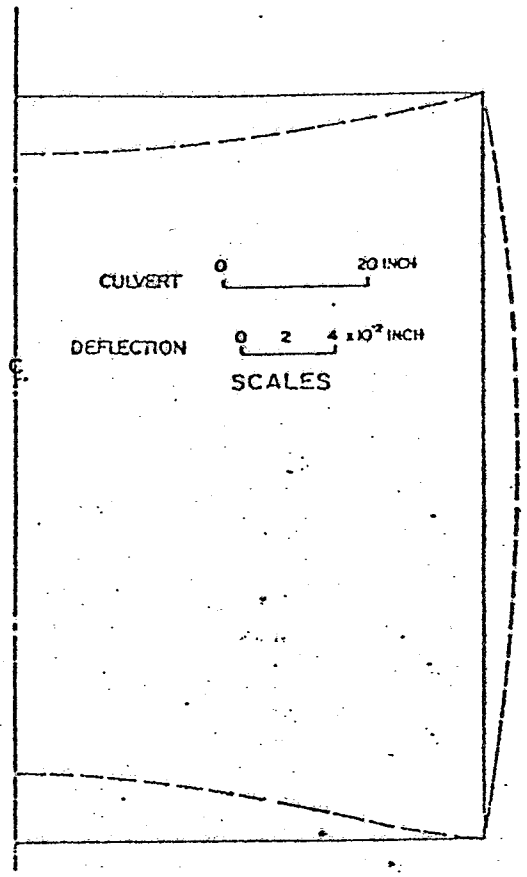

SCHEMATIC VIEW OF CULVERT RELATIVE DEFLECTIONS
UNDER 22 FT OF SOIL COVER

FIGURE 2.20

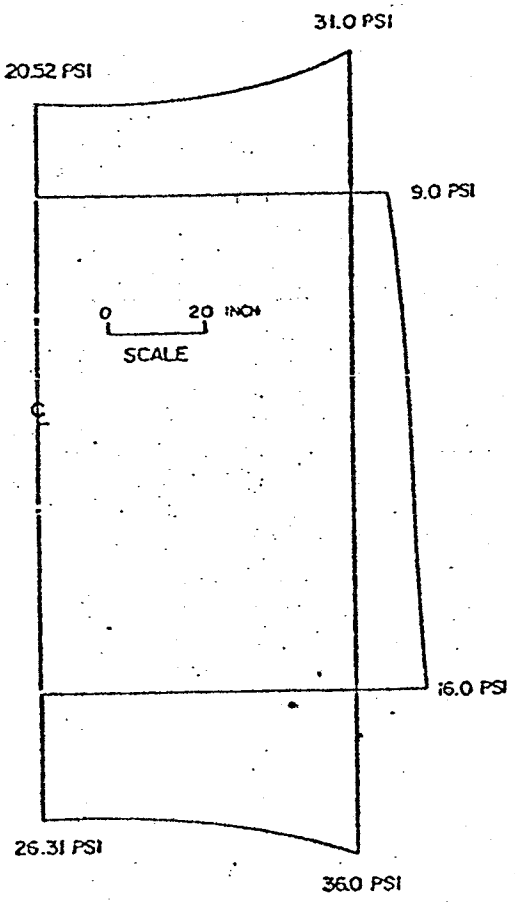

CALCULATED EARTH PRESSURES
ON 8x10-13 BOX CULVERT

FIGURE 2.21

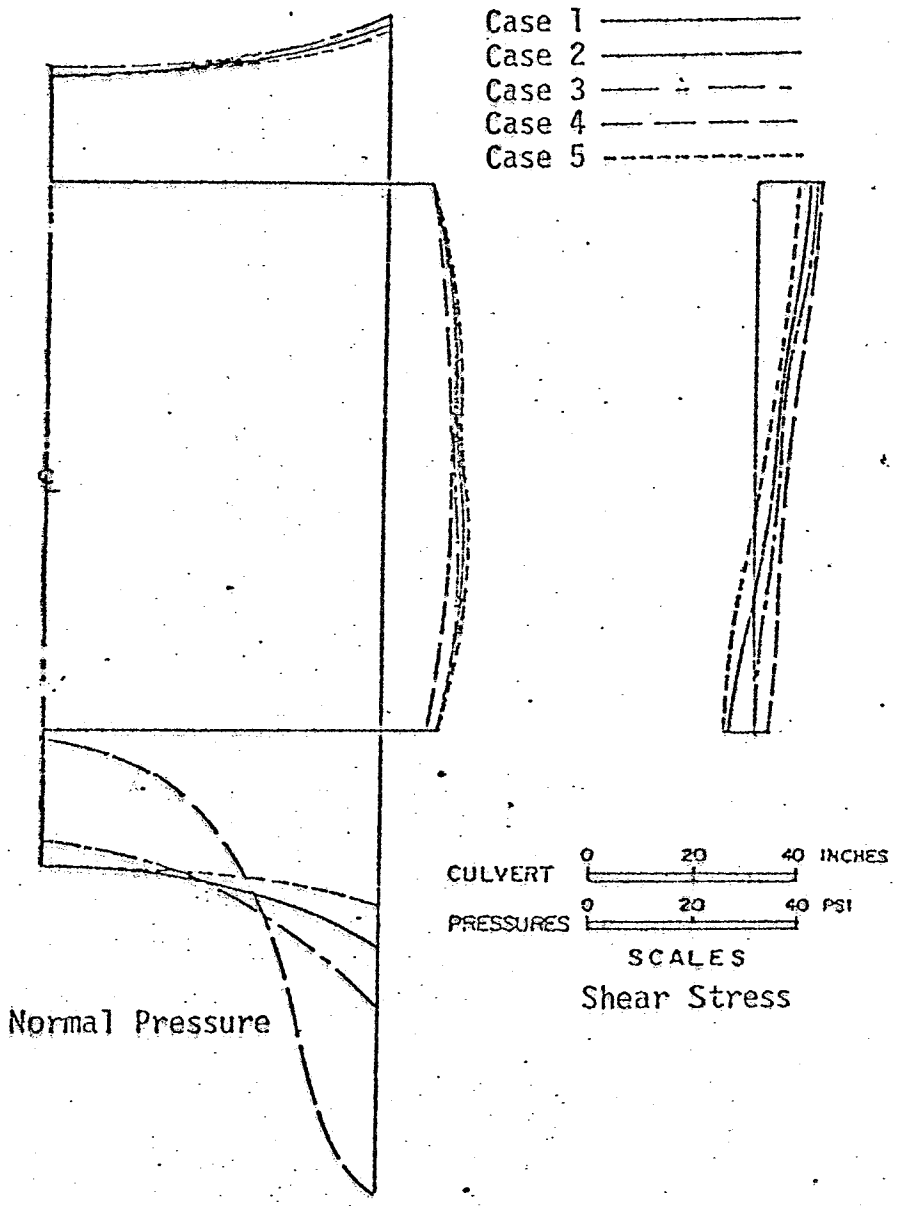

CALCULATED EARTH PRESSURE FOR DIFFERENT BEDDING AND FOUNDATION SOIL PROPERTIES.

FIGURE 2.22

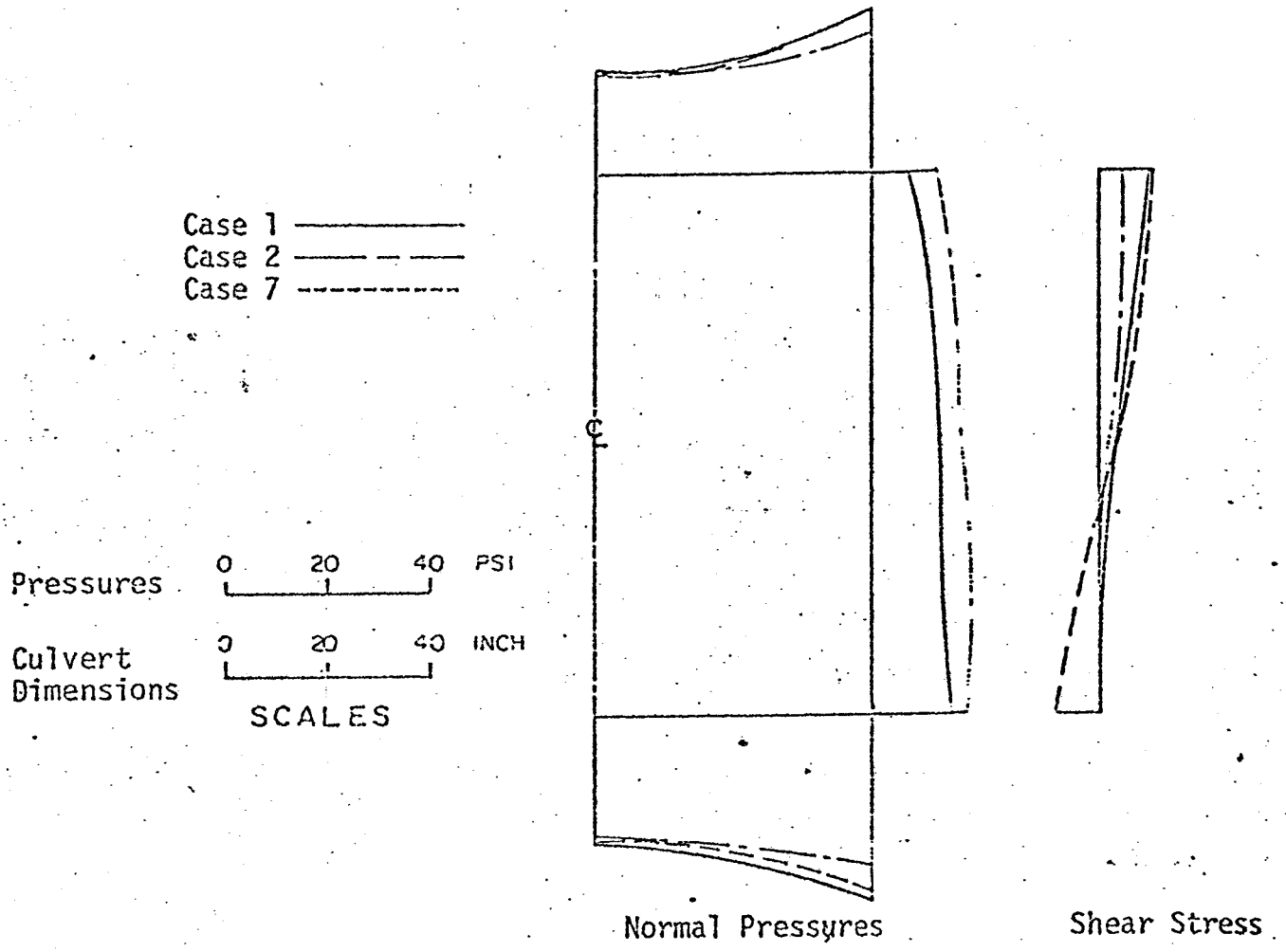

CALCULATED EARTH PRESSURES FOR DIFFERENT SOIL PROPERTIES

FIGURE 2.23

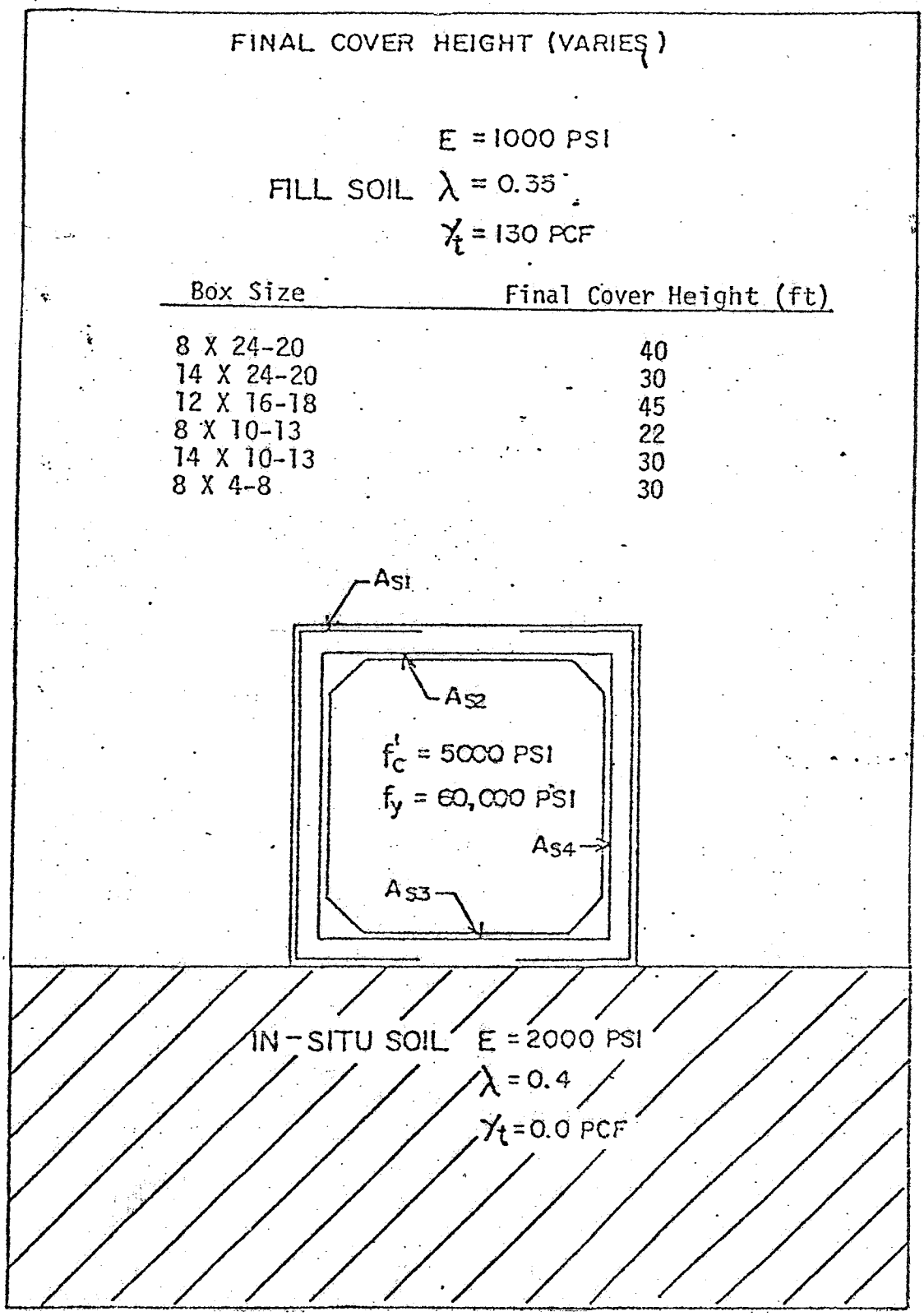

CANDE INPUT DATA FOR DIFFERENT
BOX SIZES AND SOIL COVER

FIGURE 2.24

and [2.15]

$$\frac{P}{\sigma_s} = \frac{\text{Calculated Vertical Earth Pressure}}{\text{Overburden Earth Pressure}}$$

The variation of earth load ratio [Eq. 2.14] with depth-span ratio is given in Fig. 2.25. The height of culvert-span ratio [$^{H}/_{S}$] greatly influences the results shown. An increase in the $^{H}/_{S}$ ratio increases the corresponding earth load ratio. The variation of earth pressure ratio [Eq. 2.15] with depth-span ratio is shown in Fig. 2.26. The earth pressure ratio also increases with increasing $^{H}/_{S}$ ratio. A comparison of the variation of the earth load ratio and earth pressure ratio with $^{H}/_{S}$ ratio is given in Fig. 2.27. The curves are almost identical in shape, with values of the earth load ratio being greater than those for the earth pressure ratio.

Through their analysis, Huang, Gill and Gnaedinger derived a set of design charts for box culverts of various sizes and depths of fill. The earth load ratio may be determined using Fig. 2.28, while the earth pressure ratio may be determined using Fig. 2.29. To use these charts, the culvert height, span, and depth of fill must be known.

Finally, for the lateral earth pressures, an earth pressure coefficient K_a was derived, which may be calculated by

$$K_a = \frac{\text{Integral of Calculated K Along Wall}}{\text{Culvert height, H}} \qquad [2.16]$$

A design chart is given in Fig. 2.30 for the determination of K_a. By knowing the culvert span and the depth of fill-height ratio, the lateral earth pressure coefficient can be easily found. Although Huang et.al. have presented extensive results on the behavior of box culverts, in their analyses the nonlinear stress dependent stress-strain behavior of the soil was not modeled. Furthemore the soil-structure interface was assumed to

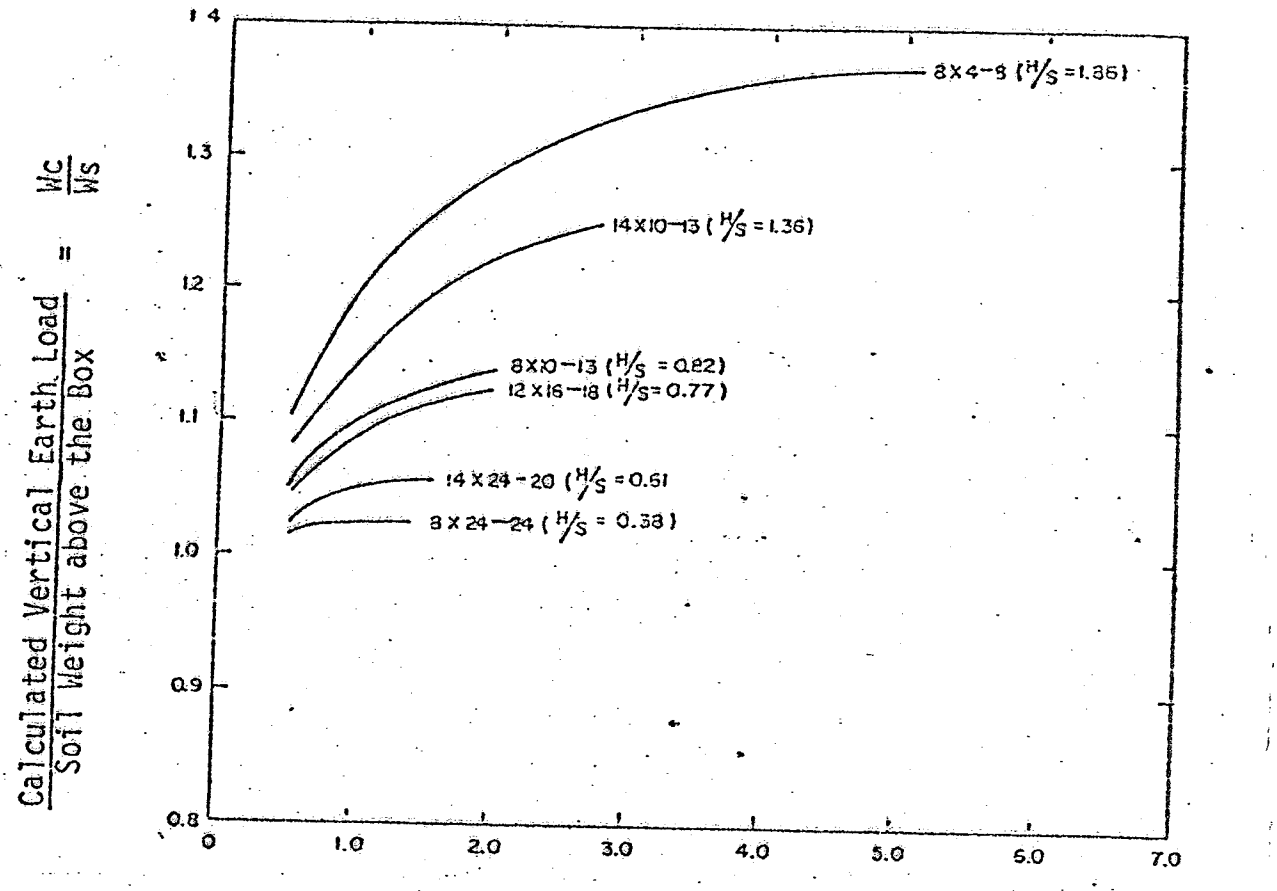

$$\frac{\text{Depth of Soil Cover (ft)}}{\text{Span of Culvert (ft)}} = \frac{D}{S}$$

CALCULATED EARTH LOAD RATIO
VS.
SOIL COVER OVER SPAN RATIOS

FIGURE 2.25

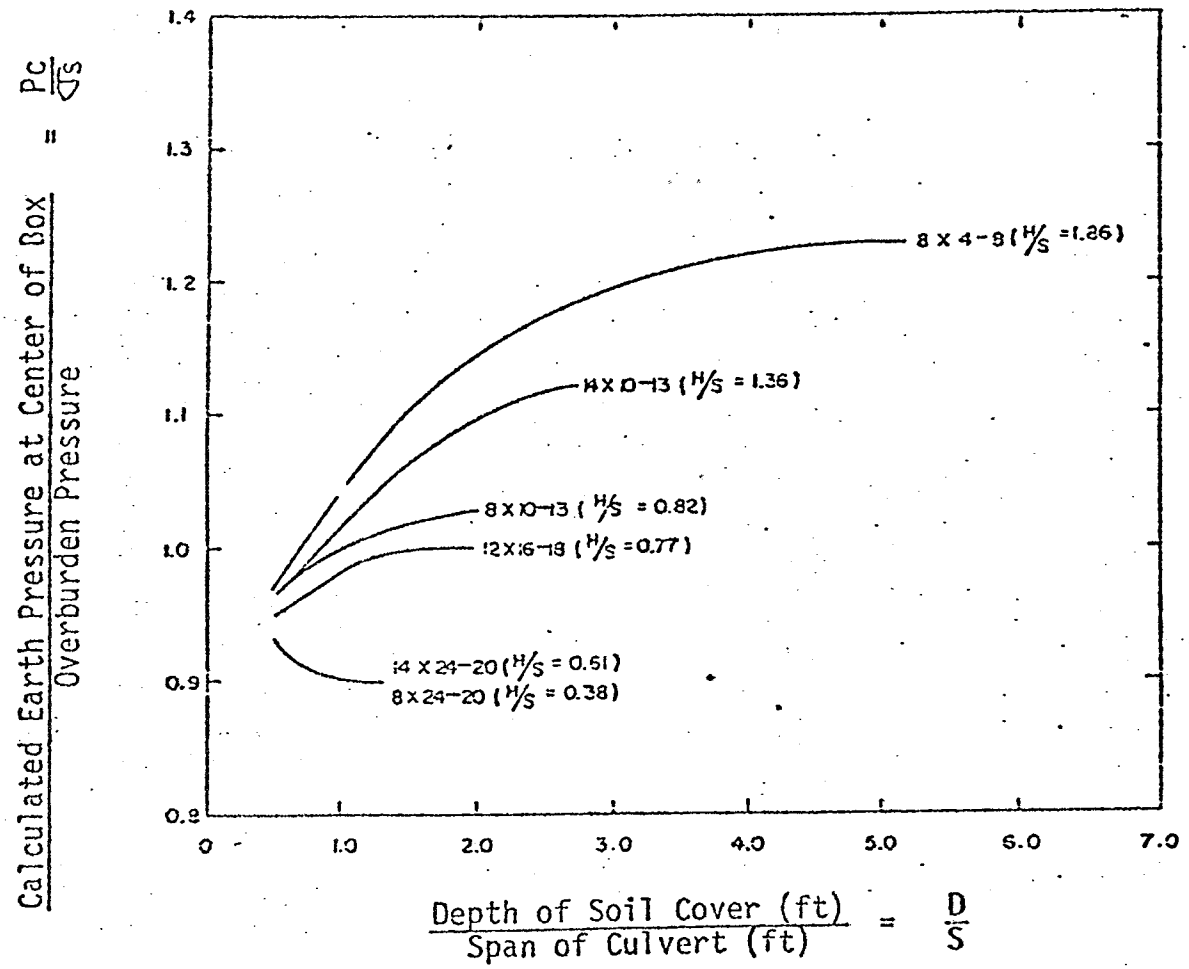

CALCULATED EARTH PRESSURE RATIO
VS.
SOIL COVER OVER SPAN RATIO

FIGURE 2.26

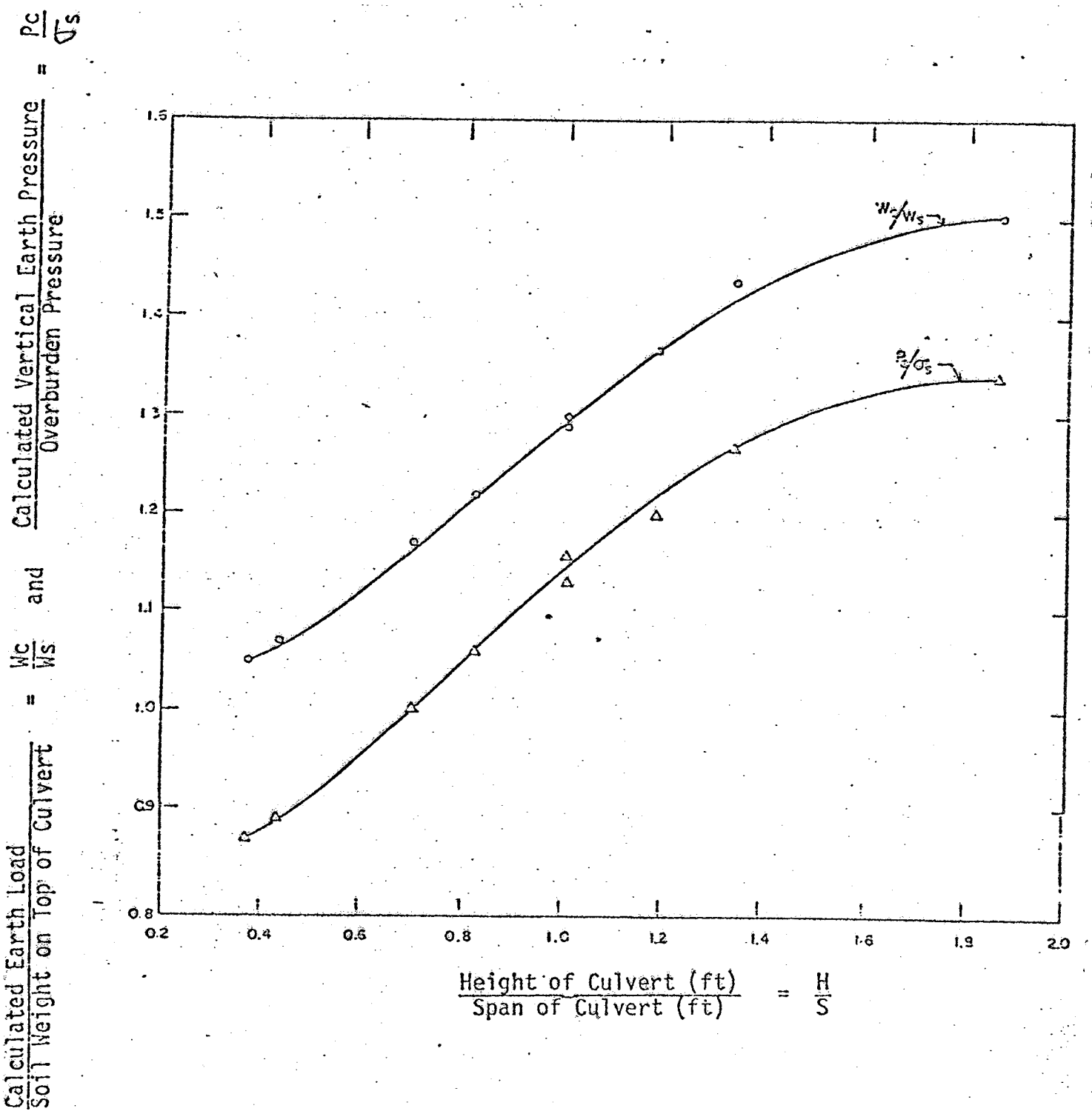

CALCULATED EARTH LOAD AND EARTH PRESSURE RATIOS
VS.
HEIGHT OF CULVERT OVER SPAN RATIO

FIGURE 2.27

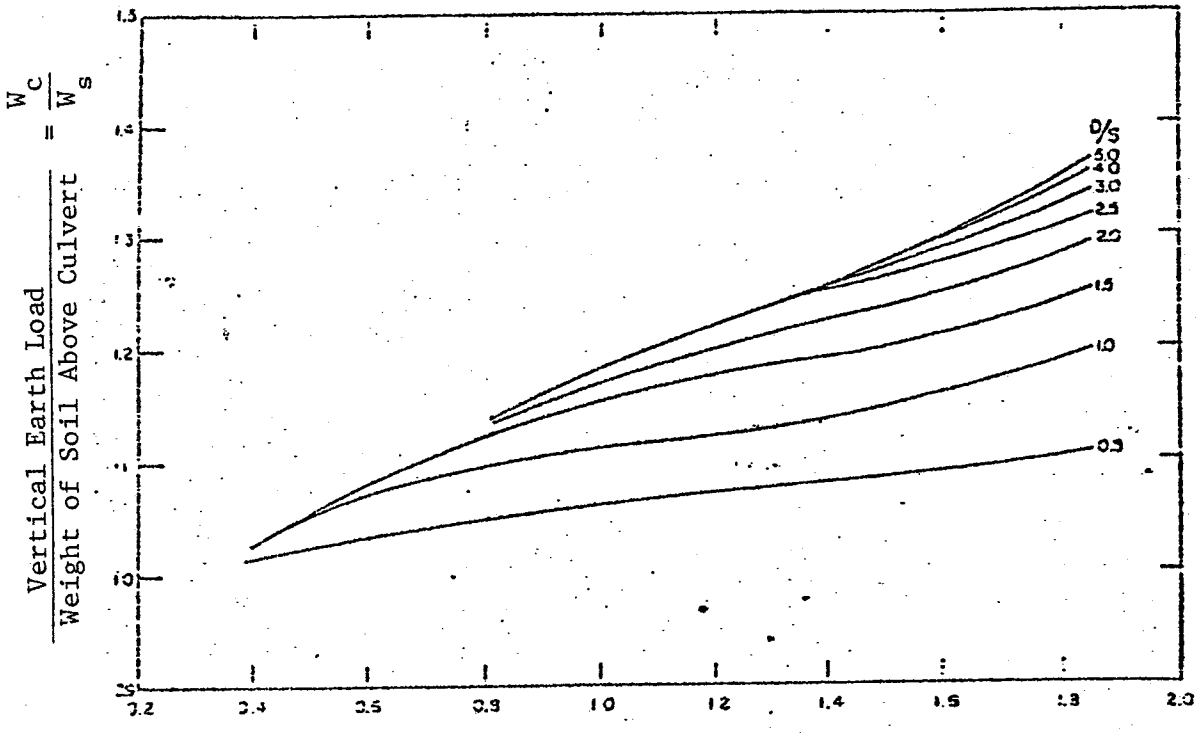

$\frac{\text{Height of Culvert}}{\text{Span of Culvert}} = \frac{H}{S}$

VERTICAL EARTH LOAD VS. $^{H}/_{S}$ RATIO

FIGURE 2.28

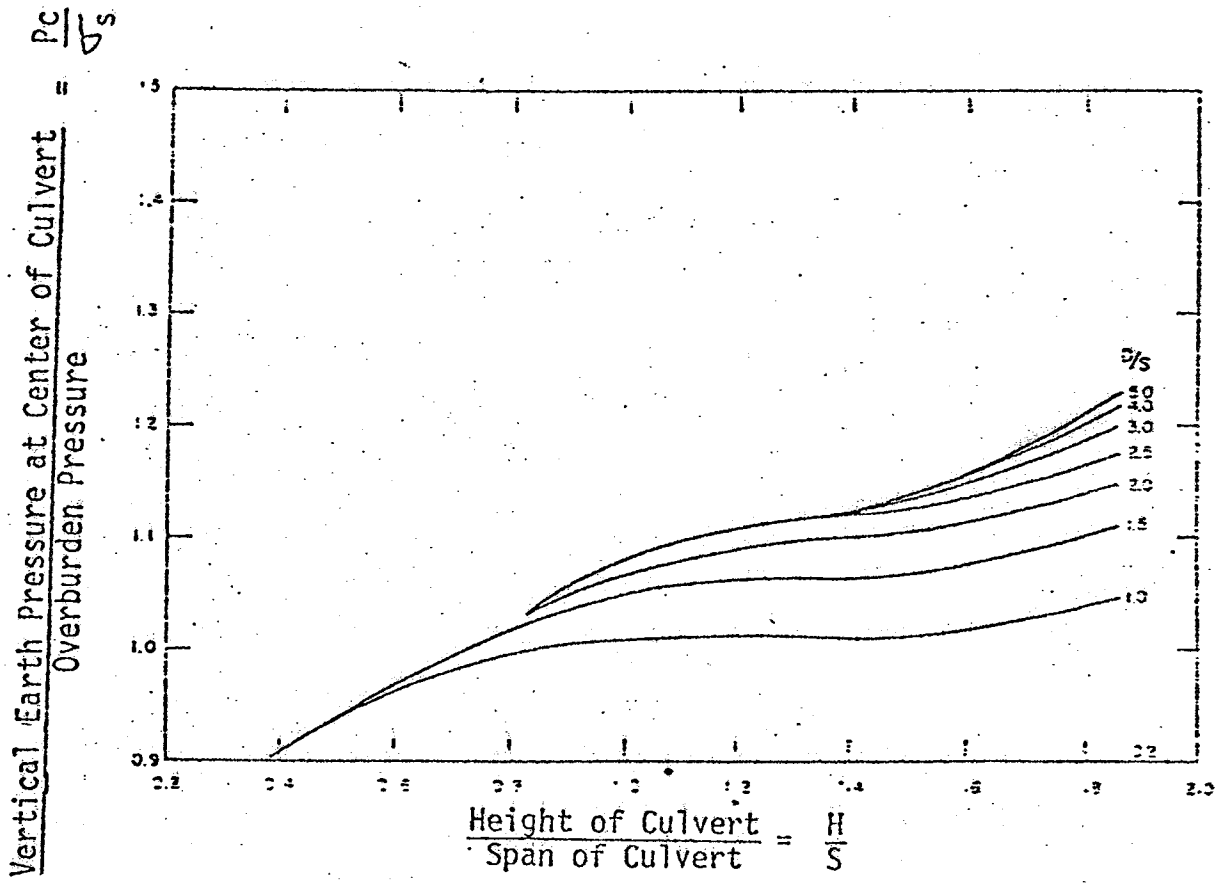

VERTICAL EARTH PRESSURE AT BOX CENTER VS. $^{H}/_{S}$ RATIO

FIGURE 2.29

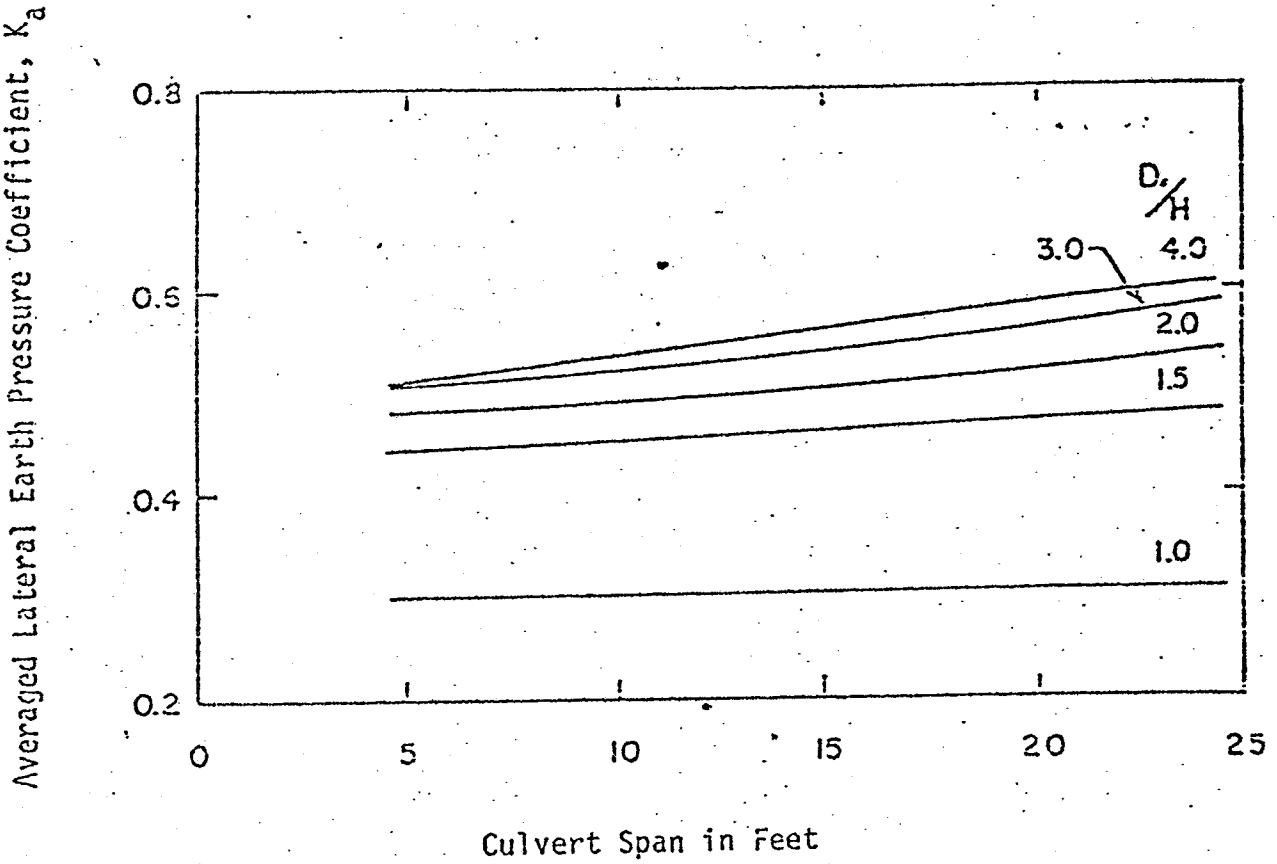

AVERAGE LATERAL EARTH PRESSURE COEFFICIENT,
K_a VS. CULVERT SPAN

FIGURE 2.30

be fully bonded.

Another program dealing with soil-structure interaction analysis is SPIDA [Soil-Pipe Interaction Design Analysis] [5]. This program is presently being evaluated by the American Concrete Pipe Association. The objective of the program is to determine the earth load and pressure distribution for circular pipes.

2.4 Empirical Solutions

Beginning in 1923, the American Railway Engineering Association [AREA] [3] conducted a series of tests at Farina, Illinois to determine culvert loading conditions. Earth pressure cells were placed on culvert sections of varying material types, which were then buried under varying depths of fill. A layout of the test site is given in Fig. 2.31a, and the results of the tests are presented in Fig. 2.31b. For a rigid culvert, the horizontal pressures are approximately 40% of the weight of the overlying soil. However, the vertical pressures are greater than the weight of the soil above the culvert.

Marston [11] also conducted many studies at the Iowa State College on the subject of culvert loading and earth pressures. The earth pressure distribution on a circular pipe under 15 feet of fill, presented by Marston [11], is given in Fig. 2.32. Three material types are given in order to evaluate the pressure differences caused by the degree of flexibility of the conduit. The rigid culvert exhibits the greatest pressures on the top and bottom portions of the conduit. However, the pressures exerted on the sides of the flexible culvert are much greater than those on the rigid culvert. This may be explained by the difference in deflection between the rigid and flexible conduit and the associated degree of arching that takes place.

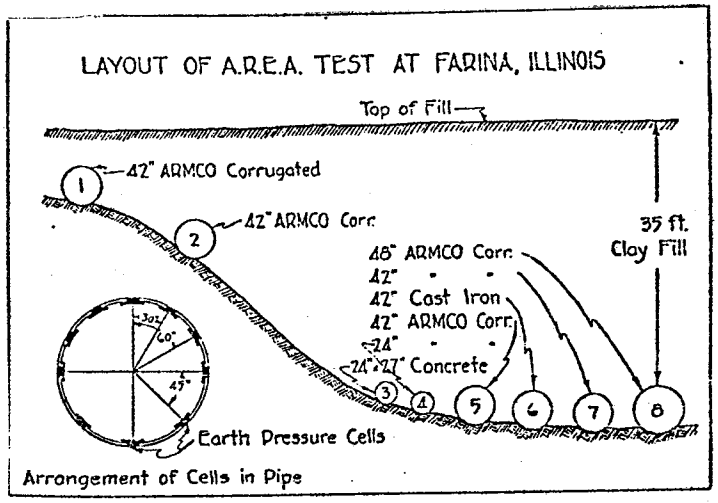

a) Field Conditions of AREA Tests

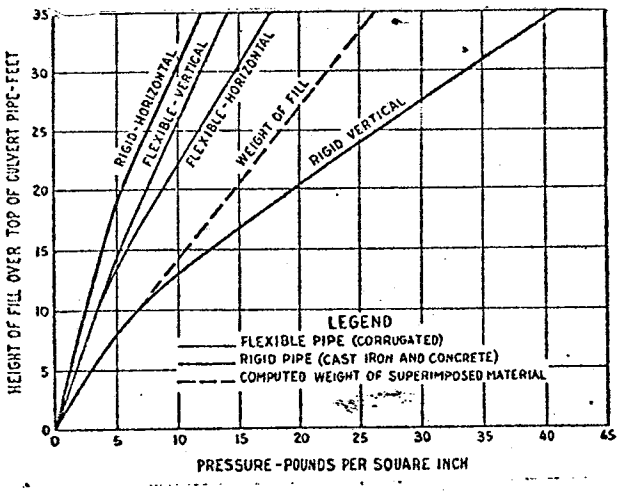

b) AREA Results

AREA TESTS AT FARINA, ILLINOIS
ON CULVERT LOADING

FIGURE 2.31

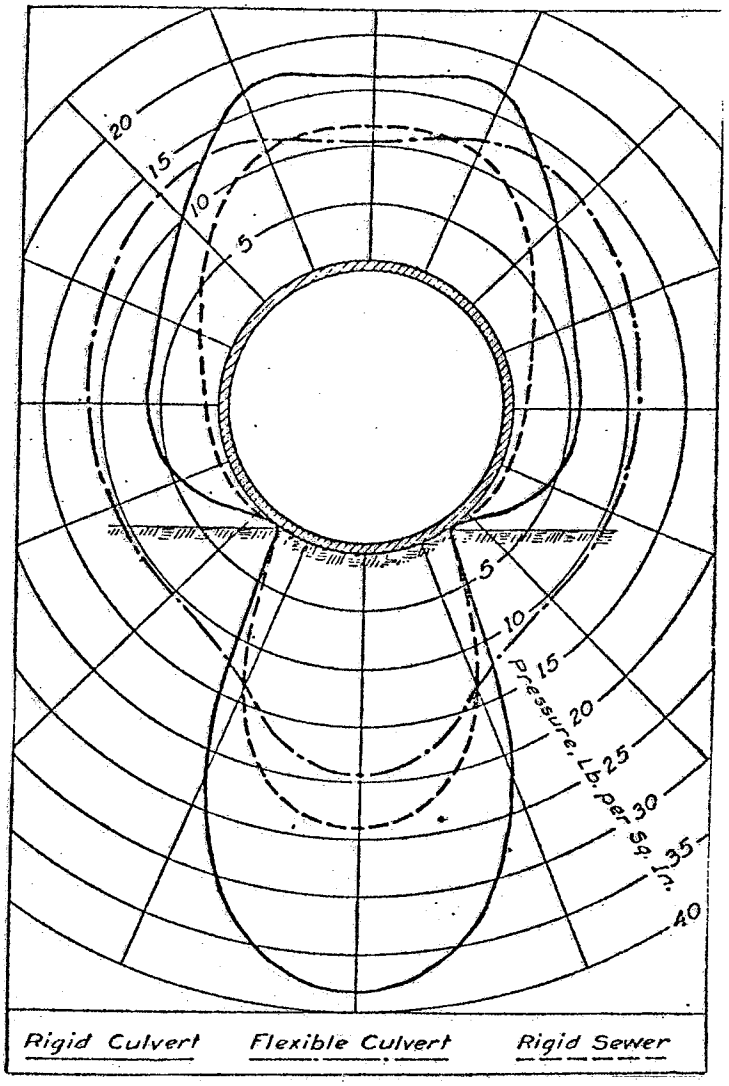

DISTRIBUTION OF RADIAL PRESSURE
ON THREE TYPES OF CONDUITS UNDER A FILL HEIGHT OF 15 FEET

FIGURE 2.32

The United States Corps of Engineers [4] use a design method for rigid conduits and culverts which depends on the construction methods used for installation. Three construction conditions are considered, and these are shown in Fig. 2.33.

Condition I applies to structures which are completely buried in a ditch with no super-imposed fill. The total dead load due to earth fill on the top of the culvert should be computed as the larger of the two values obtained by

$$W_e = C_d \ \gamma b_d^2 \qquad [2.17]$$

where C_d is obtained from Fig. 2.34,

or $$W_e = \gamma b_c H \qquad [2.18]$$

The lateral earth pressures are assumed to vary with the height of fill [H] as well as the effective width of the conduit [b_d]. When H is greater than or equal to $2b_d$, the horizontal pressure is computed at the center of the conduit using an average value for H. For a height of fill less than twice the section width, the horizontal pressure is taken as

$$P_e = \gamma H \tan^2 [45^o - \phi/2] \qquad [2.19]$$

Condition II applies to conduits and culverts completely buried in a ditch with a height of fill H above the top of the ditch. The total vertical load is taken as the larger of the two values obtained from

$$W_e = C_d \gamma b_d^2 + \frac{H_f}{H_c + H_p} [1.5 \gamma b_c H_n - \gamma C_d b_d^2] \qquad [2.20]$$

or

$$W_e = b_c H + \frac{H_f}{H_c + H_p} [1.5 \gamma b_c H - \gamma b_c H] \qquad [2.21]$$

The values of b_c, H , H_f, H_c, and b_d may be obtained as shown in Fig. 2.33.

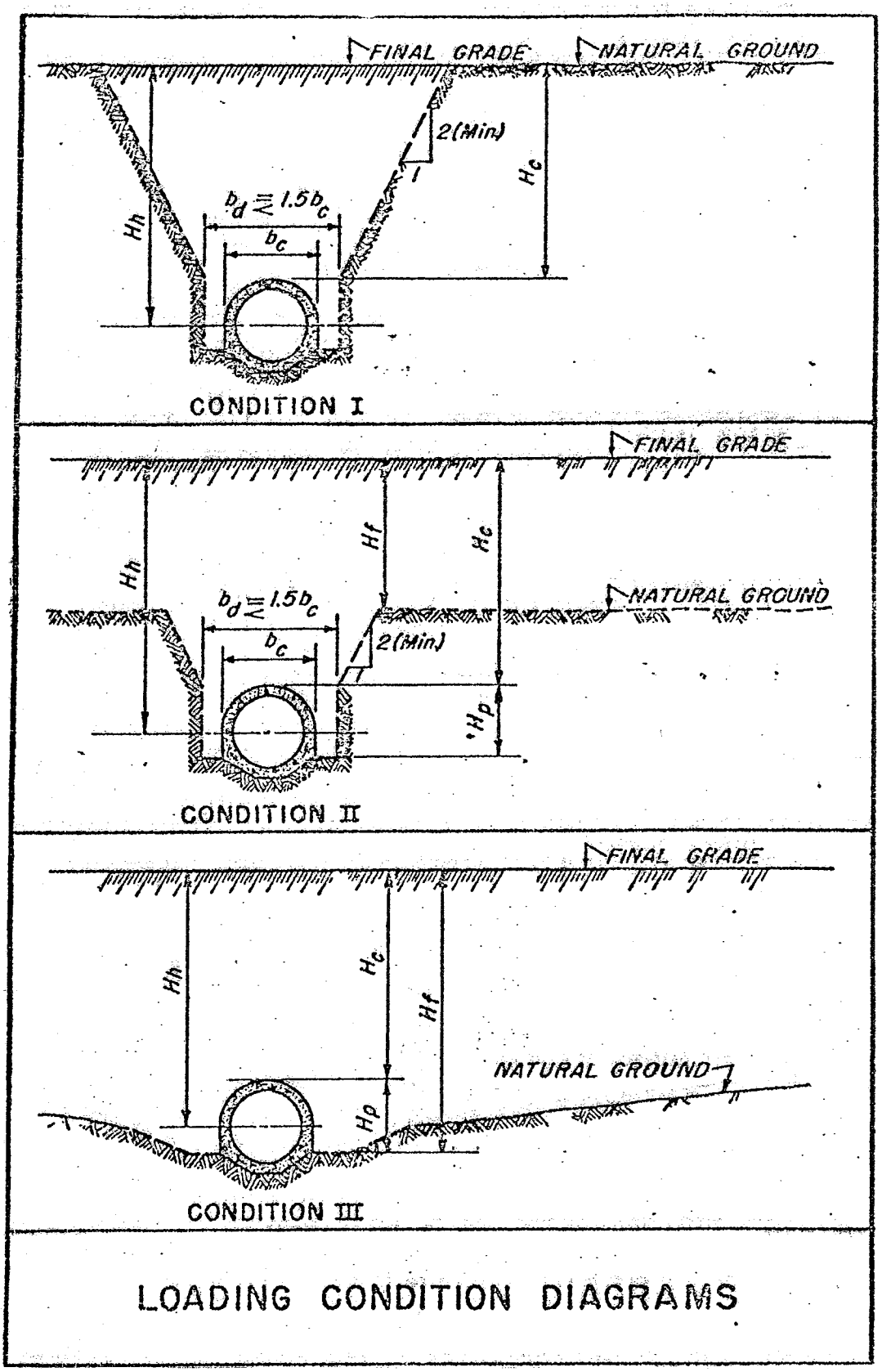

LOADING CONDITION DIAGRAMS

FIGURE 2.33

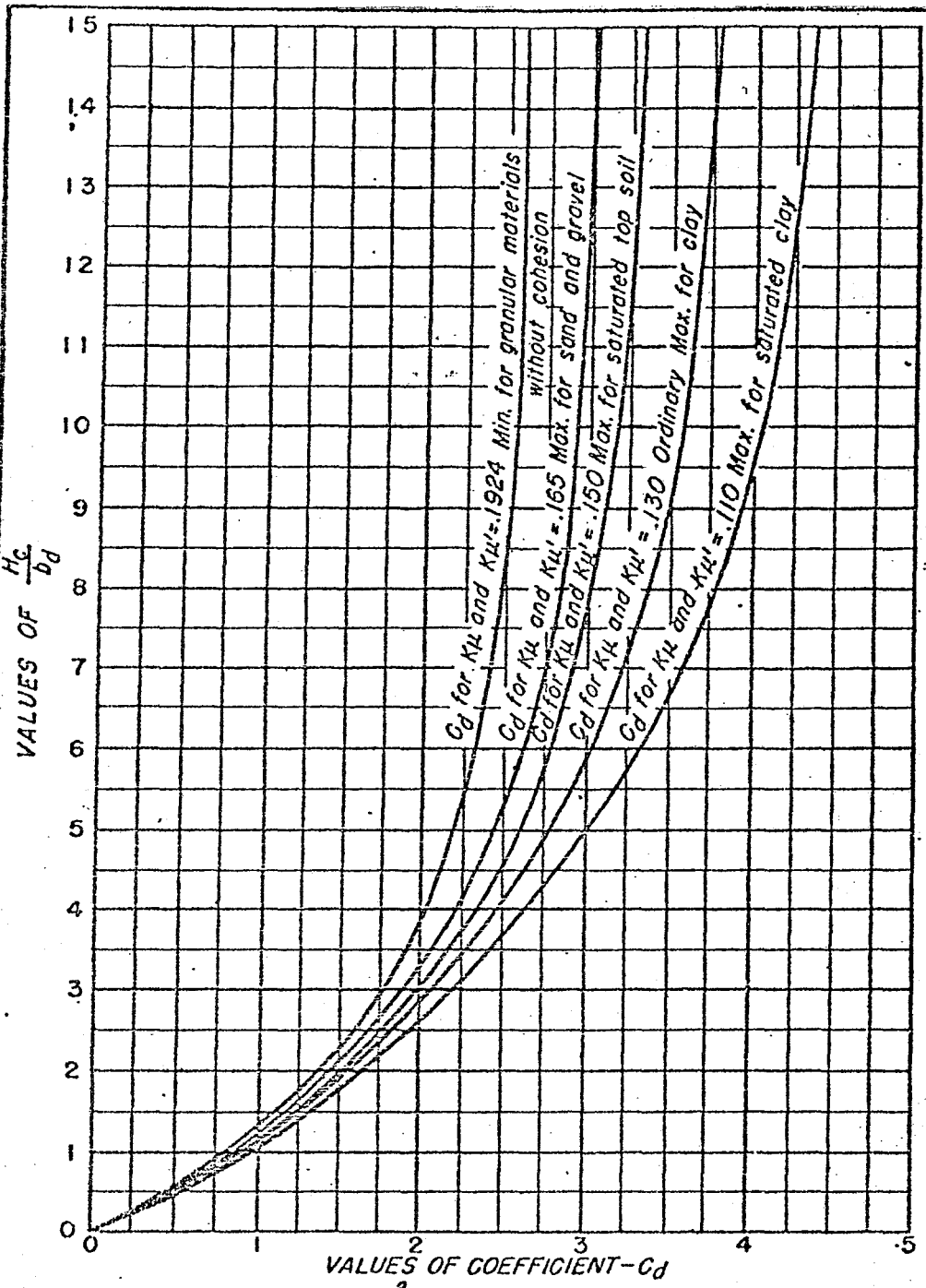

Load per unit of length, $W_c = C_d \gamma b_d^2$ (ft. lb. units)

γ = unit weight of fill materials.

b_d = breadth of ditch at top of structure

H_c = height of fill over top of structure

$$K = \frac{\sqrt{\mu^2+1}-\mu}{\sqrt{\mu^2+1}+\mu}$$

μ = the "coefficient of internal friction" in the fill materials, abstract number.

μ' = the "coefficient of sliding friction" between the fill materials and the sides of the ditch, abstract number.

DEAD LOAD COMPUTATION ANALYSIS
DITCH CONDITION – CONDUITS, CULVERTS AND PIPES

FIGURE 2.34

The lateral earth pressures for a culvert in condition II are computed by

$$P_e = H \tan^2 (45 - \phi/2) + \frac{H_f}{(H_c + H_p)} [0.5 H - \gamma H \tan^2(45-\phi/2)] \quad [2.22]$$

Condition III applies to culverts projecting above the embankment subgrade, or trench conditions not meeting the requirements of conditions I or II. Two extreme cases are developed. Case I is considered when the ratio of horizontal pressures to unit vertical load, W_e, is equal to 0.33, which indicates that the vertical loading is three times greater than the lateral loading. For this case,

$$W_e = 1.5 \gamma b_c H \quad [2.23]$$

and the horizontal pressures are given by

$$p_e = 0.5 \gamma H \quad [2.24]$$

The other extreme case of Condition III is considered when the ratio of horizontal loading to vertical loading is 1.0, which indicates the horizontal pressures equal the vertical pressures. For this case,

$$W_e = \gamma b_c H \quad [2.25]$$

and

$$p_e = \gamma H \quad [2.26]$$

The amount of surface load transmitted to an underground structure may be computed by the method shown in Fig. 2.35. This pressure is uniformly distributed over the top of the culvert.

The American Association of State Highway and Transportation Officials [AASHTO] [1] specifications also deal with design loadings on box culverts for bridge installations. The vertical and horizontal pressures due to soil fill may be estimated by using an equivalent fluid pressure. For reinforced concrete box culverts, the suggested equivalent weight for

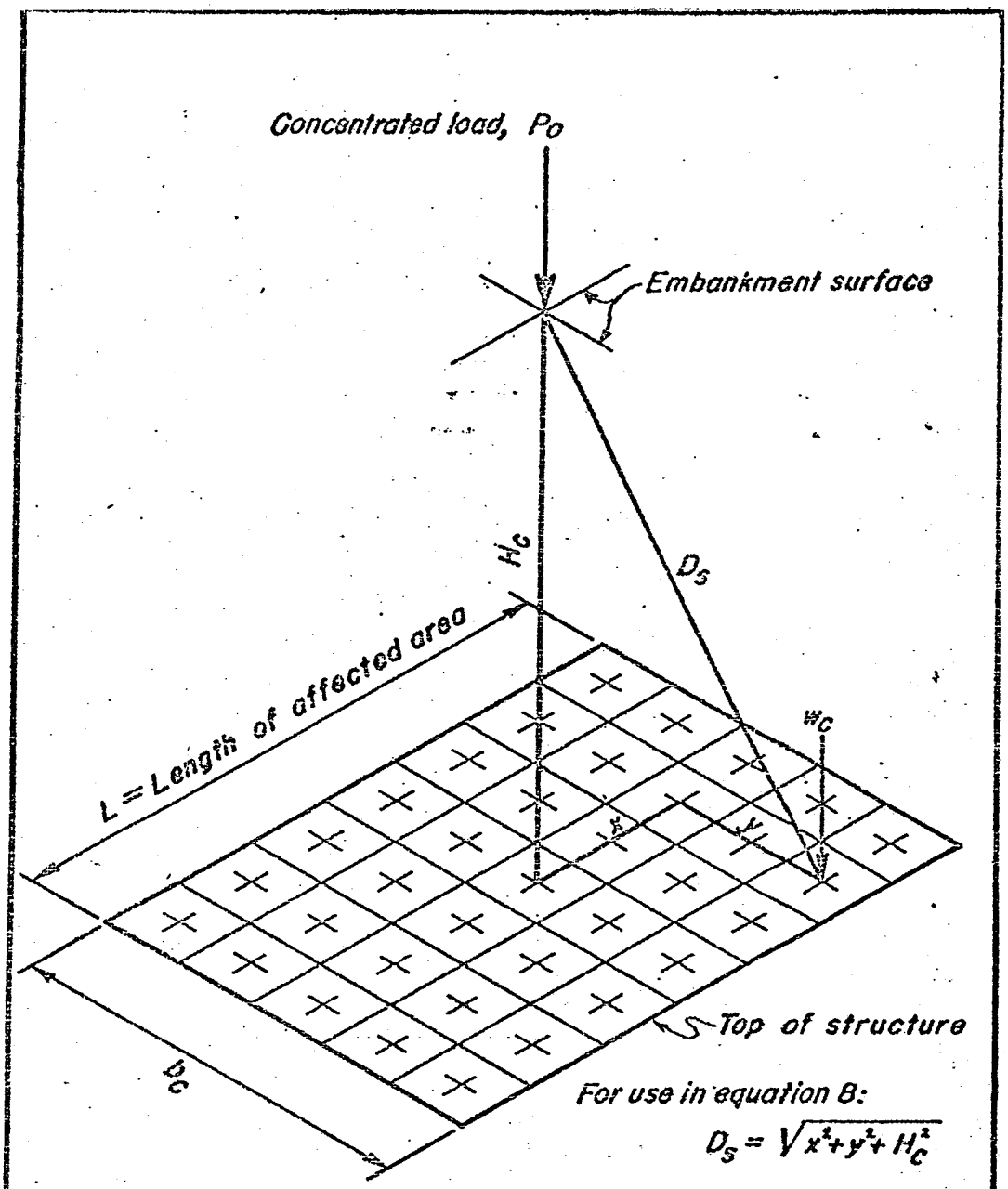

COMPUTATION OF SURFACE LOAD TRANSMITTED TO UNDERGROUND STRUCTURES

FIGURE 2.35

vertical pressure is 120 pcf, while 25% of this is used to compute lateral earth pressures.

The American Society of Testing and Materials [ASTM] [2] specifications also present the design loads for box culverts. These are very similar to the AASHTO specifications. For the vertical earth pressures, ASTM recommends that the pressure be taken as the weight of a column of earth of a width equal to the outside width dimension of the box section and of a height equal to the depth of cover over the top of the section. Lateral earth pressures are taken as a minimum of 0.25 times the vertical pressure. Design tables are given in the ASTM specifications, in which an assumed unit weight of 120 pcf is used for computations. This is equal to the equivalent weight suggested by the AASHTO specifications.

CHAPTER 3

MATERIAL PROPERTIES

3.1 Soil Properties

In order to perform finite element analyses of the field behavior of the 8' x 8' RC box culvert, the properties of the foundation soils and the backfill soils should be represented correctly. As part of this study a number of laboratory tests were conducted on representative soil samples from the site and the results are discussed in this chapter.

3.1.1 Laboratory Tests

Good quality samples of the backfill soils and the foundation soils were obtained from this site and sieve analyses were conducted. The grain size curves for the backfill and foundation materials are shown in Figs. 3.1 and 3.2. From these figures it is clear that the two soils are very similar and therefore further soil tests were performed on backfill soils only. Standard AASHTO compaction tests were performed in the laboratory and the compaction curve for the soil at site is given in Fig. 3.3. The maximum dry density of this backfill is 116 pcf and the optimum water content of 8.5%. Triaxial samples were prepared in the laboratory at the following compaction conditions:

a] Soil 1 95% Standard Maximum Dry Density,
Dry of Optimum

b] Soil 2 100% Standard Maximum Dry Density,
Optimum Water Content

c] Soil 3 95% Standard Maximum Dry Density,
Wet of Optimum

Triaxial stress-strain tests were performed at three confining pressures,

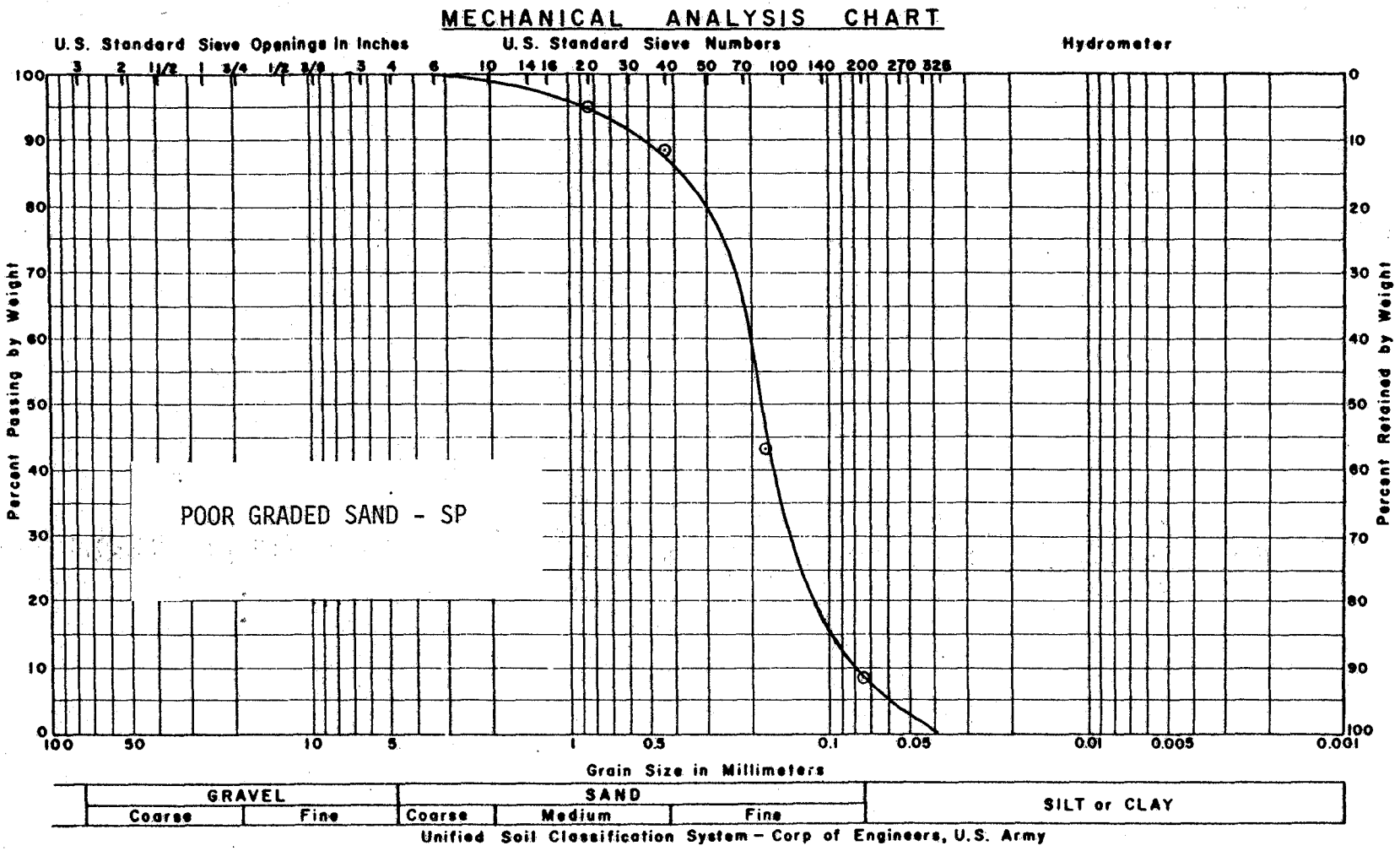

FIGURE 3.1

SOIL CLASSIFICATION - BACKFILL SAMPLES

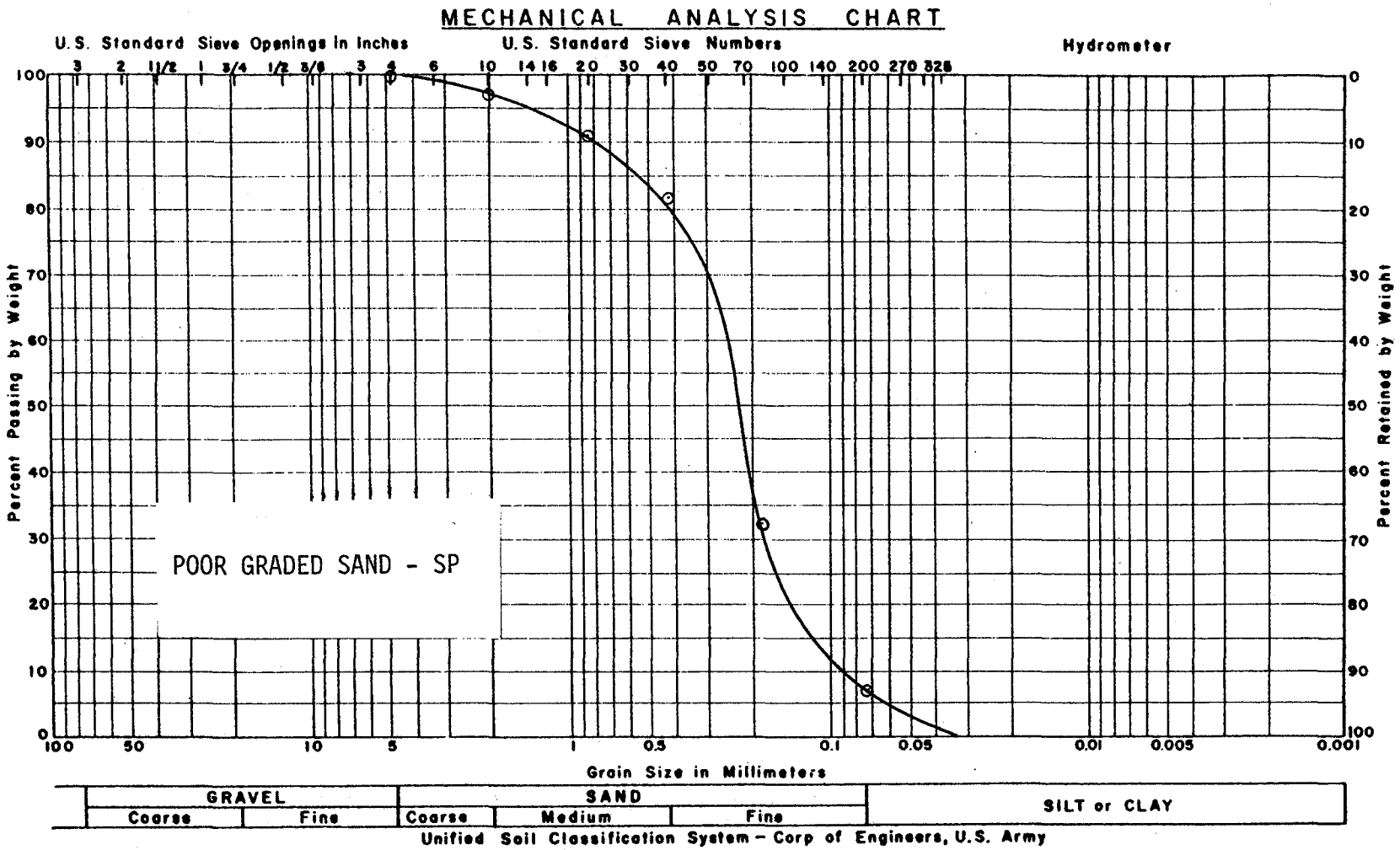

FIGURE 3.2

SOIL CLASSIFICATION - FOUNDATION SAMPLES

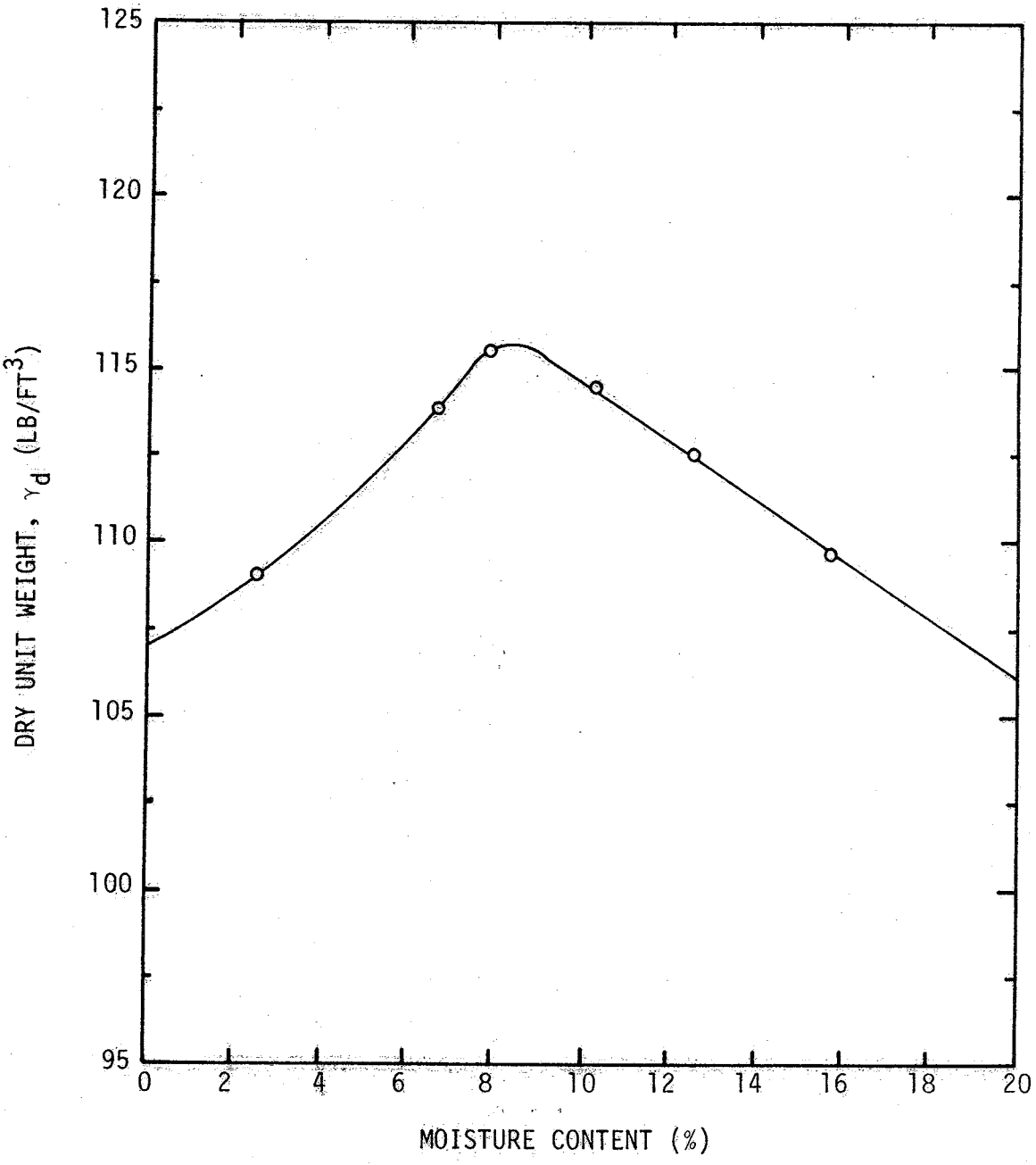

VARIATION OF DRY UNIT WEIGHT WITH MOISTURE CONTENT

FIGURE 3.3

5, 10, and 20 psi, and the results are shown in Figs. 3.4-3.6. Using the stresses at the failure condition, the q-p plots [modified Mohr-Coloumb plots] were prepared and these are shown in Figs. 3.7-3.9.

3.1.2 Hyperbolic Stress-Strain Model Parameters Used in the Analyses

The hyperbolic stress-strain relationships were developed by Duncan et.al. [1970, 1978] for use in nonlinear incremental analyses of soil deformations. In each increment of such analyses the stress-strain behavior of the soil is treated as being linear and the relationship between stress and strain is assumed to be governed by the generalized Hooke's Law of elastic deformations, which may be expressed as follows for conditions of plane strain:

$$\begin{Bmatrix} \Delta\sigma_x \\ \Delta\sigma_y \\ \Delta\tau_{xy} \end{Bmatrix} = \begin{bmatrix} [M_b + M_d] & [M_b - M_d] & 0 \\ [M_b - M_d] & [M_b + M_d] & 0 \\ 0 & 0 & M_d \end{bmatrix} \begin{Bmatrix} \varepsilon_x \\ \varepsilon_y \\ \gamma_{xy} \end{Bmatrix}$$

in which $\Delta\sigma_x$, $\Delta\sigma_y$ = normal stress

$\Delta\tau_{xy}$ = shear stress

ε_x, ε_y = normal strains

γ_{xy} = shear strain

M_d = G = shear modulus

M_b = plain strain bulk modulus

The parameters M_d and M_b are related to Young's modulus and bulk modulus by the following equations:

$$M_d = \frac{E}{2[1 + \nu]}$$

$$M_b = \frac{3B}{2[1 + \nu]}$$

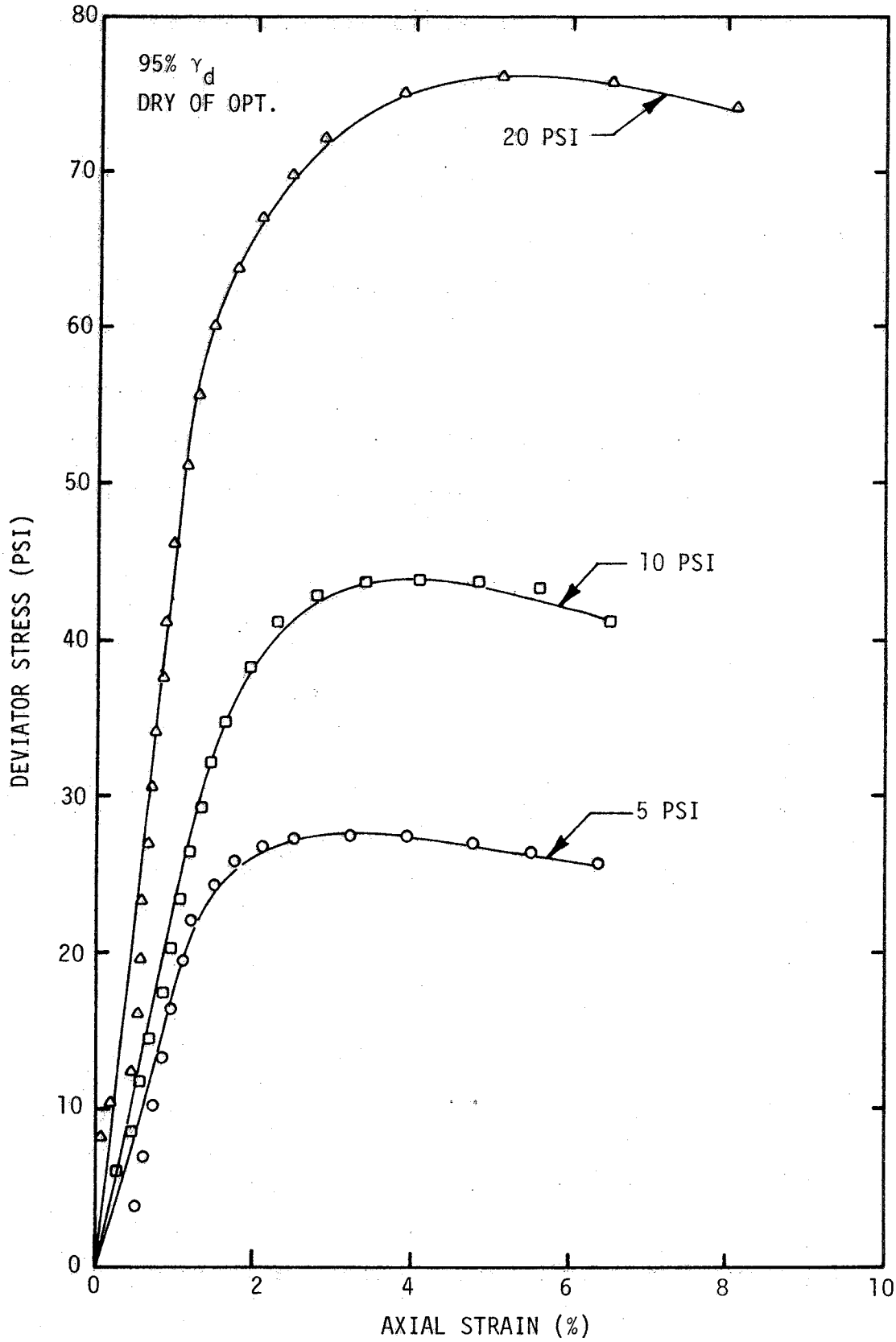

VARIATION OF DEVIATOR STRESS WITH AXIAL STRAIN SOIL 1 RESULTS

FIGURE 3.4

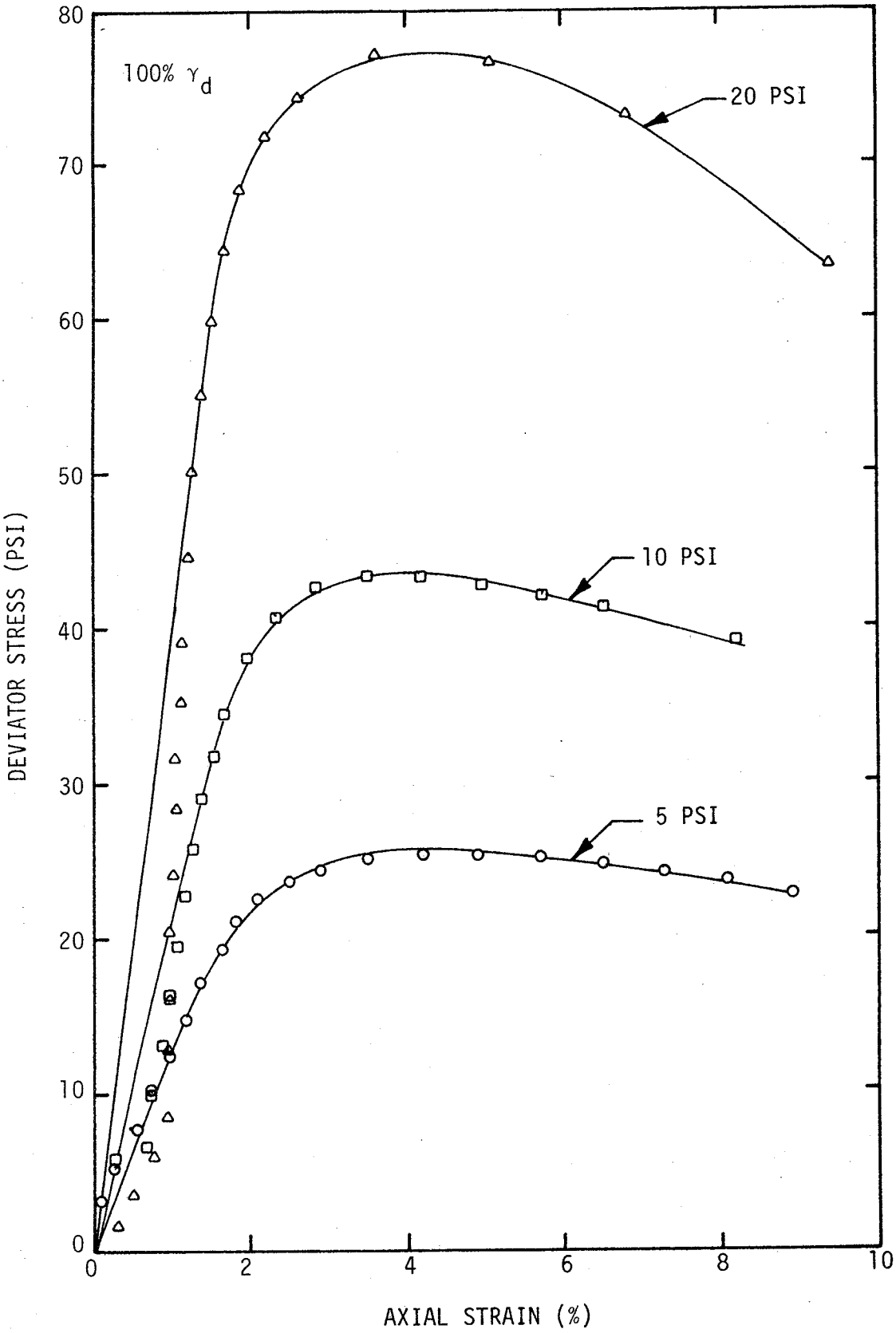

VARIATION OF DEVIATOR STRESS WITH AXIAL STRAIN SOIL 2 RESULTS

FIGURE 3.5

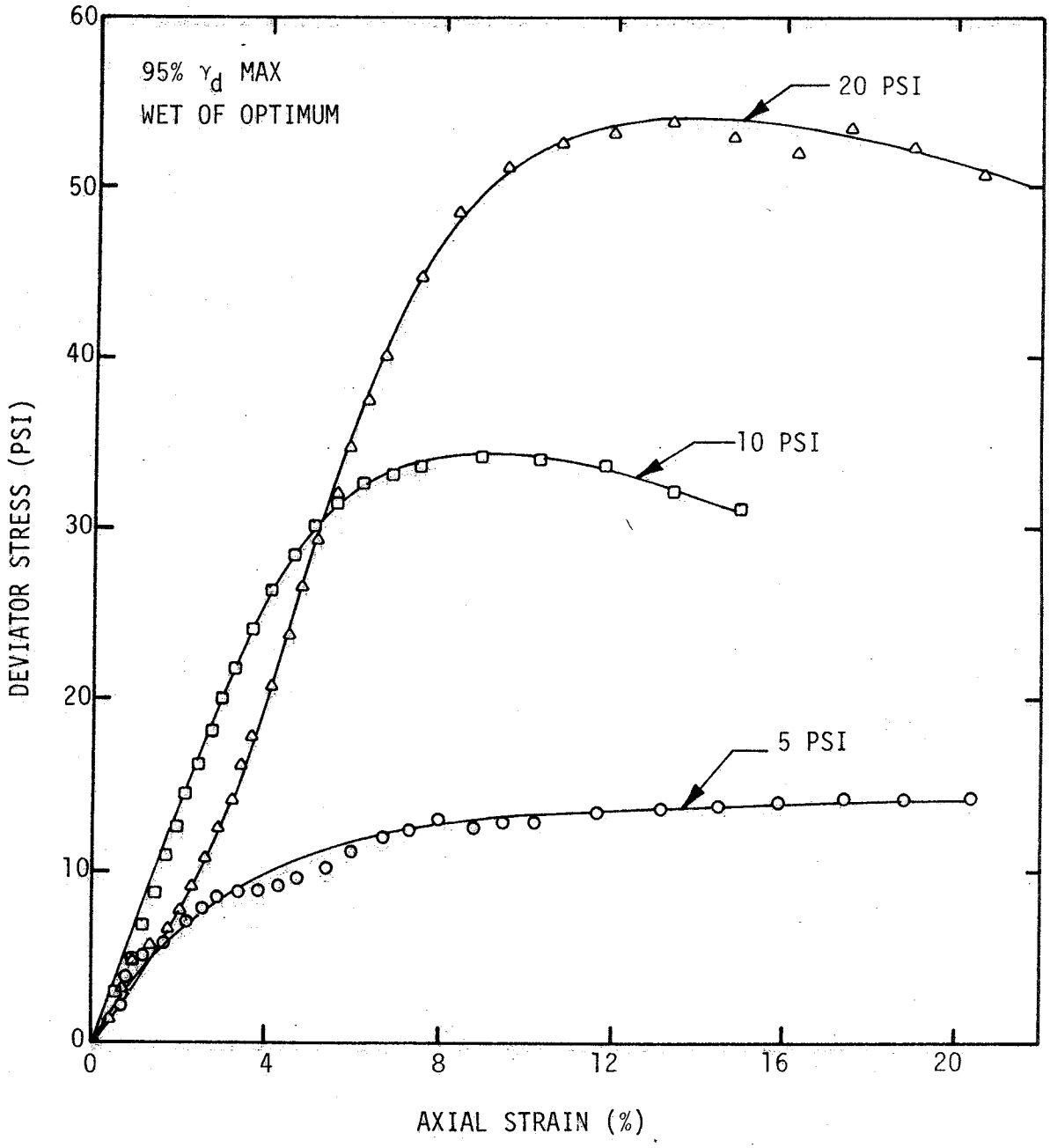

VARIATION OF DEVIATOR STRESS WITH AXIAL STRAIN SOIL 3 RESULTS

FIGURE 3.6

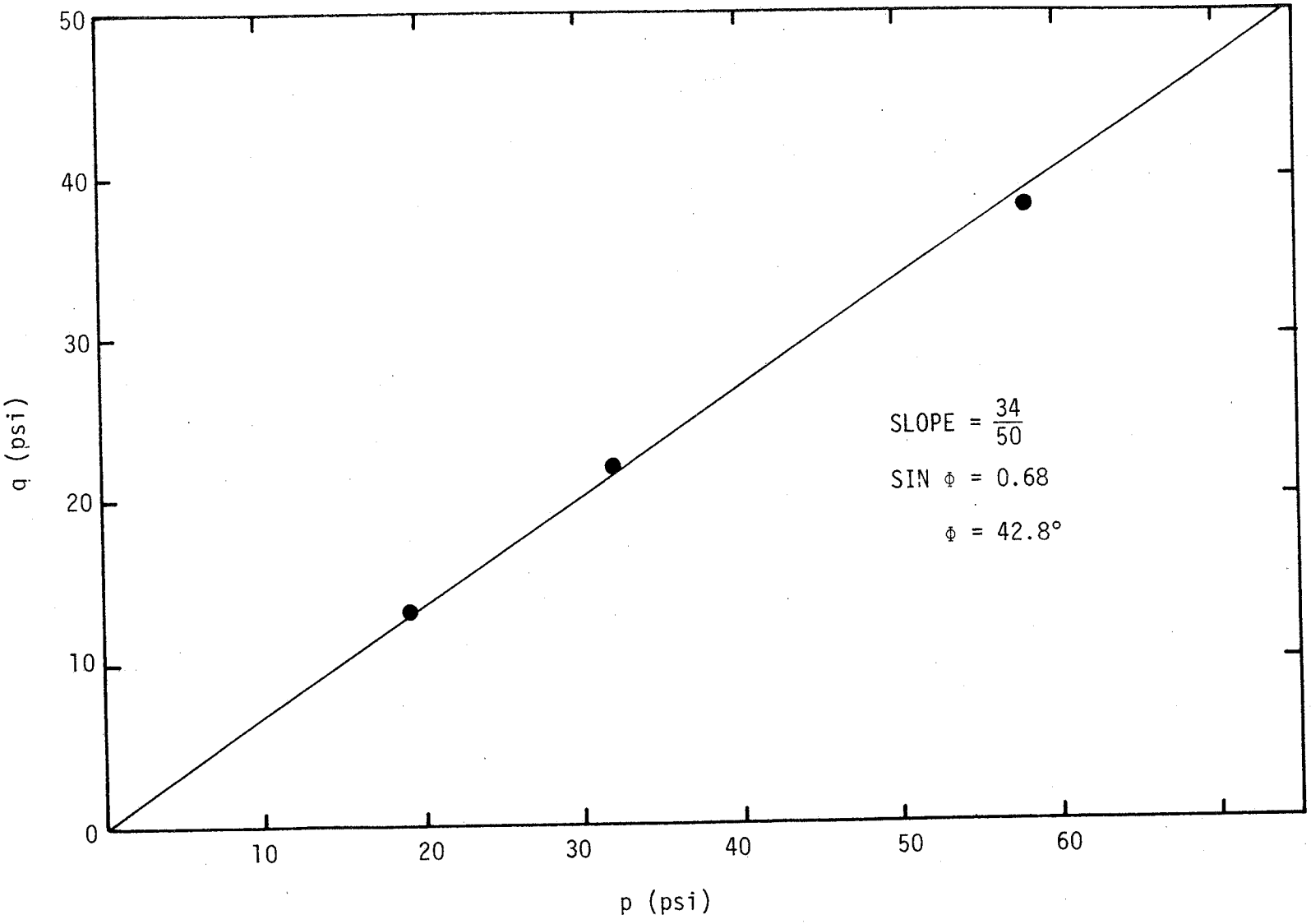

FIGURE 3.7

q-p DIAGRAM FOR DETERMINATION OF FRICTION ANGLE SOIL 1 RESULTS

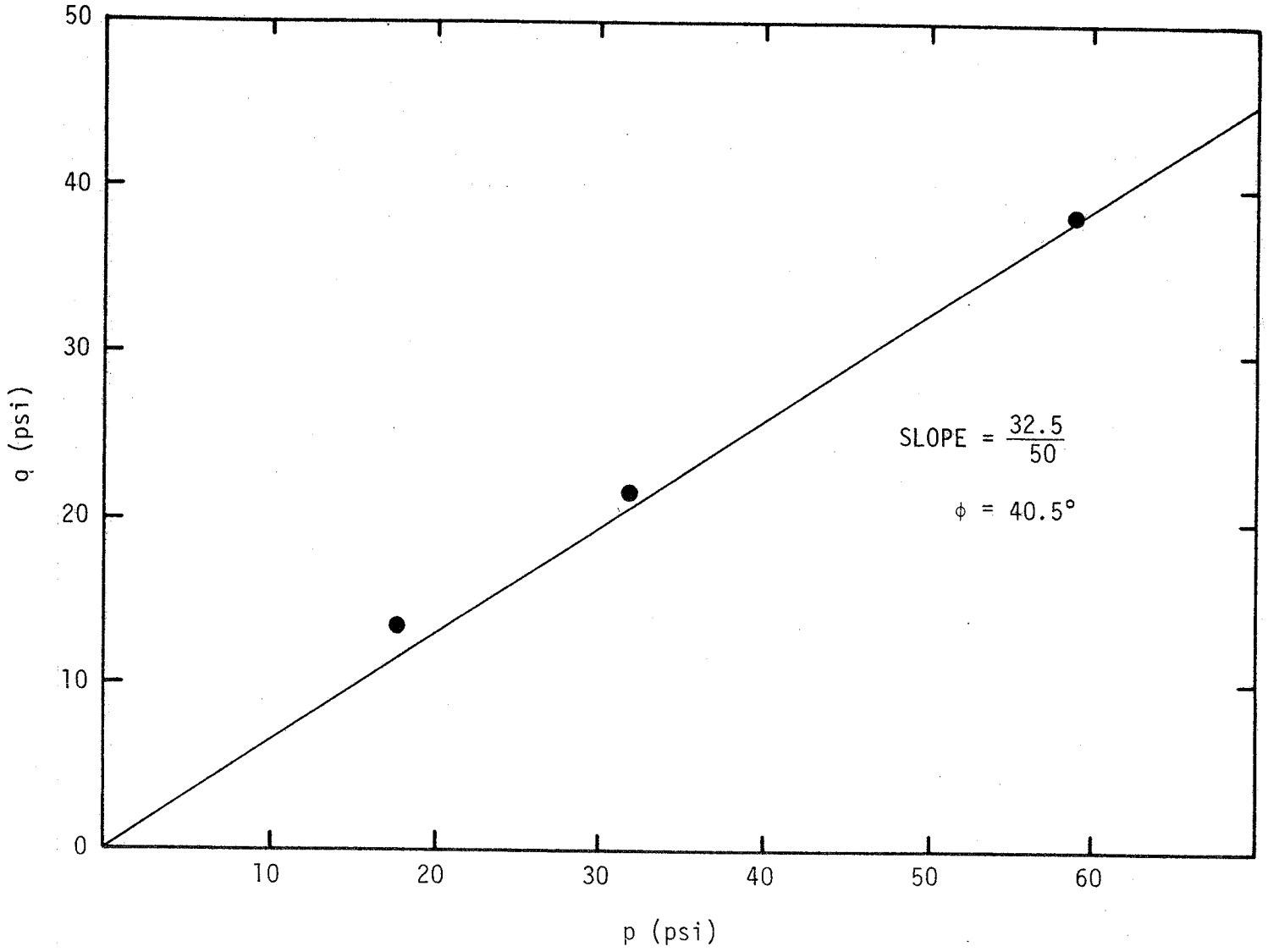

FIGURE 3.8

q-p DIAGRAM FOR DETERMINATION OF FRICTION ANGLE SOIL 2 RESULTS

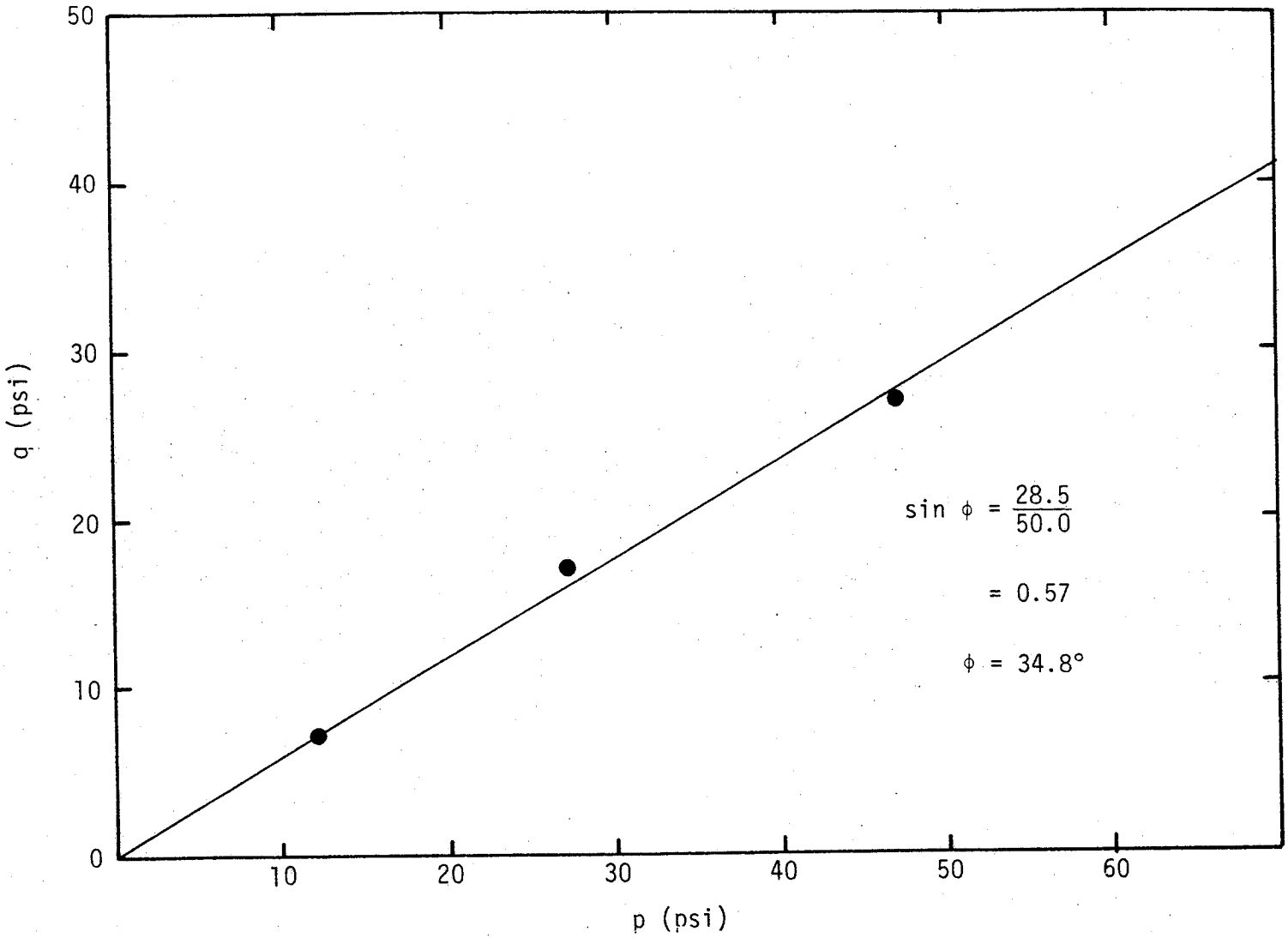

q-p DIAGRAM FOR DETERMINATION OF FRICTION ANGLE SOIL 3 RESULTS

FIGURE 3.9

and $$\nu = \frac{3B-E}{6B} \qquad [4]$$

Using these equations, the relationships between strain increments and the corresponding stress increments may be expressed in terms of the parameters E [Young's modulus] and B [Bulk modulus]. These relationships thus account for three important characteristics of the stress-strain behavior of soils, namely nonlinearity, stress-dependency, and inelasticity. The procedures used to account for these characteristics are discussed in the following paragraphs.

Nonlinear Stress-Strain Curves Represented by Hyperbolas. Duncan et.al.[1970, 1978] have shown that the stress-strain curves for a number of soils could be approximated reasonably accurately by hyperbolas like the one shown in Fig. 3.10. This hyperbola can be represented by an equation of the form:

$$[\sigma_1-\sigma_3] = \frac{\varepsilon}{\frac{1}{E_i} + \frac{\varepsilon}{(\sigma_1-\sigma_3)ult}} \qquad [5]$$

While other types of curves could also be used, these hyperbolas have two characteristics which make their use convenient:

[1] The parameters which appear in the hyperbolic equation have physical significance. E_i is the initial tangent modulus or initial slope of the stress-strain curve and $[\sigma_1-\sigma_3]_{ult}$ is the asymptotic value of stress difference which is related closely to the strength of the soil. The value of $[\sigma_1-\sigma_3]_{ult}$ is always greater than the compressive strength of the soils, as discussed subsequently.

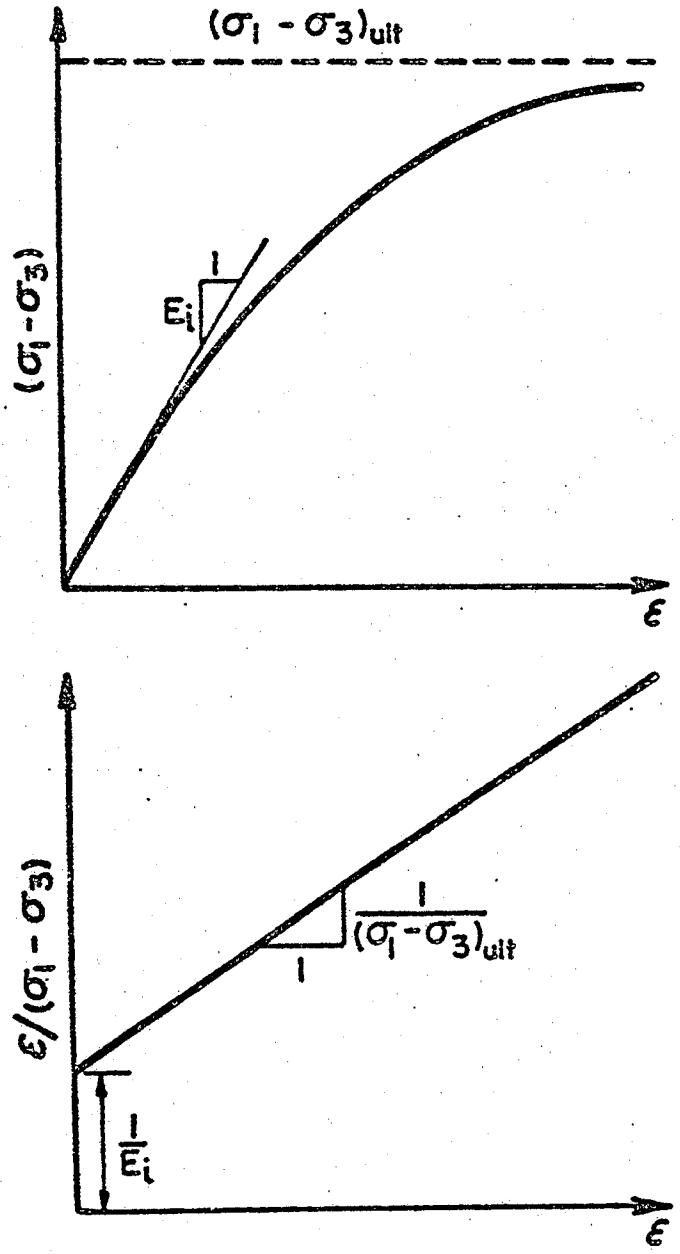

REAL

$$(\sigma_1 - \sigma_3) = \frac{\varepsilon}{\frac{1}{E_i} + \frac{\varepsilon}{(\sigma_1 - \sigma_3)_{ult}}}$$

TRANSFORMED

$$\frac{\varepsilon}{(\sigma_1 - \sigma_3)} = \frac{1}{E_i} + \frac{\varepsilon}{(\sigma_1 - \sigma_3)_{ult}}$$

FIGURE 3.10

HYPERBOLIC REPRESENTATION OF A STRESS-STRAIN CURVE

[2] The values of E_i and $[\sigma_1-\sigma_3]_{ult}$ for a given stress-strain curve can be determined easily. If the hyperbolic equation is transformed as shown in the lower part of Fig. 3.10, it represents a linear relationship between $\varepsilon/[\sigma_1-\sigma_3]$ and ε. Thus, to determine the best-fit hyperbola for the stress-strain curve, values of $\varepsilon/[\sigma_1-\sigma_3]$ are calculated from the test data and are plotted against ε. The best-fit straight line on this transformed plot corresponds to the best-fit hyperbola on the stress-strain plot.

Stress Dependent Stress-Strain Behavior Represented by Varying E_i and $[\sigma_1-\sigma_3]_{ult}$ with Confining Pressure. For all soils except fully saturated soils tested under unconsolidated-undrained conditions, an increase in confining pressure will result in a steeper stress-strain curve and a higher strength, and the values of E_i and $[\sigma_1-\sigma_3]_{ult}$ therefore increases with increasing confining pressure. This stress-dependency is taken into account by using empirical equations to represent the variation of E_i and $[\sigma_1-\sigma_3]_{ult}$ with confining pressure.

The variation of E_i with σ_3 is represented by an equation of the following form,

$$E_i = Kp_a\left(\frac{\sigma_3}{p_a}\right)^n \qquad [6]$$

The variation of E_i with σ_3 corresponding to this equation is shown in Fig. 3.11. The parameter K in equation [6] is the modulus number, and n is the modulus exponent. Both are dimensionless numbers. P_a is atmospheric pressure, introduced into the equation to make conversion from one system of units to another more convenient. The values of K and n are

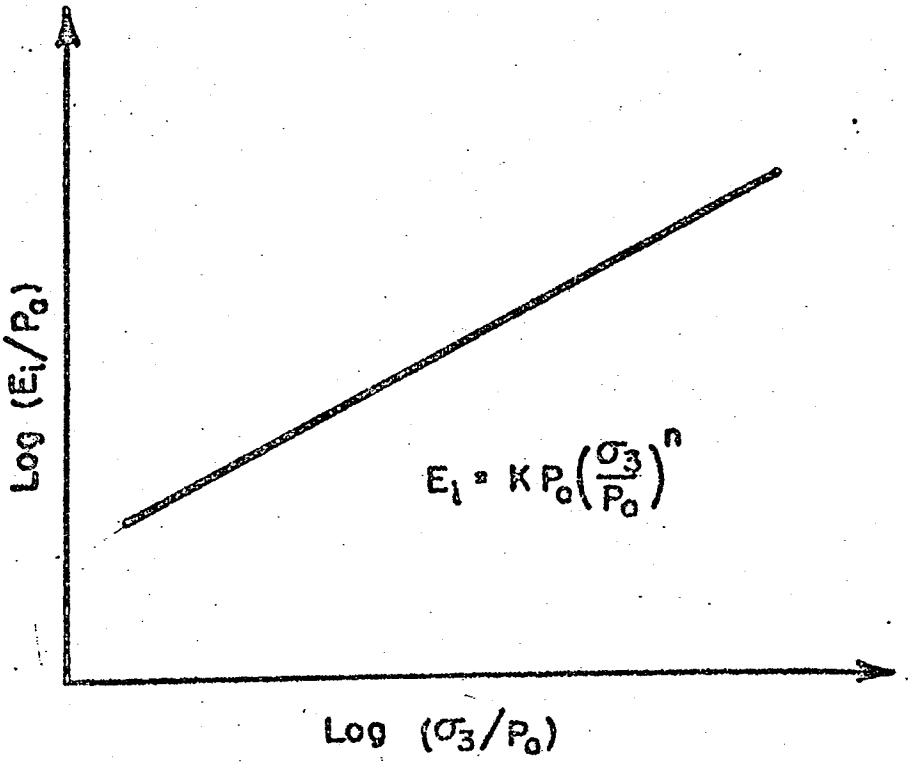

VARIATION OF INITIAL TANGENT MODULUS
WITH CONFINING PRESSURE

FIGURE 3.11

the same for any system of units, and the units of E_i are the same as the units of P_a. To change from one system of units to another it is only necessary to introduce the appropriate value of p_a in equation [6].

The variation of $[\sigma_1-\sigma_3]_{ult}$ with σ_3 is accounted for as shown in Fig. 3.12 by relating $[\sigma_1-\sigma_3]_{ult}$ to the compressive strength or stress difference at failure, $[\sigma_1-\sigma_3]_f$, and then using the Mohr-Coulomb strength equation to relate $[\sigma_1-\sigma_3]_f$ to σ_3. The values of $[\sigma_1-\sigma_3]_{ult}$ and $[\sigma_1-\sigma_3]_f$ are related by:

$$[\sigma_1-\sigma_3]_f = R_f[\sigma_1-\sigma_3]_{ult} \qquad [7]$$

in which R is the failure ratio. Because $[\sigma_1-\sigma_3]_f$ is always smaller than $[\sigma_1-\sigma_3]_{ult}$, the value of R_f is always smaller than unity, and varies from 0.5 to 0.9 for most soils.

The variation of $[\sigma_1-\sigma_3]_f$ with σ_3 is represented by the familar Mohr-Couloub strength relationship, which can be expressed as follows:

$$[\sigma_1-\sigma_3]_f = \frac{2c\cos\phi + 2\sigma_3\sin\phi}{1 - \sin\phi} \qquad [8]$$

in which c and ϕ are the cohesion intercept and the friction angle, as shown in Fig. 3.12

Summary of Hyperbolic Parameters. In all, nine parameters are employed in the hyperbolic stress-strain relationships for soils used in the the analyses. These parameters and their functions within the relationships, are listed in Table 3.1.

The hyperbolic relationships outlined previously have proven quite useful for a wide variety of practical problems for the following reasons:

[1] The parameter values can be determined from the results of conventional triaxial compression tests.

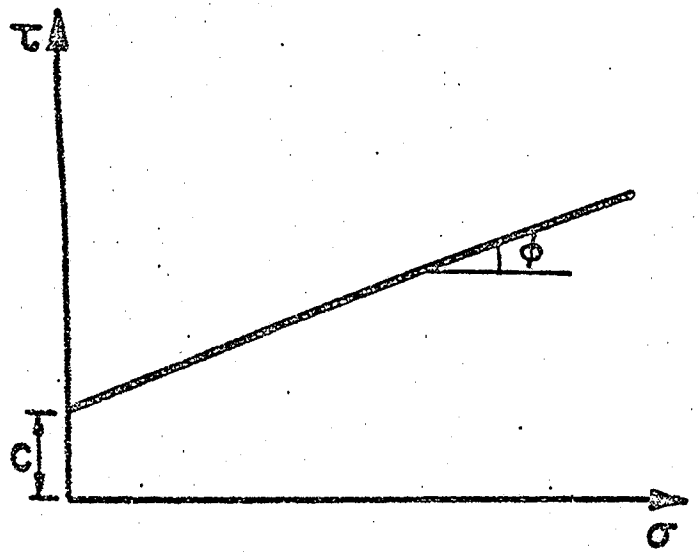

$$(\sigma_1 - \sigma_3)_f = \frac{2C \cos\phi + 2\sigma_3 \sin\phi}{1 - \sin\phi}$$

$$(\sigma_1 - \sigma_3)_f = R_f (\sigma_1 - \sigma_3)_{ult}$$

VARIATION OF STRENGTH WITH CONFINING PRESSURE

FIGURE 3.12

TABLE 3.1 SUMMARY OF THE HYPERBOLIC PARAMETERS

Parameter	NAME	FUNCTION
K, K_{ur}	Modulus number	Relate E_i and E_{ur} to σ_3
n	Modulus exponent	
c	Cohesion intercept	Relate $[\sigma_1-\sigma_3]$ to σ_3
ϕ,$\Delta\phi$	Friction angle parameters	
R_f	Failure ratio	Relates $[\sigma_1-\sigma_3]_{ult}$ to $[\sigma_1-\sigma_3]$
K_b	Bulk modulus number	Value of B/P_a at $\sigma_3 = P_a$
m	Bulk modulus exponent	Change in B/P_a for ten-fold increase in σ_3

[2] The same relationships can be used for effective stress analyses [using data from drained tests] and total stress analyses [using data from unconsolidated-undrained tests].

[3] Values of the parameters have been calculated for many different types of soils and this information can be used to estimate reasonable values of the parameters in cases where the available data are insufficient to define the parameters for all of the soils involved in a particular problem. The information is also quite useful for assessing the reliability of parameter values derived from laboratory test results.

In order to model the field behavior of soils around the culvert accurately, the above described hyperbolic stress-strain models were used in the finite element analyses. The triaxial stress-strain test data were reduced as shown in Figs. 3.13 - 3.15 and the hyperbolic model parameters for the backfill and foundation soils were obtained. The hyperbolic parameters used in this study are summarized in Table 3.2.

3.1.3 Soil Properties Used in the Analyses With No-Slip and Full-Slip Interface conditions.

In order to study the effects of Culvert-Soil interface on the results obtained by the Finite Element Analyses, two separate analyses were performed, in which one is with a no-slip interface and the other with a full-slip interface. To simulate the worst compaction condition the backfill at this site would ever experience, soil properties that are more conservative than that of Soil 3, were used in these analyses.

3.2 Structural Properties

The RC box culvert was modeled as a series of beam elements, connected at common nodes, in the finite element analyses. The geometry and the

Soil: Soil 1
95% γ_d, DRY

Data for Deviatoric Modulus Parameters							
		70 % Stress Level			95 % Stress Level		
σ_3 ①	$(\sigma_1-\sigma_3)_f$ ②	$(\sigma_1-\sigma_3)$ ③	ε_a ④	$\frac{\varepsilon_a}{(\sigma_1-\sigma_3)}$ ⑤	$(\sigma_1-\sigma_3)$ ⑥	ε_a ⑦	$\frac{\varepsilon_a}{(\sigma_1-\sigma_3)}$ ⑧
5	27.5	19.25	0.011	5.714×10^{-4}	26.13	0.019	7.271×10^{-4}
10	44.0	30.80	0.014	4.545×10^{-4}	41.80	0.025	5.981×10^{-4}
20	76.0	53.20	0.012	2.256×10^{-4}	72.20	0.029	4.017×10^{-4}

Pa =

$\frac{\sigma_3}{Pa}$ ⑫	$\frac{1}{(\sigma_1-\sigma_3)_{ult}}$ ⑬	R_f ⑭	$\frac{E_i}{Pa}$ ⑮	$\frac{B}{Pa}$ ⑯
0.3401	1.946×10^{-2}	0.54	190.4	
0.6803	1.305×10^{-2}	0.57	250.3	
1.361	1.036×10^{-2}	0.79	671.7	

$$\frac{1}{(\sigma_1-\sigma_3)_{ult}} = \frac{⑧-⑤}{⑦-④}$$

$$R_f = ② \times ⑬$$

Average R_f = 0.63

$$\frac{E_i}{Pa} = \frac{2.0}{⑤ + ⑧ - ⑬ \times [④ + ⑦]} - \frac{1}{Pa}$$

$$\frac{B}{Pa} = \frac{⑪}{Pa}$$

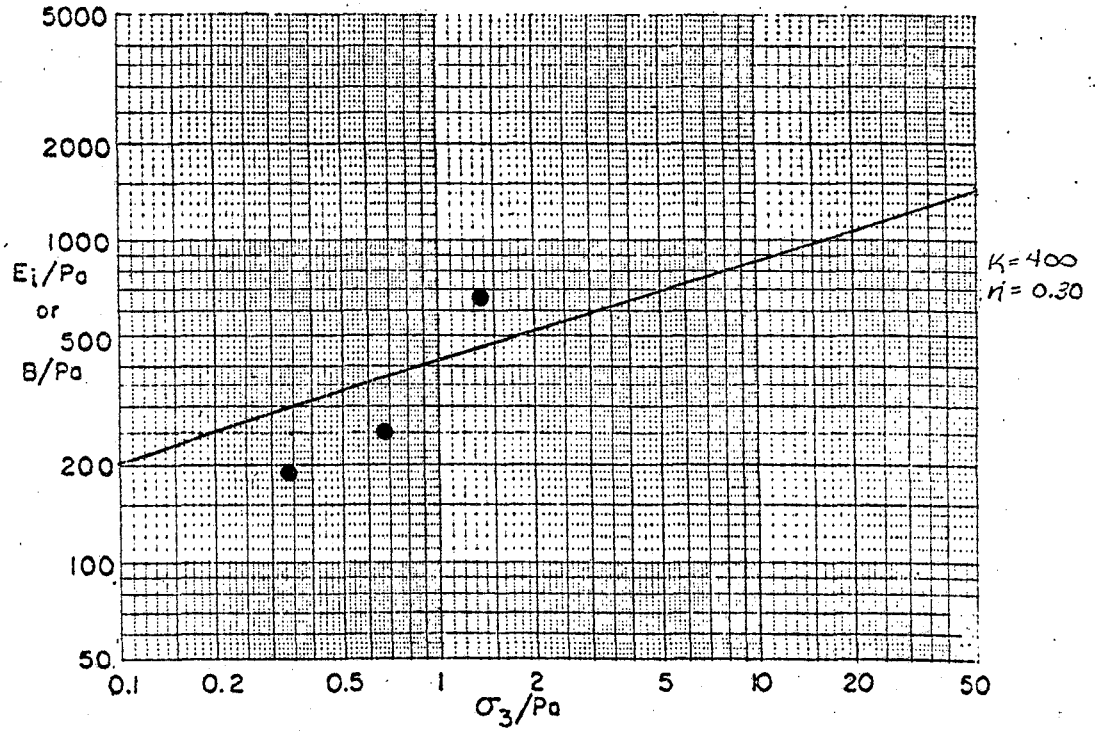

FORM FOR COMPUTING HYPERBOLIC PARAMETERS

FIGURE 3.13

Soil: Soil 2, 100% $\gamma_{d\,max}$

Data for Deviatoric Modulus Parameters							
		70 % Stress Level			95 % Stress Level		
σ_3 ①	$(\sigma_1-\sigma_3)_f$ ②	$(\sigma_1-\sigma_3)$ ③	ε_a ④	$\frac{\varepsilon_a}{(\sigma_1-\sigma_3)}$ ⑤	$(\sigma_1-\sigma_3)$ ⑥	ε_a ⑦	$\frac{\varepsilon_a}{(\sigma_1-\sigma_3)}$ ⑧
5	25.5	17.85	0.0140	7.843×10^{-4}	24.23	0.028	1.156×10^{-3}
10	43.5	30.45	0.0145	4.762×10^{-4}	41.33	0.025	6.049×10^{-4}
20	77.5	54.25	0.0132	2.433×10^{-4}	73.63	0.024	3.260×10^{-4}

Pa =

$\frac{\sigma_3}{Pa}$ ⑫	$\frac{1}{(\sigma_1-\sigma_3)_{ult}}$ ⑬	R_f ⑭	$\frac{E_i}{Pa}$ ⑮	$\frac{B}{Pa}$ ⑯
0.3401	2.655×10^{-2}	0.68	165	
0.6803	1.226×10^{-2}	0.53	228	
1.361	7.657×10^{-3}	0.59	478	

$$\frac{1}{(\sigma_1-\sigma_3)_{ult}} = \frac{⑧-⑤}{⑦-④}$$

$$R_f = ② \times ⑬$$

Average R_f = 0.60

$$\frac{E_i}{Pa} = \frac{2.0}{⑤+⑧-⑬\times[④+⑦]} - \frac{1}{Pa}$$

$$\frac{B}{Pa} = \frac{⑪}{Pa}$$

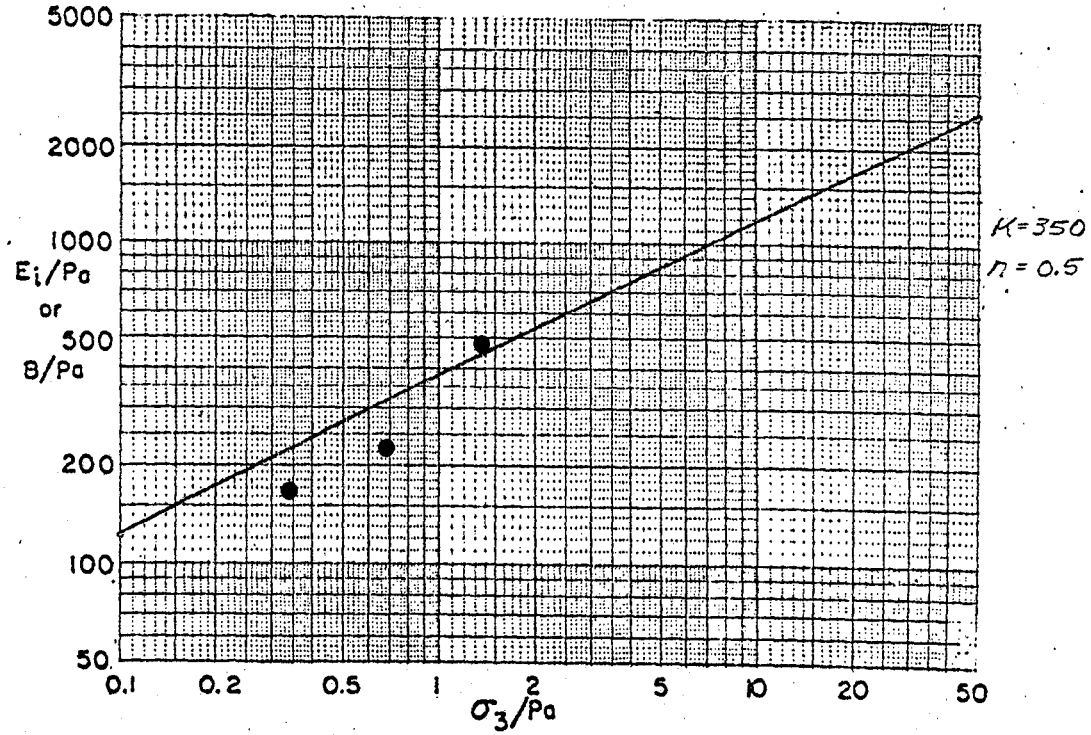

FORM FOR COMPUTING HYPERBOLIC PARAMETERS

FIGURE 3.14

Soil: Soil 3, 95% γ_d, WET

Data for Deviatoric Modulus Parameters							
		70 % Stress Level			95 % Stress Level		
σ_3 ①	$(\sigma_1-\sigma_3)_f$ ②	$(\sigma_1-\sigma_3)$ ③	ε_a ④	$\frac{\varepsilon_a}{(\sigma_1-\sigma_3)}$ ⑤	$(\sigma_1-\sigma_3)$ ⑥	ε_a ⑦	$\frac{\varepsilon_a}{(\sigma_1-\sigma_3)}$ ⑧
5	14.3	10.010	0.042	4.196×10^{-3}	13.6	0.134	9.853×10^{-3}
10	34.5	24.15	0.045	1.863×10^{-3}	32.8	0.064	1.951×10^{-3}
20	54.0	37.80	0.063	1.667×10^{-3}	51.3	0.097	1.891×10^{-3}

Pa =

$\frac{\sigma_3}{Pa}$ ⑫	$\frac{1}{(\sigma_1-\sigma_3)_{ult}}$ ⑬	R_f ⑭	$\frac{E_i}{Pa}$ ⑮	$\frac{B}{Pa}$ ⑯
0.3401	6.149×10^{-2}	0.88	42.16	
0.6803	4.632×10^{-3}	0.16	41.12	
1.361	6.588×10^{-3}	0.36	54.34	

$$\frac{1}{(\sigma_1-\sigma_3)_{ult}} = \frac{⑧-⑤}{⑦-④}$$

R_f = ② × ⑬

Average R_f = 0.47

$$\frac{E_i}{Pa} = \frac{2.0}{⑤+⑧-⑬\times[④+⑦]} - \frac{1}{Pa}$$

$$\frac{B}{Pa} = \frac{⑪}{Pa}$$

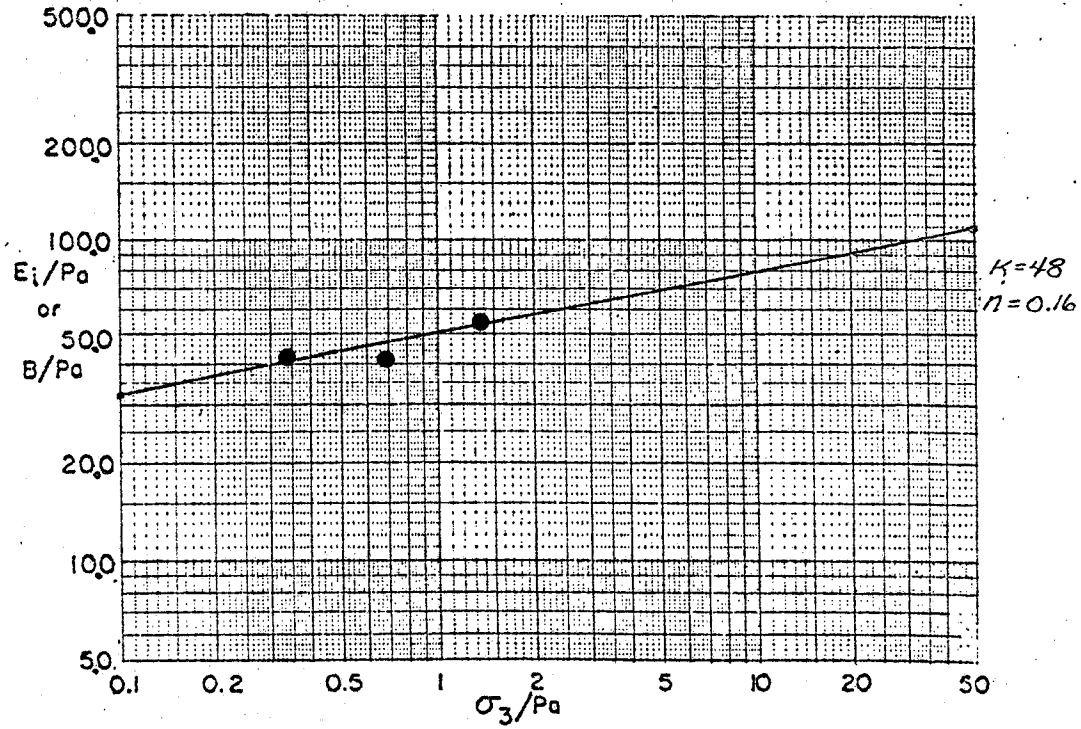

FORM FOR COMPUTING HYPERBOLIC PARAMETERS

FIGURE 3.15

Table 3.2 SOIL PROPERTIES USED IN FINITE ELEMENT ANALYSIS

PROPERTY	Soil 1 95% γ_{max} Dry of Opt.	Soil 2 100% γ_{max}	Soil 3 95% γ_{max} Wet of Opt.
Dry Unit Wt., γ_d [kcf]	0.110	0.116	0.110
Moisture Content, w [%]	3.6	7.9	13.0
Moist Unit Wt, γ [kcf]	0.114	0.125	0.125
Modulus Number, K	400	350	50
Modulus Exponent, n	0.3	0.5	0.2
Failure Ratio, R_f	0.6	0.6	0.6
Bulk Modulus No., K_b	75	125	40
Bulk Modulus Exponent, m	0.2	0.2	0.2
Angle of Friction, ϕ	42.8	40.5	34.8
Reduction in Angle, $\Delta\phi$	7	7	5
Cohesion, c	0	0	0
Earth Pressure Coef., K_o	0.5	0.5	0.5

sectional properties of the culvert used in the analyses are discussed in the sections below.

3.2.1 Geometry of the Culvert

The culvert analyzed in this study is a Reinforced Concrete Box Culvert and a cross-section is shown in Fig. 3.16. The side walls have a thickness of 8 inches and the bottom and top slabs have a thickness of 7 inches. Longitudinal and Transverse Steel are present in the concrete sections for reinforcement.

3.2.2 Sectional Properties Used in the Analyses

The culvert was represented by a series of beam elements, as shown in Fig. 3.16, in the analyses. The cross-sectional properties for the plane strain analyses were calculated by transforming areas of steel into concrete and the sectional properties used in the analyses are summarized in Table 3.3.

3.2.3 Soil-Structure Interface Properties

In order to allow for the effects of slip at the culvert-soil interface, special interface elements shown in Fig. 3.17 were employed in the analyses. The shear spring constant can be defined a low value for a full-slip connection between the soil and the culvert. A high value for the shear spring constant will yield a no-slip condition. Both types of analyses were performed and the properties used for the soil-structure interface are given in Table 3.4.

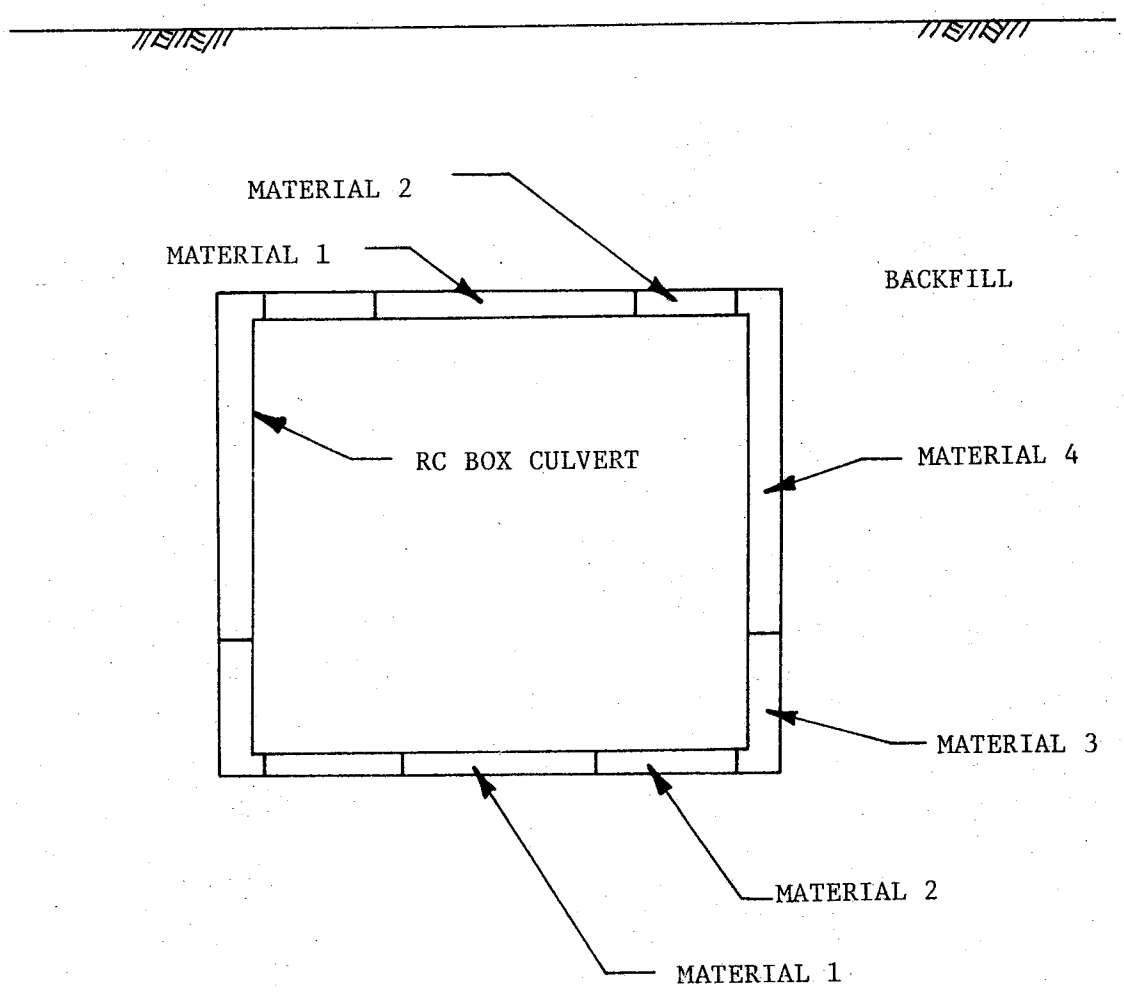

CROSS-SECTION OF BOX CULVERT

FIGURE 3.16

Table 3.3. STRUCTURAL PROPERTIES USED IN THE ANALYSES

PROPERTY	MATERIAL TYPE NO.			
	1	2	3	4
Young's Modulus, E [ksf]	519119.0	519119.0	519119.0	519119.0
Moment of Inertia, I [ft]	0.0170	0.0172	0.0256	0.0253
Cross Sectional Area, A [ft]	0.601	0.612	0.700	0.689
Shear Area, ASH [ft]	0.601	0.612	0.700	0.689
Weight Per Unit Length [kips/ft]	0.0875	0.0875	0.100	0.100
C - Top [ft]	0.287	0.289	0.336	0.333
C - Bottom [ft]	0.297	0.294	0.331	0.333

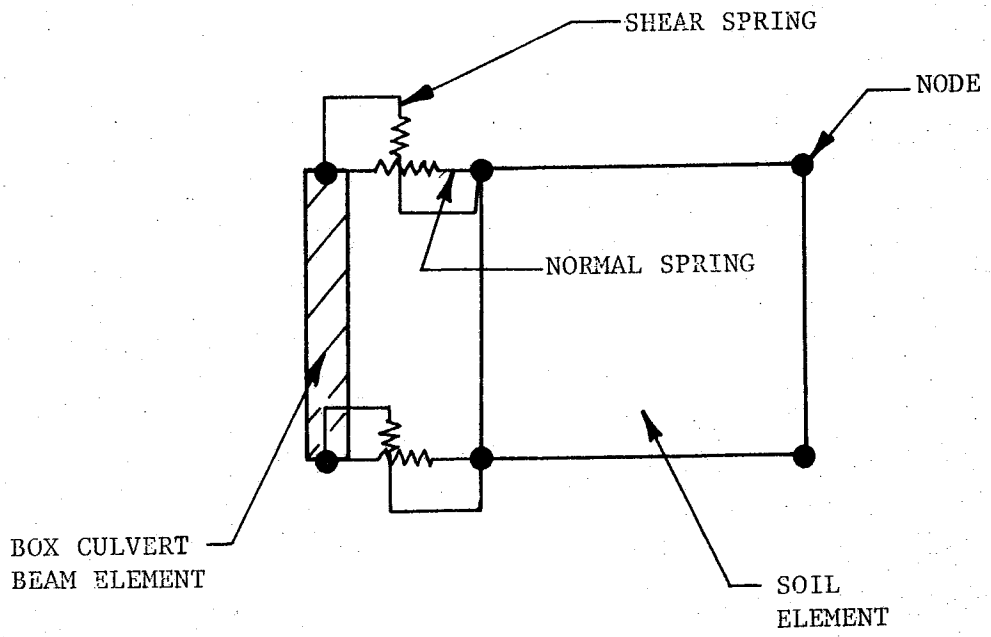

DEFINITION SKETCH OF INTERFACE ELEMENT

FIGURE 3.17

Table 3.4. INTERFACE ELEMENT PROPERTIES USED IN ANALYSES

PROPERTY	Full-Slip Condition [Low Spring Constants]		No-Slip Condition [High Spring Constants]	
MATERIAL NO.	1	2	1	2
Adhesion, C	0	0	0	0
Wall Friction Angle, ϕ	36.0	32.0	36.0	32.0
Reduction in Angle, $\Delta\phi$	5.0	4.0	5.0	4.0
Normal Spring Coeff.	1.0×10^6	1.0×10^6	1.0×10^6	1.0×10^6
Shear Spring Coeff.	1.00	1.00	1.0×10^7	1.0×10^7
Unloading Shear Spring Coeff.	1.00	1.00	1.0×10^7	1.0×10^7
Modulus Exponent, n	0.40	0.25	0.40	0.25
Failure Ratio, R_f	0.70	0.70	0.70	0.70

CHAPTER 4

FINITE ELEMENT ANALYSES

4.1 Introduction

The finite element analysis program SSTIPN was used to analyze the behavior of the reinforced concrete box culvert during backfill placement around and over the structure. Through this analysis, earth pressures, bending moments, stresses, strains, and deflections in the culvert were determined.

The full finite element mesh for this study is shown in Fig. 4.1. Due to symmetry of construction, only half of the mesh was used for the backfilling analysis as shown in Fig. 4.2. This was done in order to reduce the computing time required for the finite element analyses. However, the program SSTIPN has the capability of analyzing unsymmetrical cases.

4.2 Behavior of the Culvert Under Backfill Loads

4.2.1 Earth Pressures

The pressures exerted on the culvert were detemined directly from the results of the finite element program. The variation of earth pressure with depth of fill was plotted for seven locations on the perimeter of the culvert which correspond to the placement of pressure cells on the 8' x 8' RC box culvert to be instrumented in a related study.

In order to study the influence of the soil-culvert interface on the results, separate analyses were performed, with full-slip and no-slip interfaces. The full-slip condition provides no resistance to slippage along the wall of the culvert. This is represented in the analyses by assigning small values for the shear spring constant and for the unloading shear spring constant. The components of an interface element in the full-slip condition are shown in Fig. 4.3a. The no-slip condition is

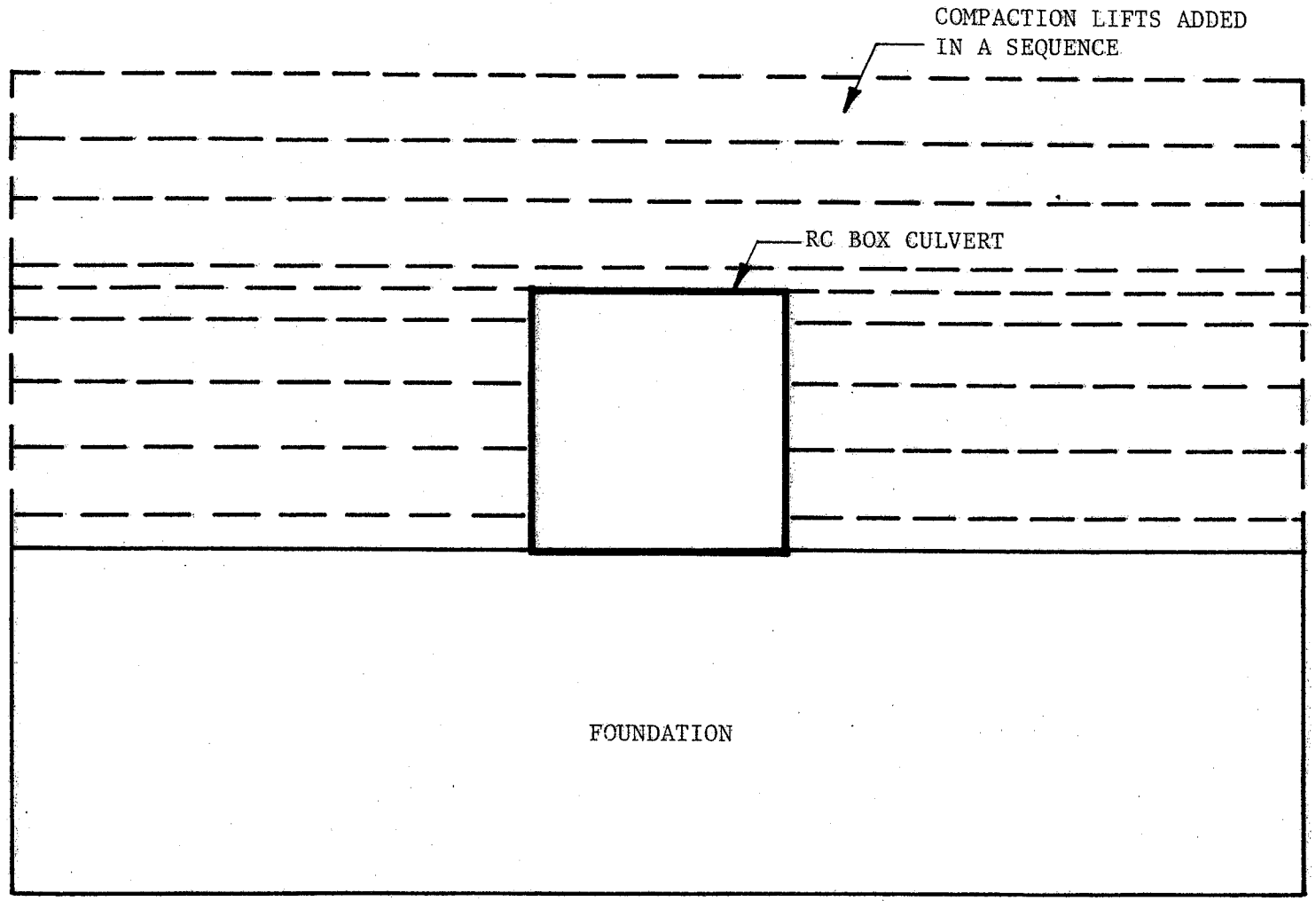

FULL FINITE ELEMENT MESH

FIGURE 4.1

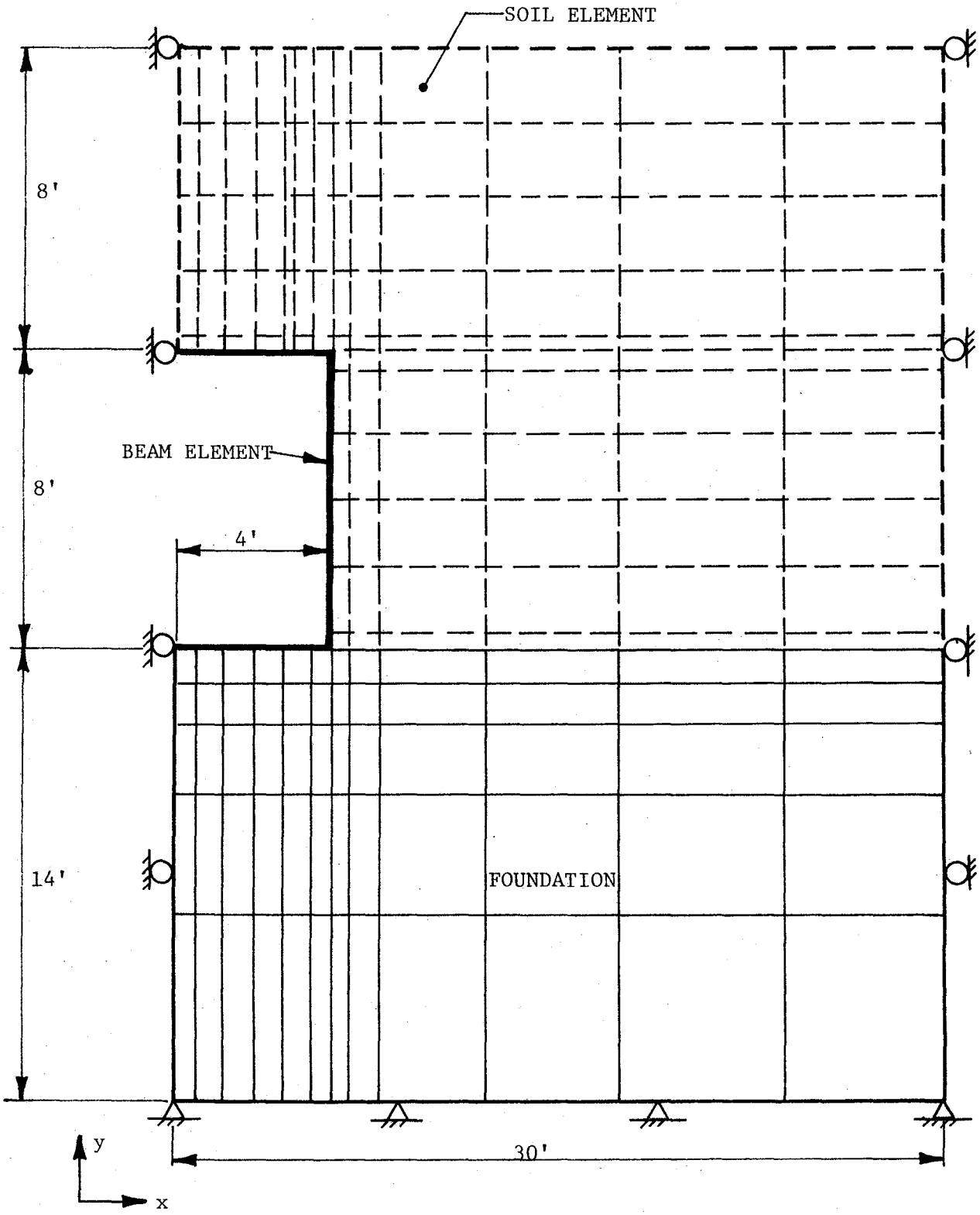

HALF MESH USED IN FINITE ELEMENT PROGRAM

FIGURE 4.2

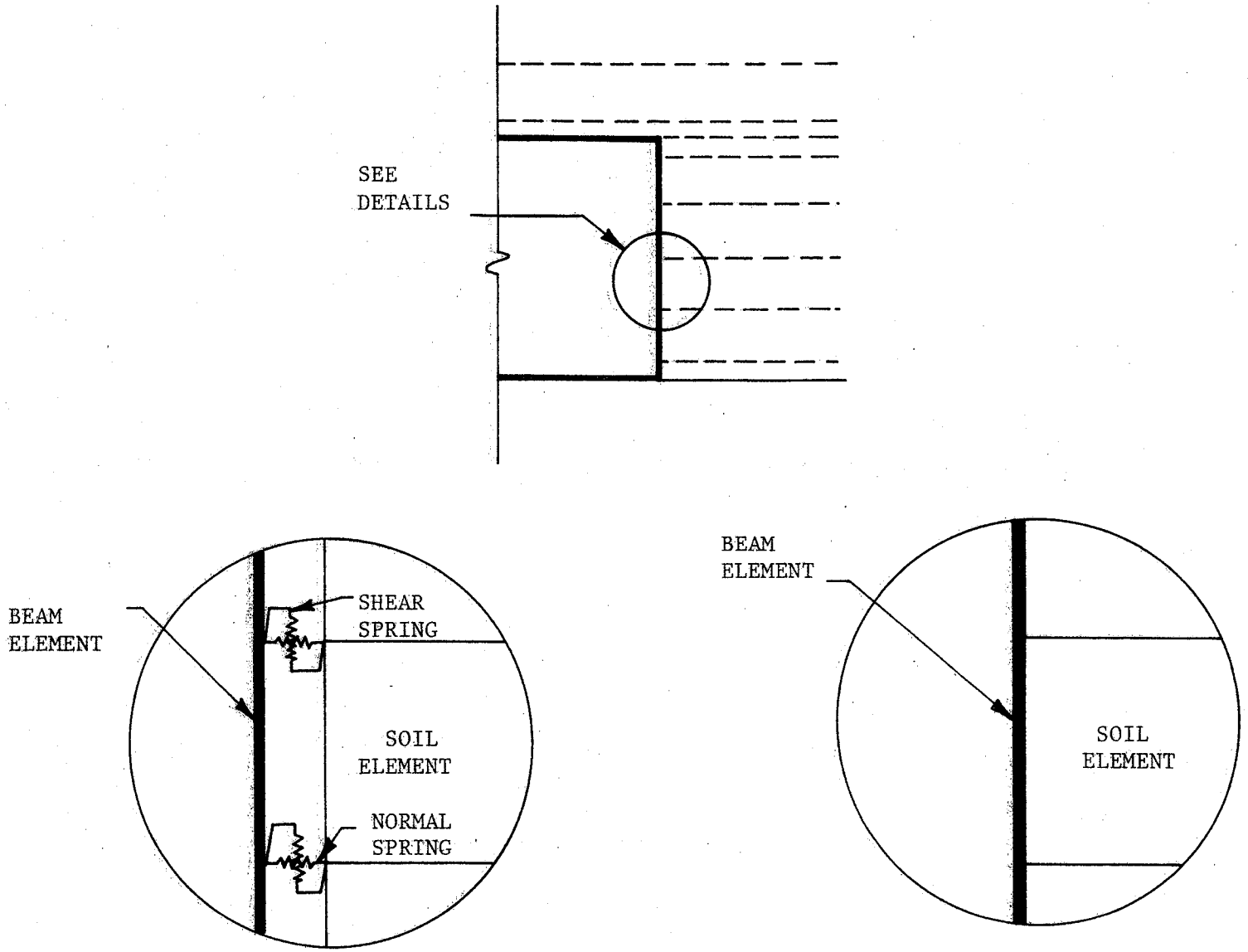

a. FULL - SLIP CONDITION
DETAIL

b. NO SLIP CONDITION
DETAIL

FIGURE 4.3 DETAILS OF SOIL - STRUCTURE INTERFACE

modeled by rigidly attaching the soil elements, around the perimeter of the culvert, to the structural beam elements. In this manner, no slippage is allowed. This is shown in Fig. 4.3b.

The effects of full-slip and no-slip conditions on calculated earth pressures are shown in Figs. 4.4 - 4.10, for the seven pressure cell locations.

Pressure cell P-1 is located near the bottom of the culvert on the vertical wall. The variation of earth pressures with depth of fill for this pressure cell is shown in Fig. 4.4. The calculated earth pressures increase linearly with depth of fill and the results for full-slip and no-slip conditions are very similar.

The variation of earth pressures with depth of fill for pressure cell P-2 is shown in Fig. 4.5. Pressure cell P-2 is located approximately 3.5 feet above the bottom of the culvert on the vertical wall. The earth pressures produced by the full-slip condition are slightly greater than those from the no-slip condition.

Pressure cell P-3 is located 5.3 feet above the bottom of the culvert on the vertical wall. The earth pressures produced during the incremental backfilling operations are shown in Fig. 4.6. Again, the earth pressures calculated using the full-slip assumption are slightly greater than that calculated with the no-slip assumption.

The variation of earth pressures with depth of fill for pressure cell P-4 is given in Fig. 4.7. The pressures increase linearly with depth of fill, with the full-slip condition producing slightly greater pressures on the culvert.

Pressure cell P-5 is located at the midspan of the top slab. The calculated earth pressures for this pressure cell are shown in Fig. 4.8.

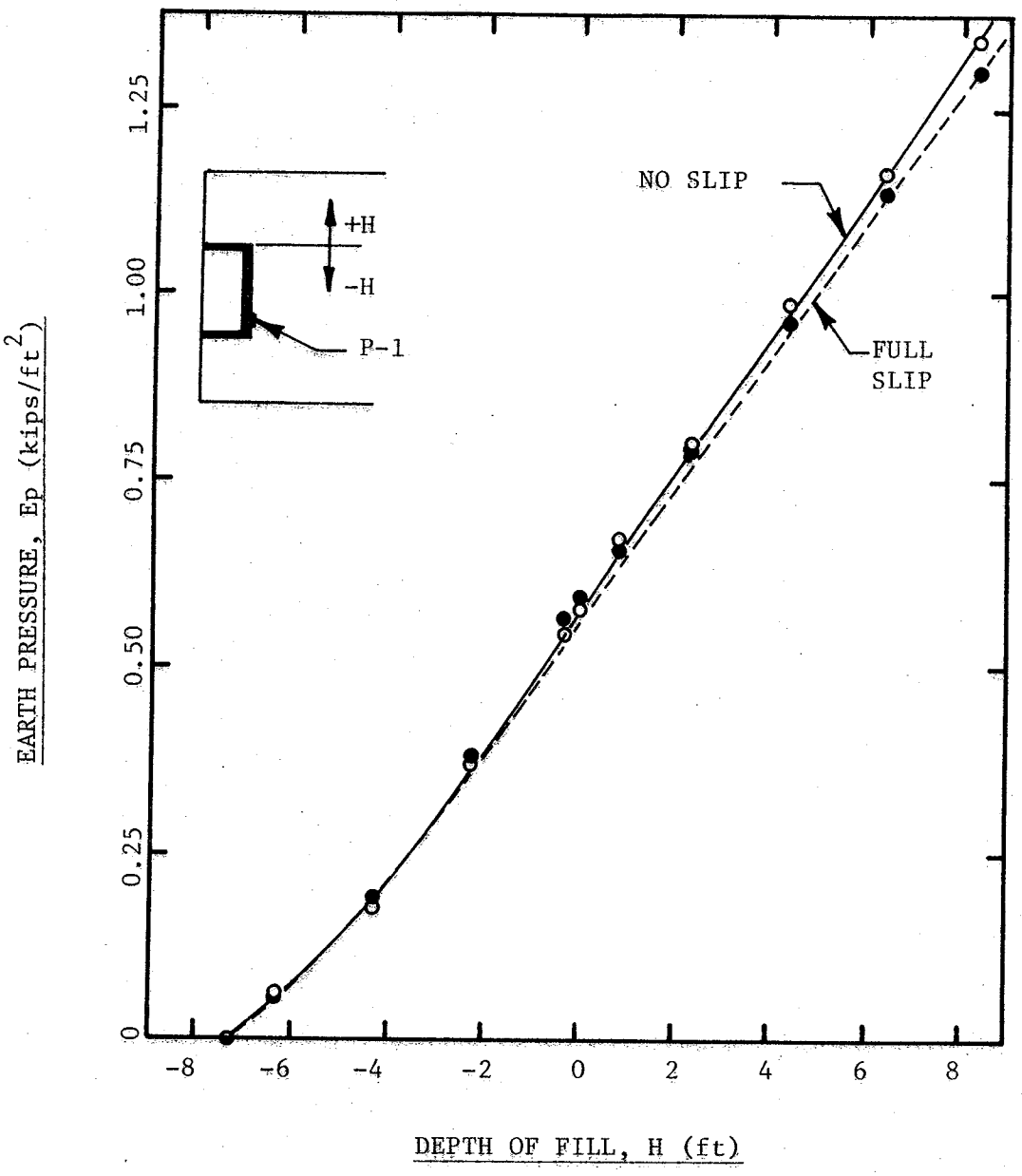

VARIATION OF EARTH PRESSURE WITH
DEPTH OF FILL FOR PRESSURE CELL P-1

FIGURE 4.4

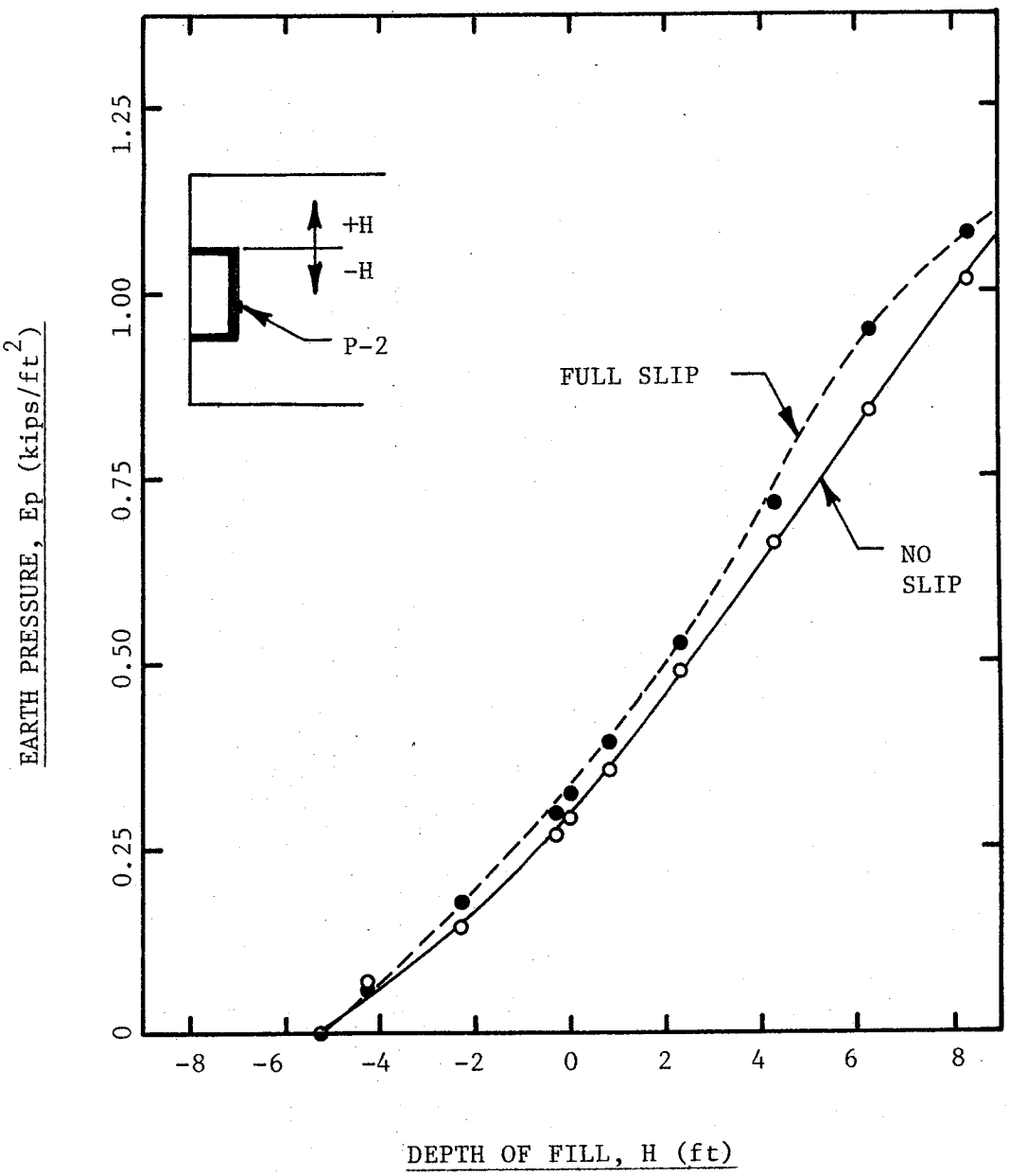

VARIATION OF EARTH PRESSURE WITH
DEPTH OF FILL FOR PRESSURE CELL P-2

FIGURE 4.5

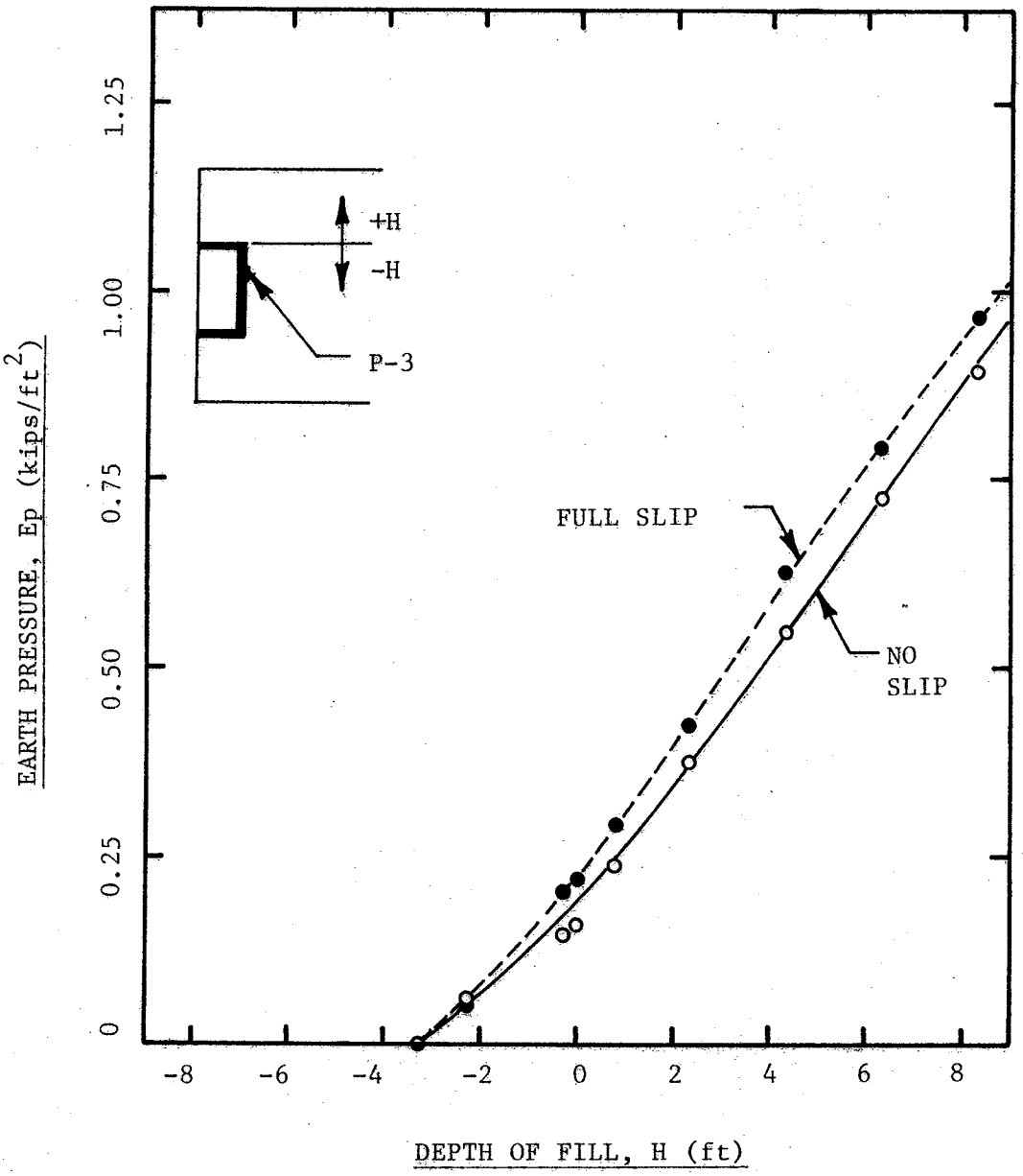

VARIATION OF EARTH PRESSURE WITH
DEPTH OF FILL FOR PRESSURE CELL P-3

FIGURE 4.6

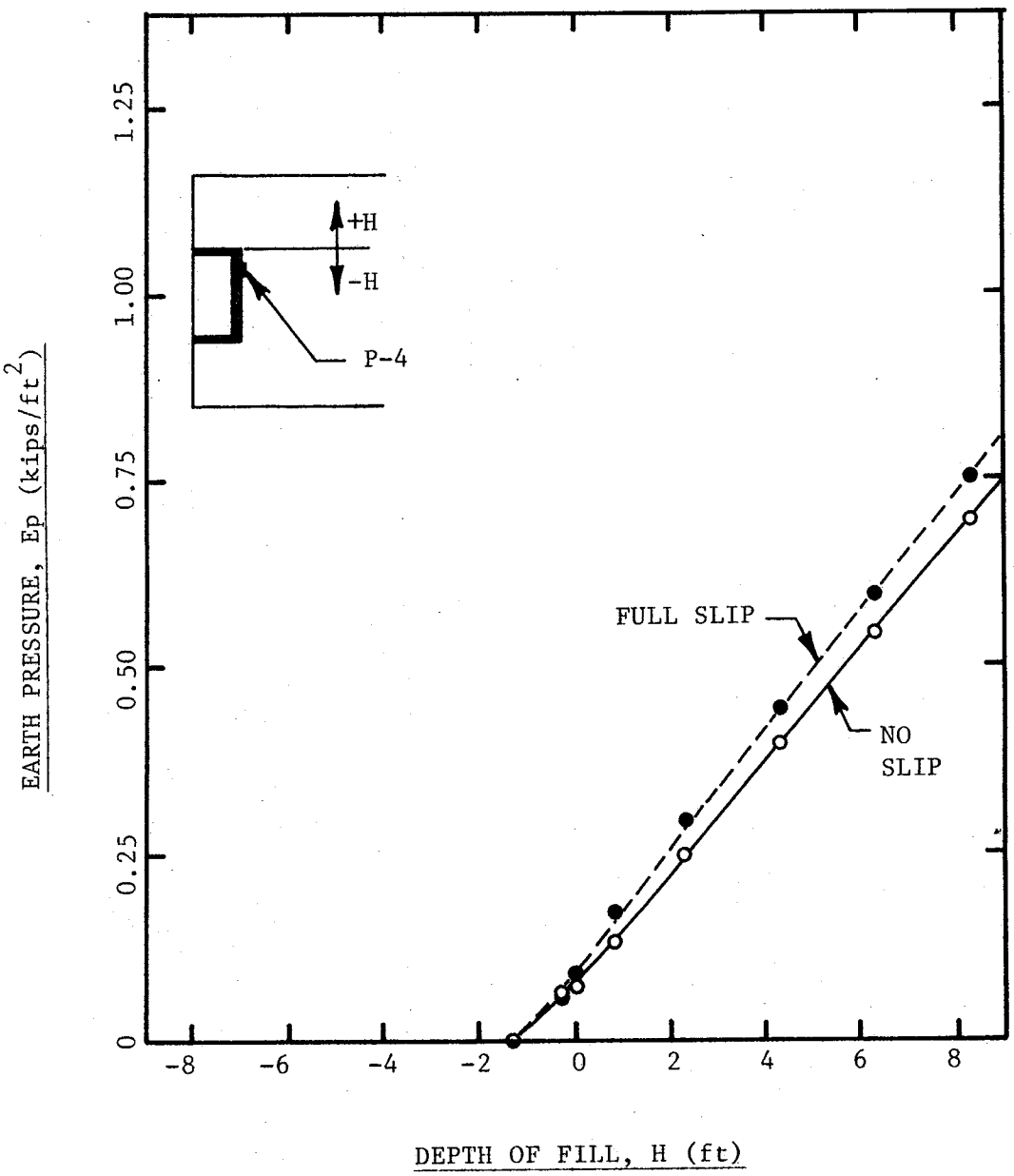

VARIATION OF EARTH PRESSURE WITH
DEPTH OF FILL FOR PRESSURE CELL P-4

FIGURE 4.7

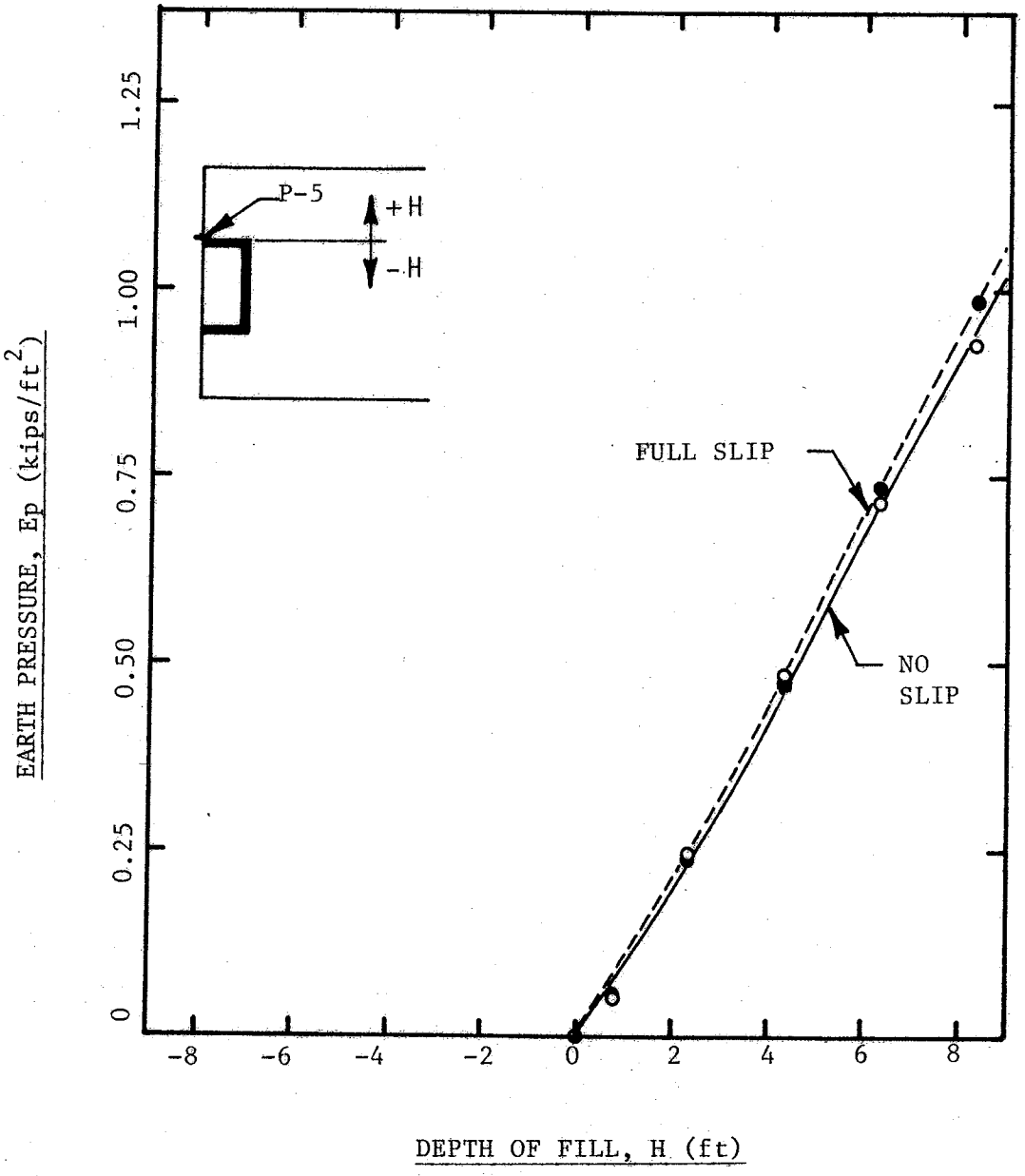

VARIATION OF EARTH PRESSURE WITH
DEPTH OF FILL FOR PRESSURE CELL P-5

FIGURE 4.8

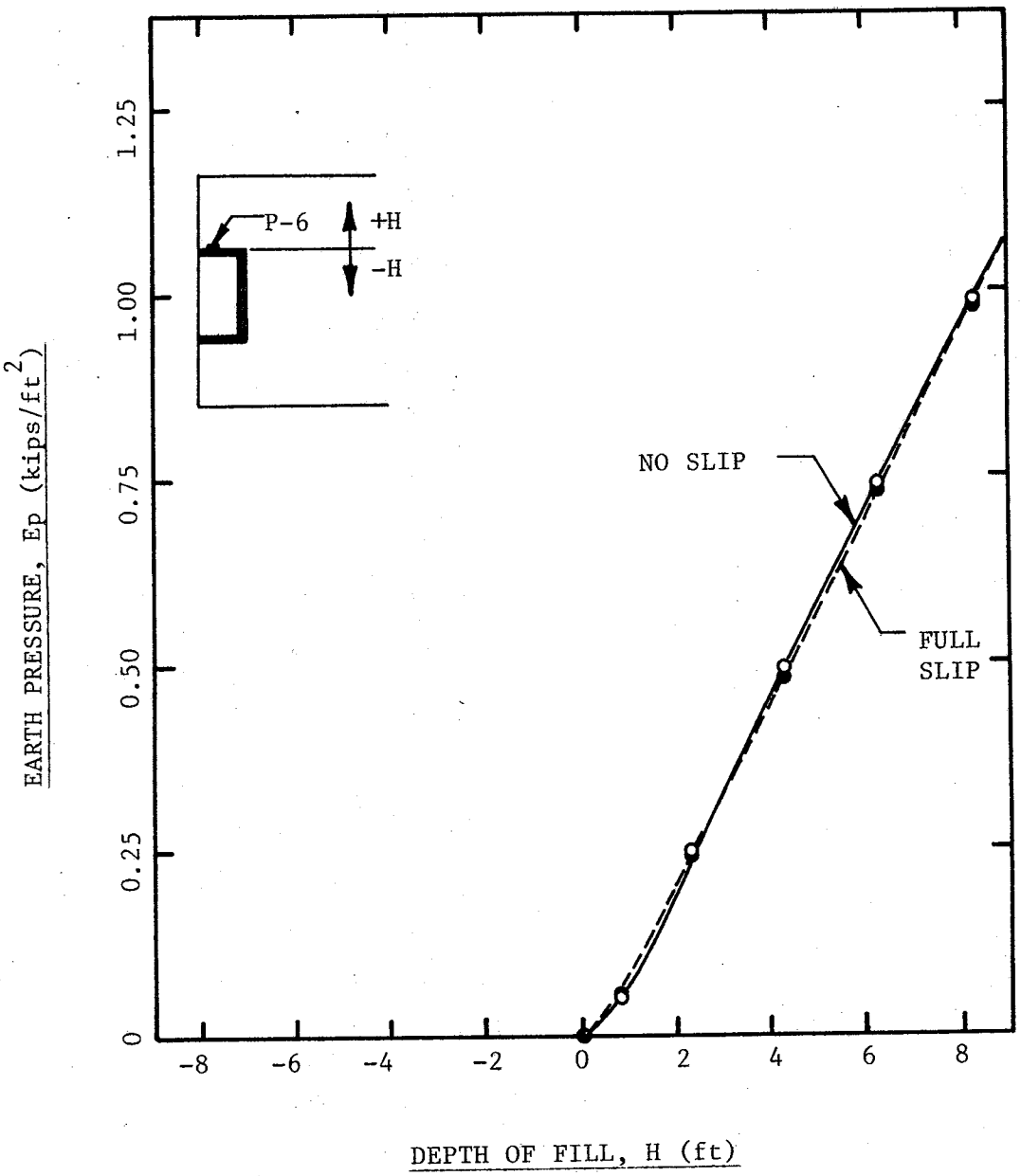

VARIATION OF EARTH PRESSURE WITH
DEPTH OF FILL FOR PRESSURE CELL P-6

FIGURE 4.9

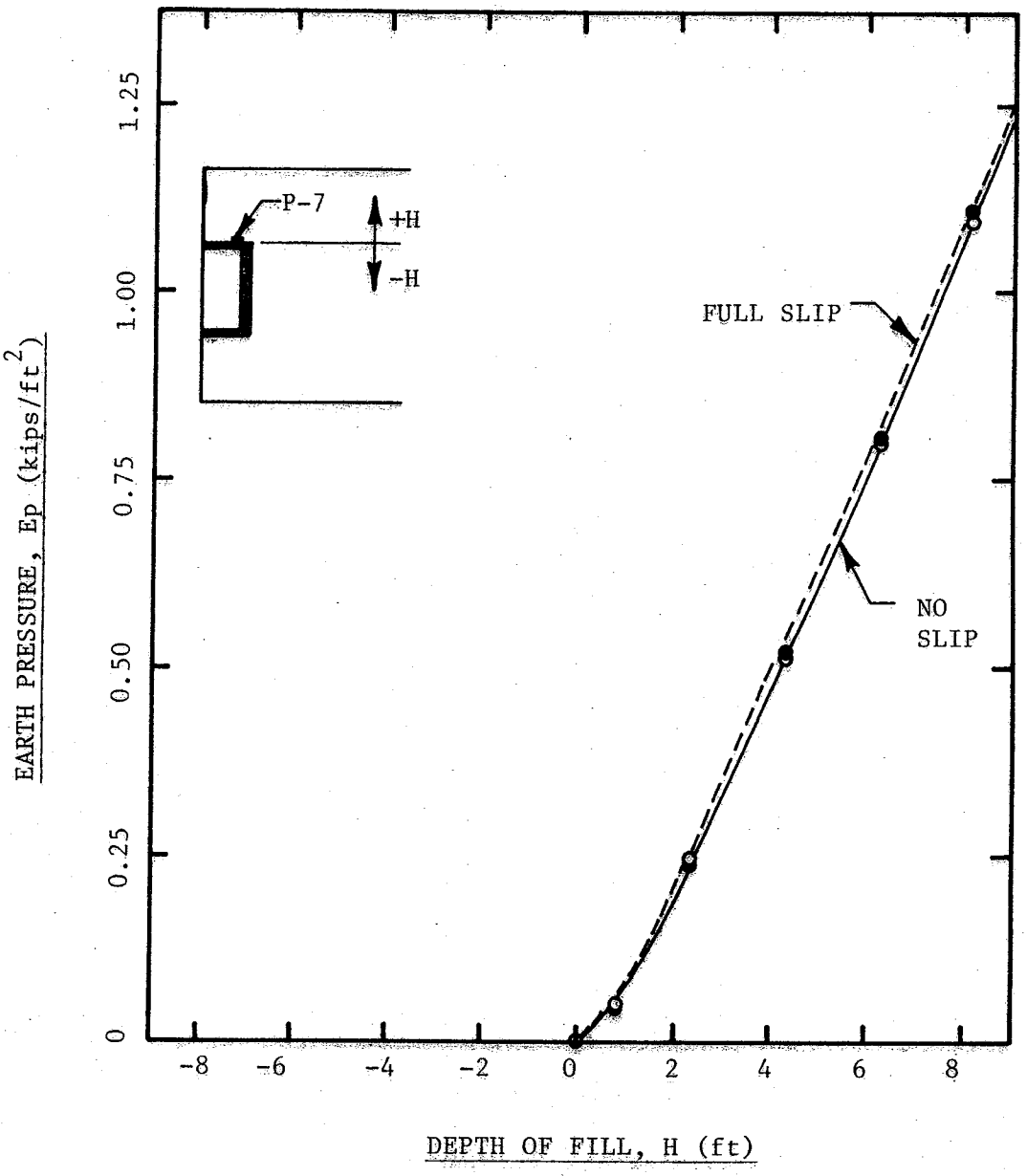

VARIATION OF EARTH PRESSURE WITH
DEPTH OF FILL FOR PRESSURE CELL P-7

FIGURE 4.10

The pressures increase linearly with depth of fill, and the results are almost identical for the no-slip and full-slip conditions.

The variation of earth pressures with depth of fill for pressure cell P-6 is shown in Fig. 4.9. Pressure cell P-6 is also located on the top slab of the culvert, approximately 1.75 feet from the center. These results are almost identical to those for pressure cell P-5.

Finally, pressure cell P-7 is located 3.0 feet from the center of the culvert on the top slab. The variation of earth pressure with depth of fill for this cell is shown in Fig. 4.10. The pressures increase linearly with depth of fill, and are slightly greater than those given by pressure cells P-5 and P-6. The results for full-slip and no-slip conditions are identical.

The earth pressures shown in these figures for the full-slip and no-slip conditions show little difference and therefore the rest of the analyses were performed using the no-slip condition only. It should be noted that in the no-slip analyses, the special soil-structure interface element can be omitted and an appreciable reduction in computing costs can be achieved. Three different soils were used for the backfill material and a number of analyses on the behavior of the culvert were made to study the effects of soil compaction conditions on earth pressures, moments, stresses, strains, and deflections. The properties of the Soils 1, 2, and 3 were given in Chapter 3.

The variation of earth pressure with depth of fill for pressure cell P-1 is shown in Fig. 4.11. Soil 1 exerts the least pressure, while Soil 3 exerts the greatest pressure on the culvert. In all cases, the pressure increases linearly with depth of fill. It should be noted that Soil 1 is compacted on the dry side of optimum water content at 95% standard AASHTO

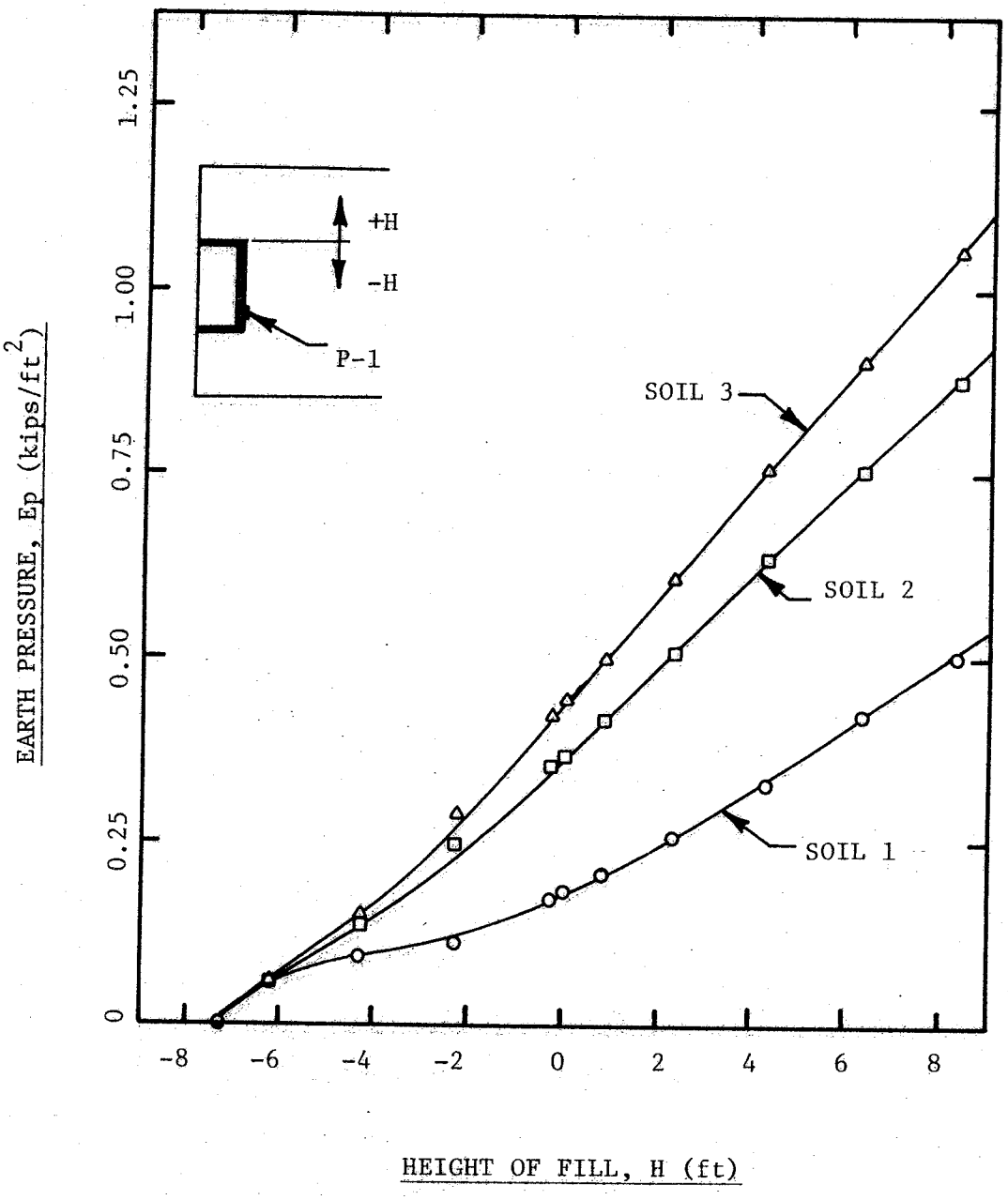

VARIATION OF EARTH PRESSURE WITH
DEPTH OF FILL FOR PRESSURE CELL P-1

FIGURE 4.11

maximum dry density, Soil 2 is compacted at 100% maximum dry density, and Soil 3 is compacted on the wet side of optimum at 95% maximum dry density.

For pressure cell P-2, the earth pressures are given in Fig. 4.12. Soil 3 exhibits the most critical behavior during backfilling.

The variation of earth pressures with depth of fill for pressure cell P-3 is given in Fig. 4.13. The pressures increase linearly with depth of fill after some backfilling.

For pressure cell P-4, the earth pressures are given in Fig. 4.14. Soil 1 exerts very low pressures at this point due to the stiffness of the soil. Soil 3 exerts very high pressures.

For pressure cells P-5, P-6, and P-7, located on the top slab, the variations in earth pressure with depth of fill are almost identical. These are shown in Figs. 4.15 - 4.17. In all cases, the earth pressures increase linearly with depth of backfill.

The distribution of earth pressures around the culvert with the backfill level at the crown of the culvert is shown in Fig. 4.18. A comparison is shown for no-slip and full-slip conditions. The difference is small except along the bottom of the culvert, where slip and soil movement produce a difference in the results. For a cover depth of 8 ft over the crown of the culvert, the distribution of earth pressures around the culvert is shown in Fig. 4.19. As before, there is a significant difference along the bottom of the culvert where the full-slip condition permits soil movement along the sides of the culvert.

The earth pressure distributions for the three soils with the backfill level at the crown are shown in Fig. 4.20. The difference in soil quality affects primarily the pressures on the walls of the culvert, with

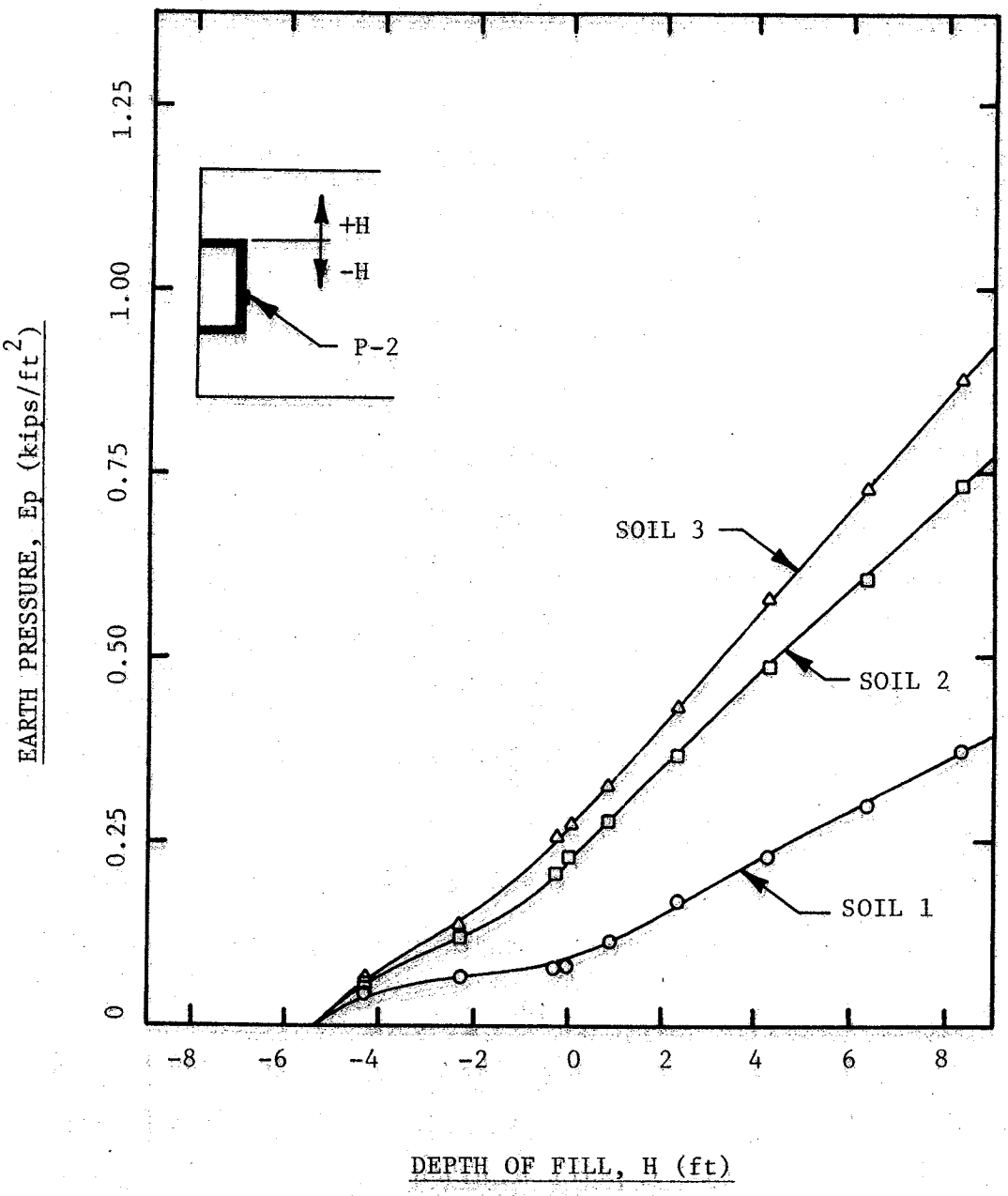

VARIATION OF EARTH PRESSURE WITH
DEPTH OF FILL FOR PRESSURE CELL P-2

FIGURE 4.12

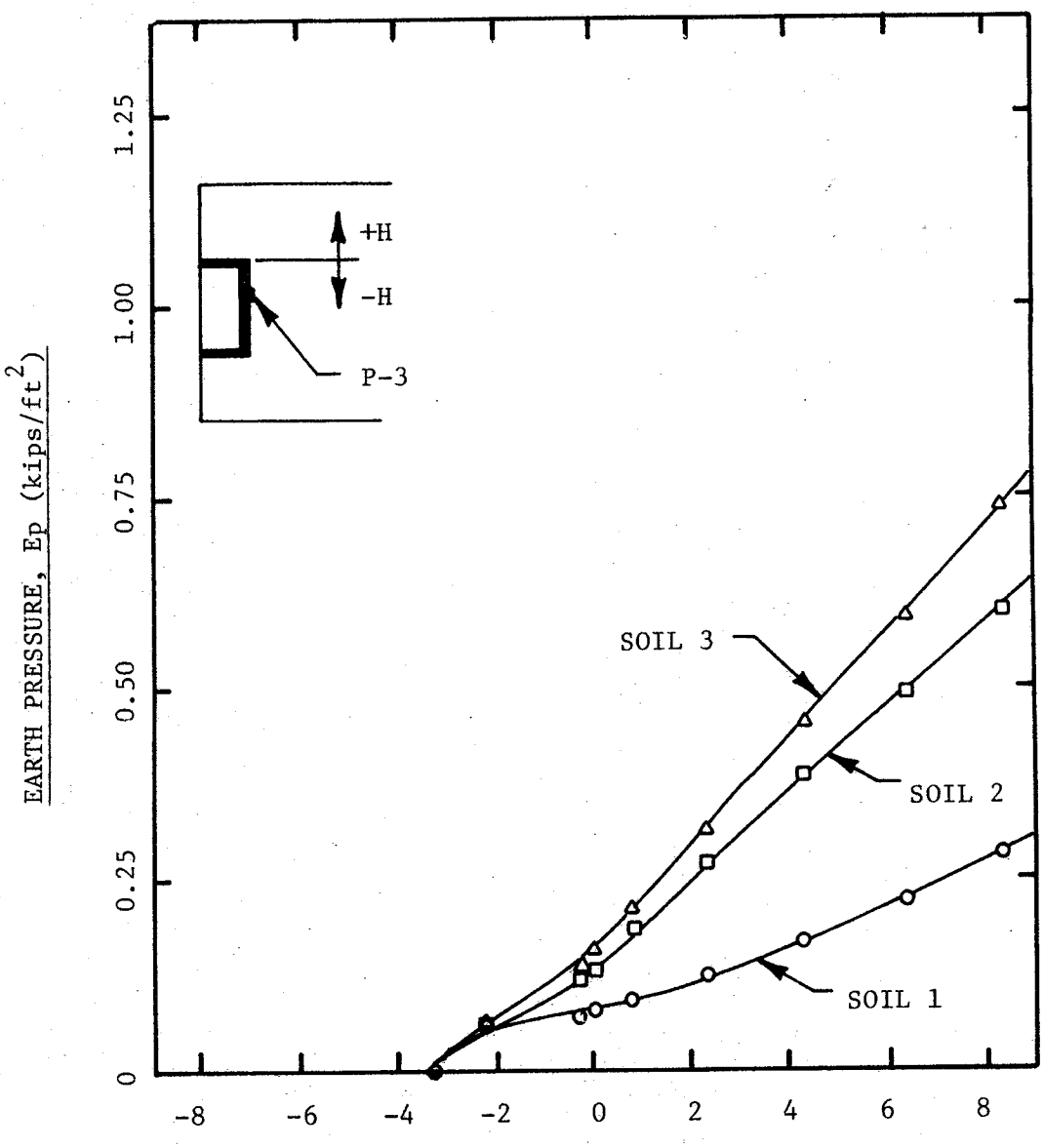

VARIATION OF EARTH PRESSURE WITH
DEPTH OF FILL FOR PRESSURE CELL P-3

FIGURE 4.13

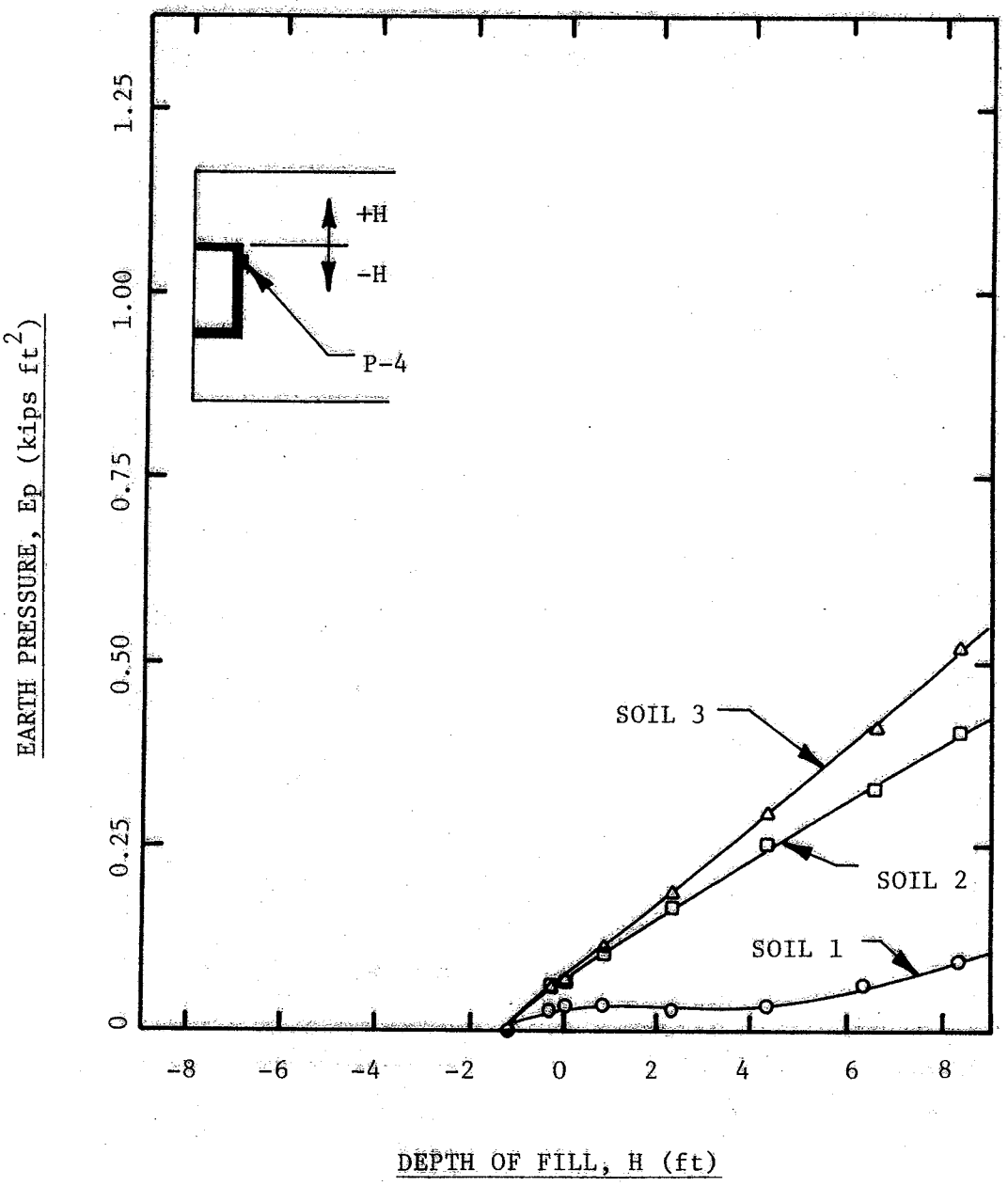

VARIATION OF EARTH PRESSURE WITH
DEPTH OF FILL FOR PRESSURE CELL P-4

FIGURE 4.14

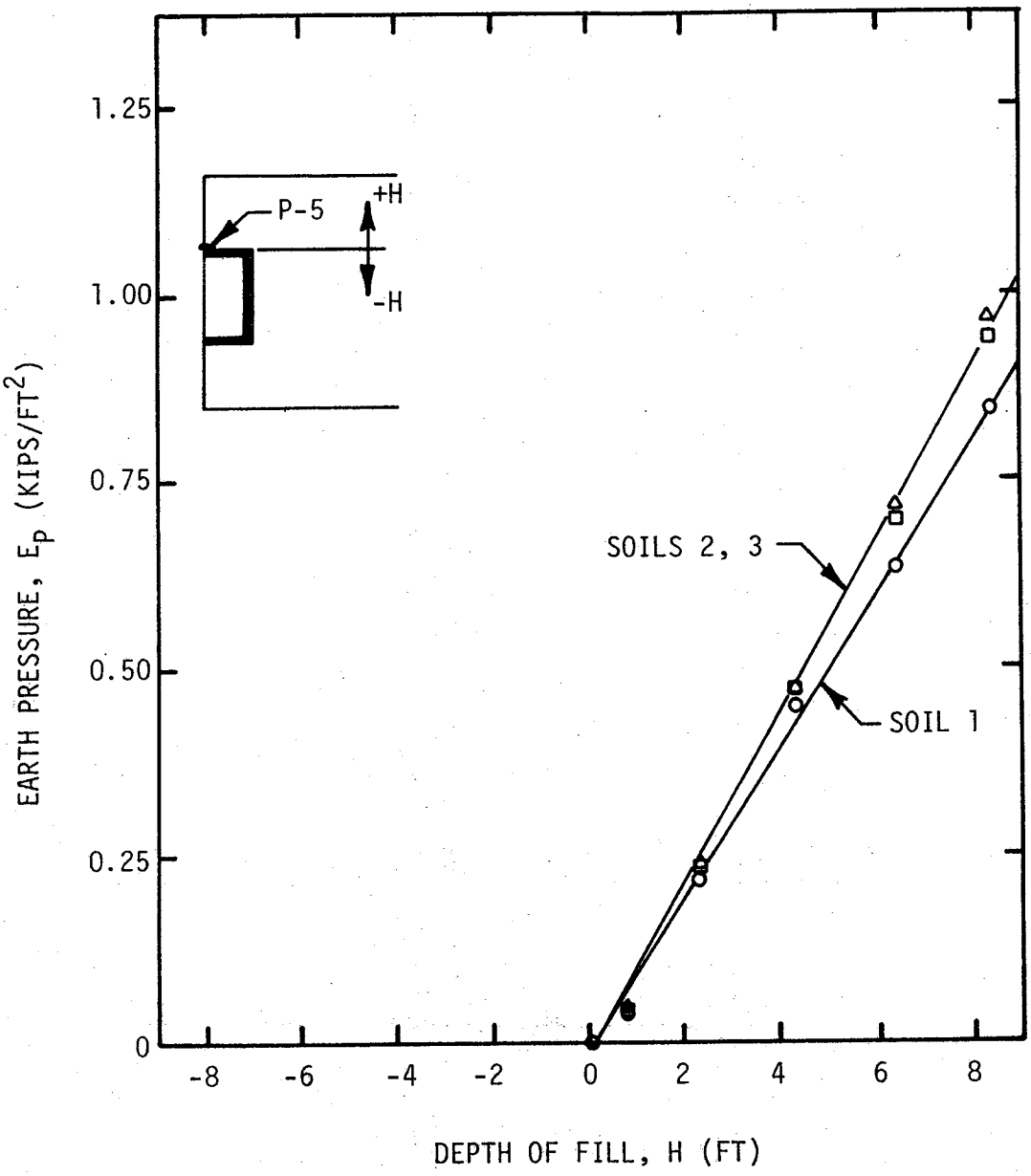

VARIATION OF EARTH PRESSURE WITH DEPTH
OF FILL FOR PRESSURE CELL P-5

FIGURE 4.15

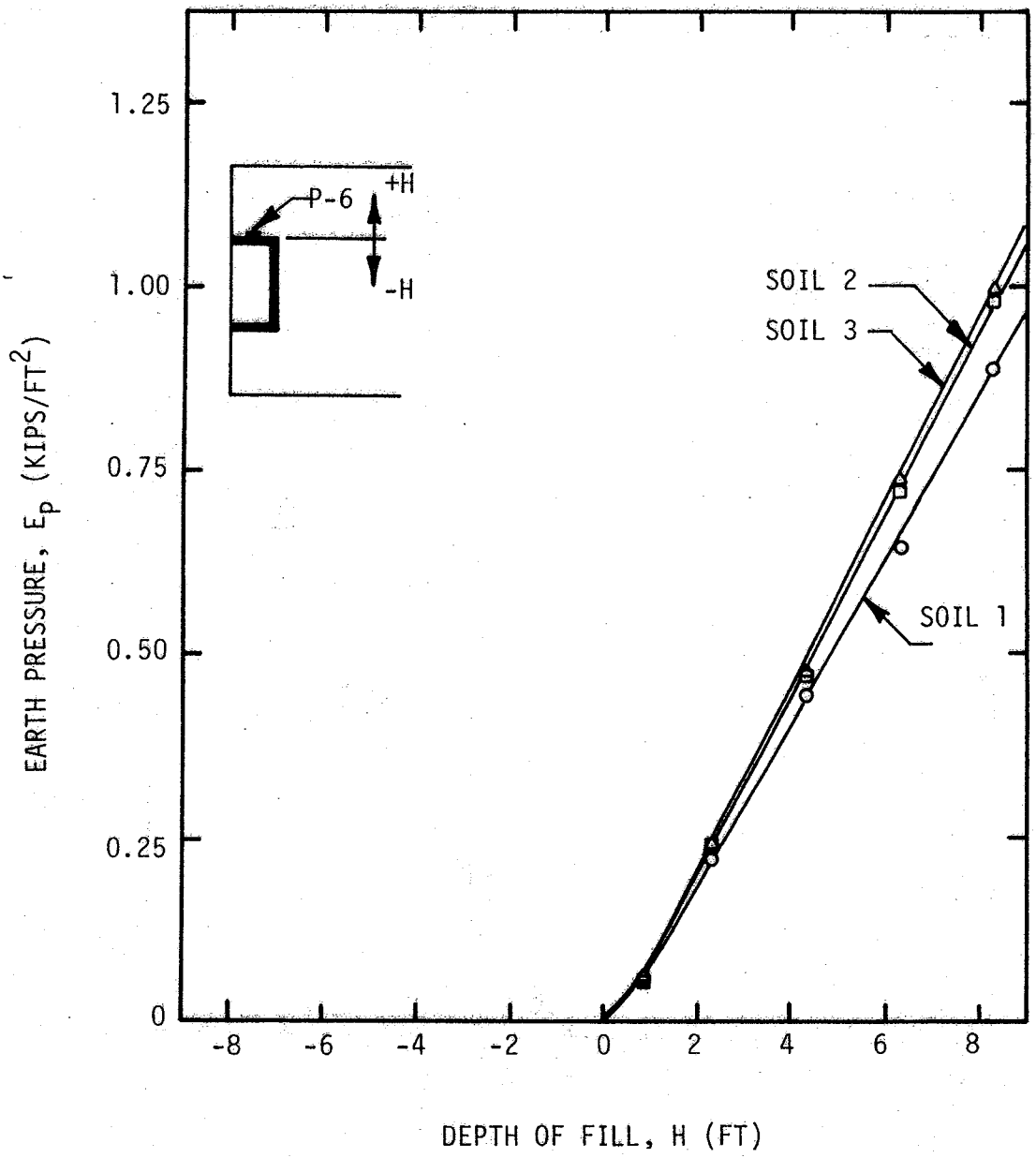

VARIATION OF EARTH PRESSURE WITH
DEPTH OF FILL FOR PRESSURE CELL P-6

FIGURE 4.16

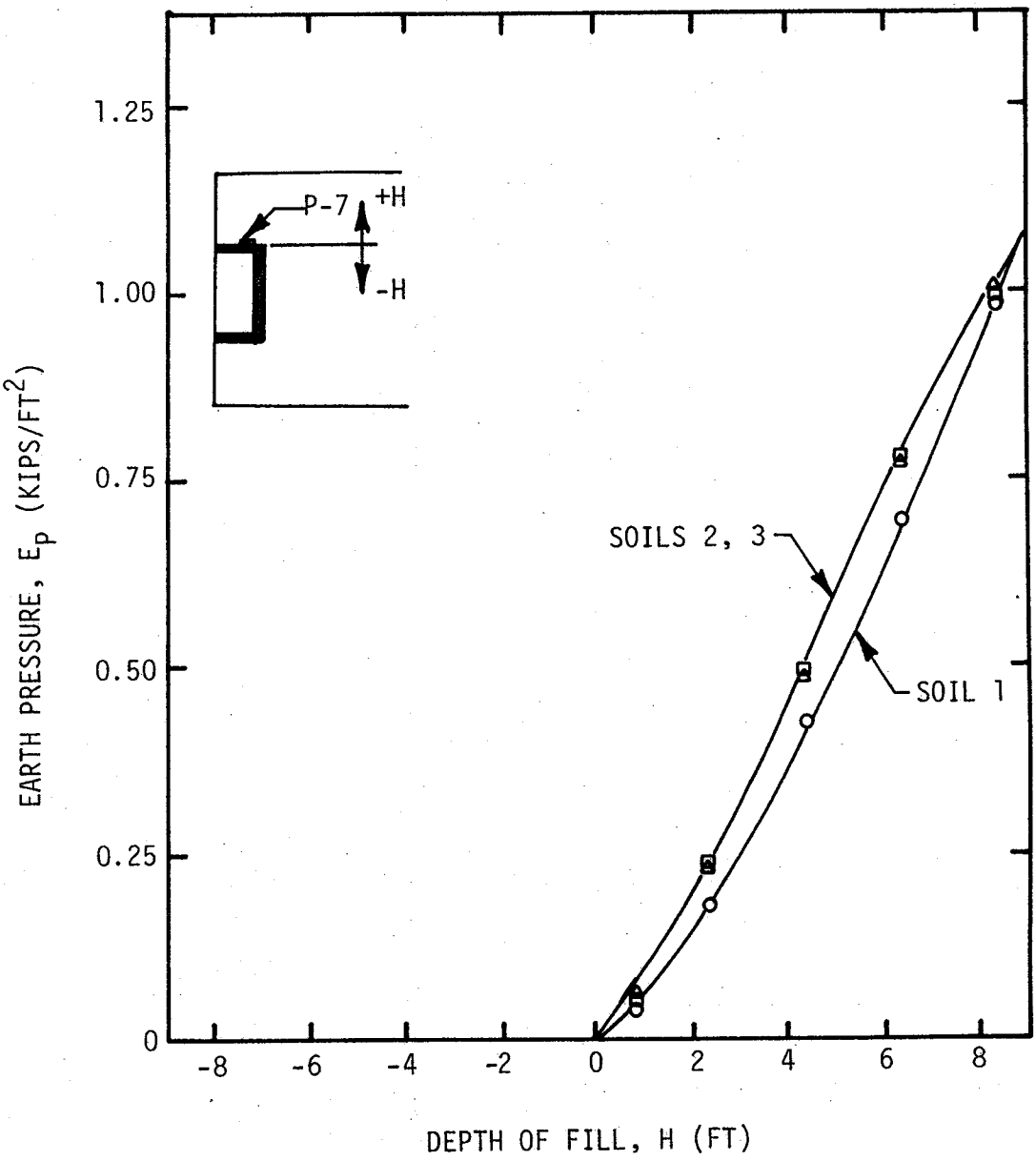

VARIATION OF EARTH PRESSURE WITH DEPTH
OF FILL FOR PRESSURE CELL P-7

FIGURE 4.17

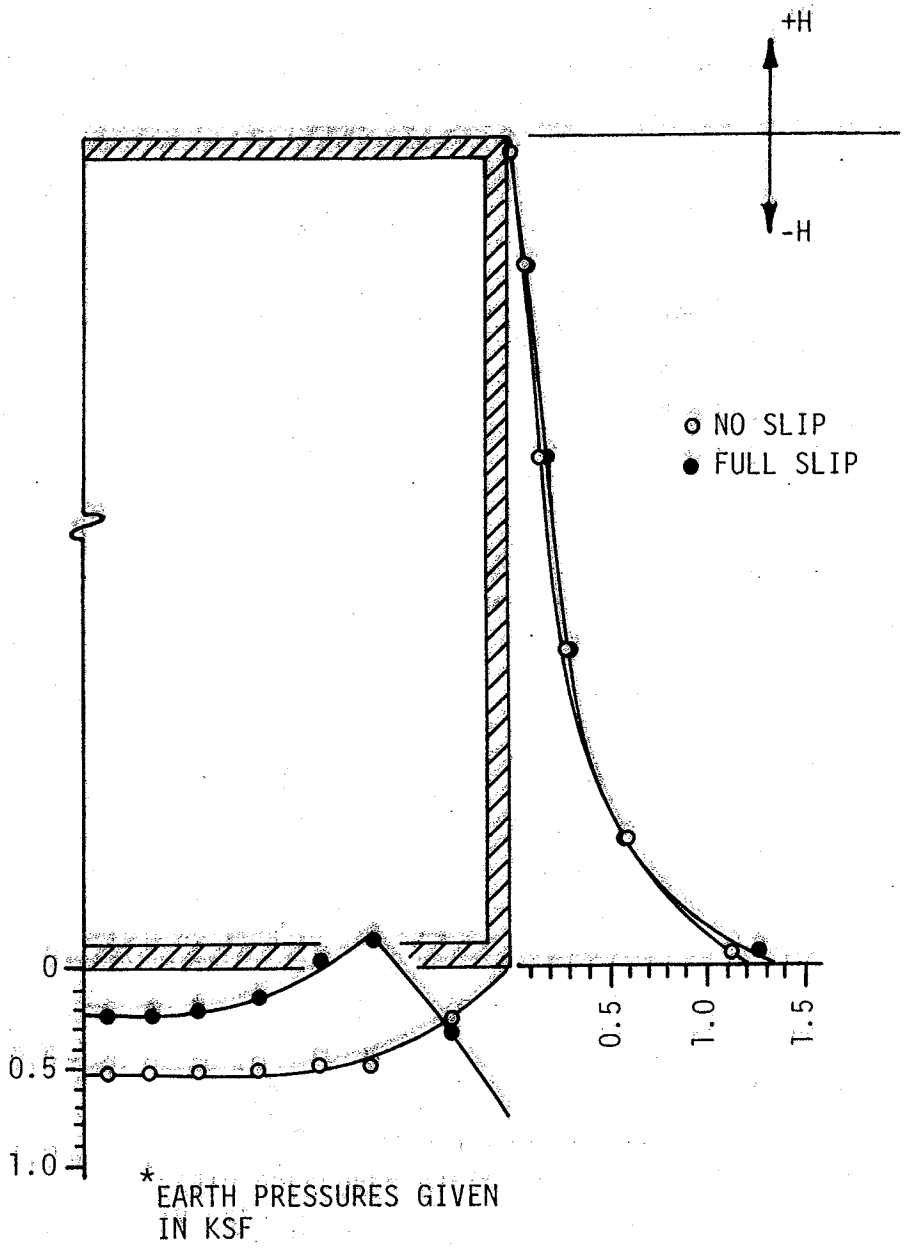

EARTH PRESSURE DISTRIBUTION AROUND THE STRUCTURE, H=0

FIGURE 4.18

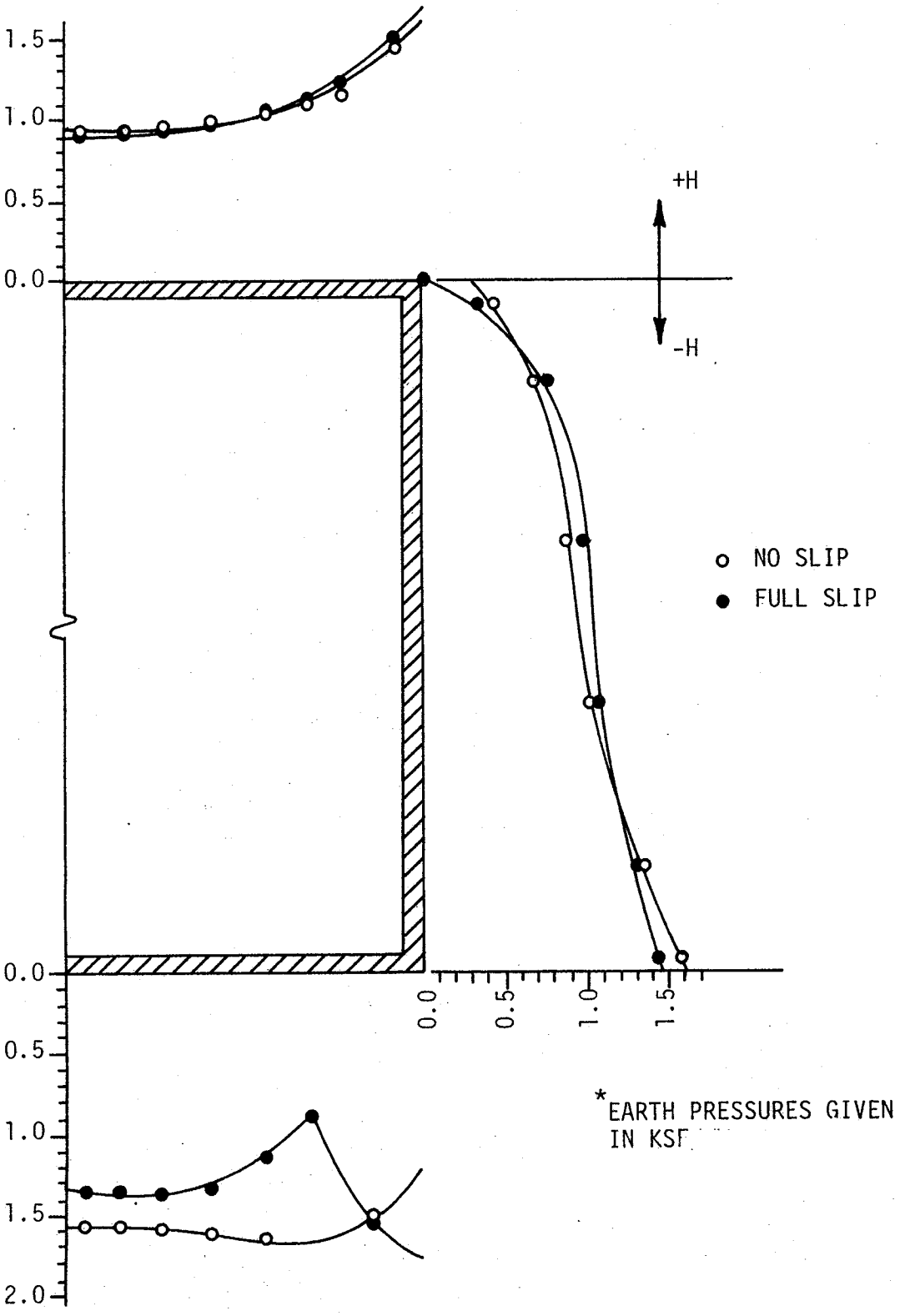

EARTH PRESSURE DISTRIBUTION AROUND THE STRUCTURE, H=8'

FIGURE 4.19

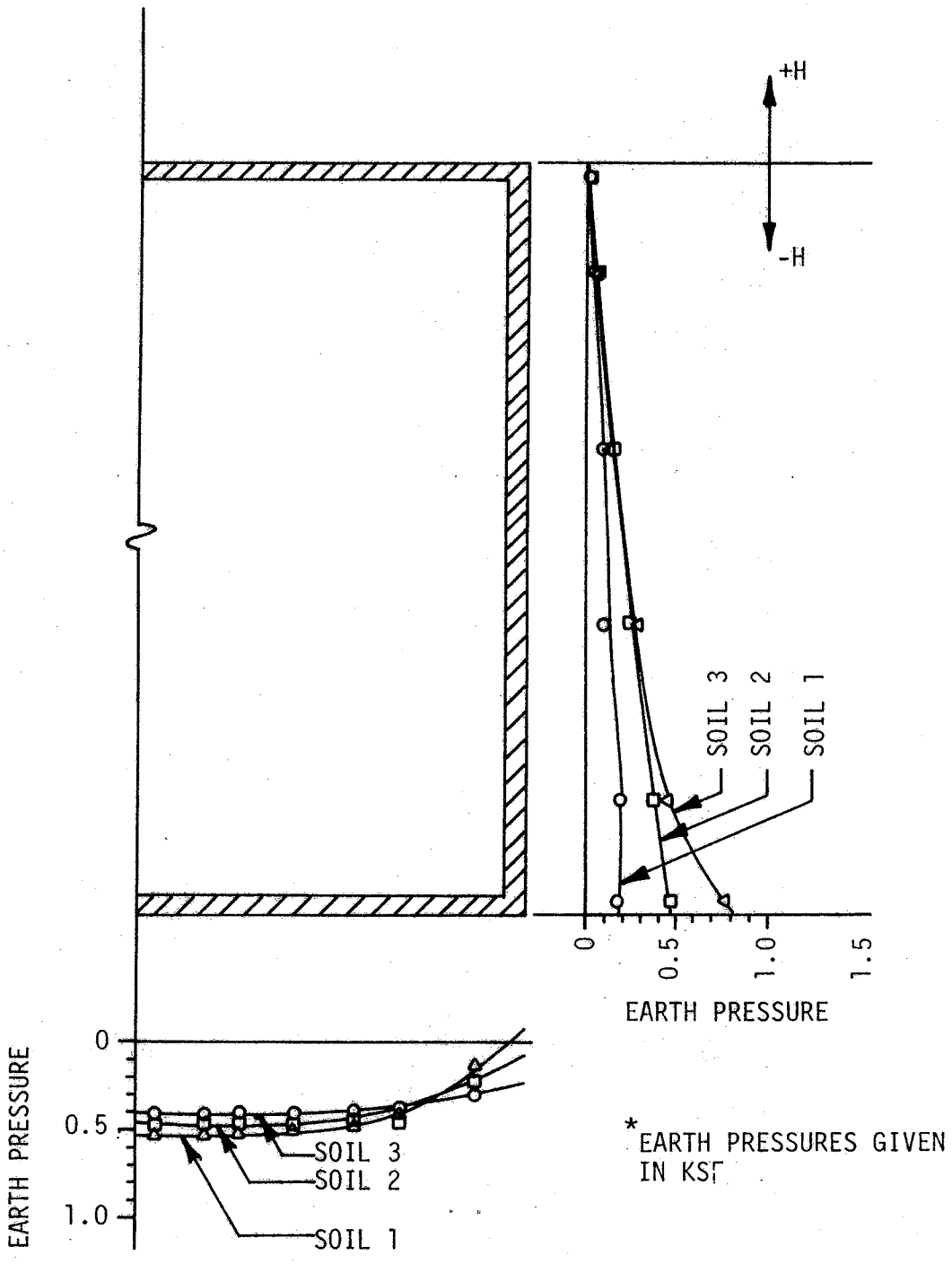

EARTH PRESSURE DISTRIBUTION AROUND THE STRUCTURE, H=0'

FIGURE 4.20

Soil 3 exerting the greatest pressure.

For a depth of fill 8 ft above the crown of the culvert, the earth pressure distributions for the three types of backfill are shown in Fig. 4.21. The difference in pressures is small along the horizontal portions of the culvert. However, along the wall of the culvert there is a significant difference in the calculated earth pressures due to varying shear stresses along the vertical planes that form the prism of soil mass above the culvert. Soil 1, which is compacted on the dry side of optimum, encourages arching considerably due to its high stiffness and shearing resistance and therefore exerts the lowest earth pressures.

4.4.2 Moments

The moments developed in the structural elements were also determined using the finite element analyses. The data on the calculated moments at critical sections around the culvert were reduced from the computer output. The critical sections of the culvert are the corners and midspan sections of the box culvert. At these points, the moments reached their local maximum values.

A comparison of the effects of no-slip and full-slip conditions on the maximum moments are shown in Figs. 4.22 - 4.26. The soil-structure interface effects are slightly more pronounced in the bending moments than they were with earth pressures. In these bending moments, positive values cause tensile stresses on the inside of the culvert. The variation of bending moment with depth of fill for the midspan of the bottom slab is shown in Fig. 4.22. For the no-slip condition the moments increase with added layers of backfill. However, the full-slip condition exhibits a negative moment when the height of fill equals the crown height. This is due to the fact that the full-slip condition permits no downward shear

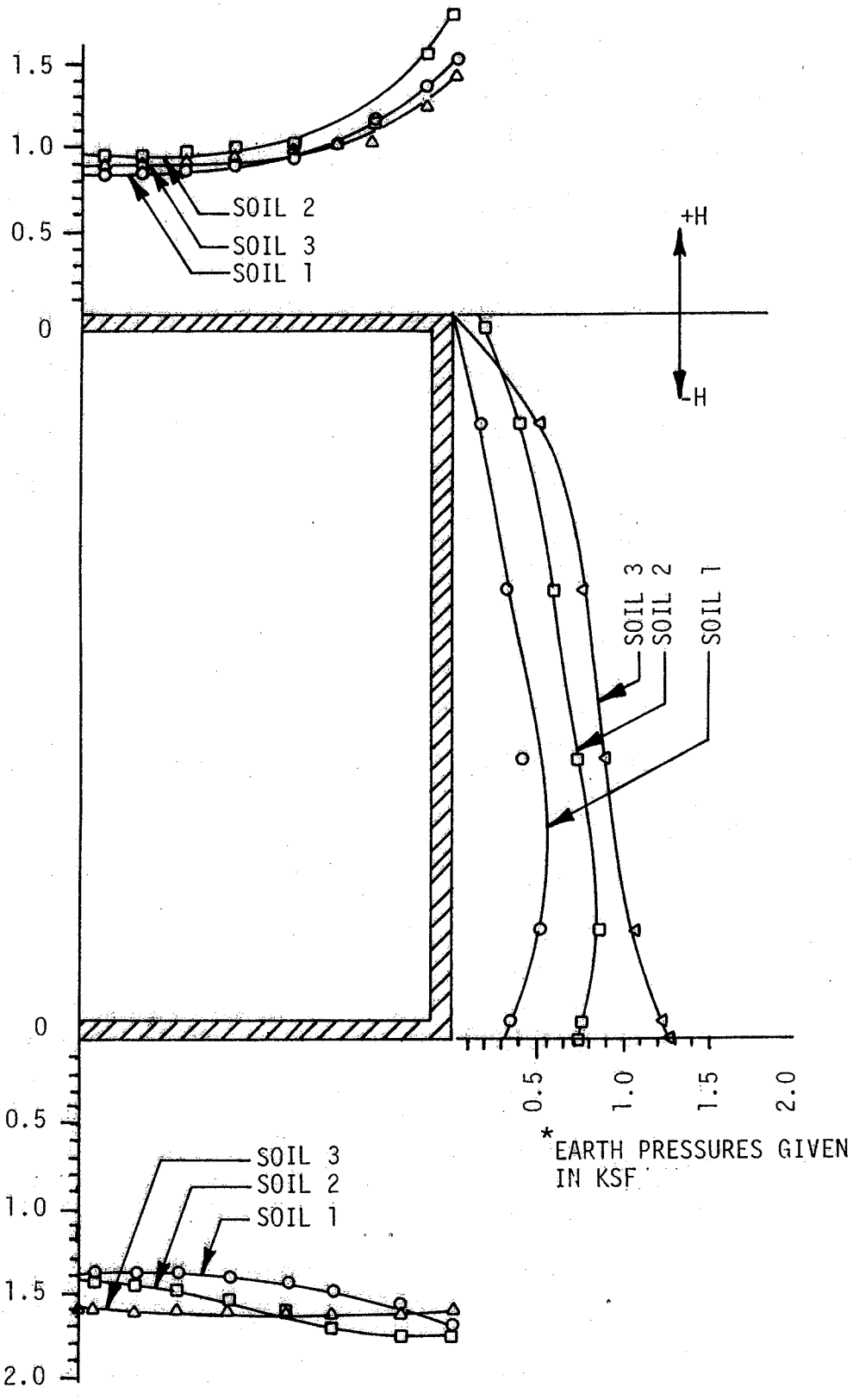

EARTH PRESSURE DISTRIBUTION AROUND THE STRUCTURE, H=8'

FIGURE 4.21

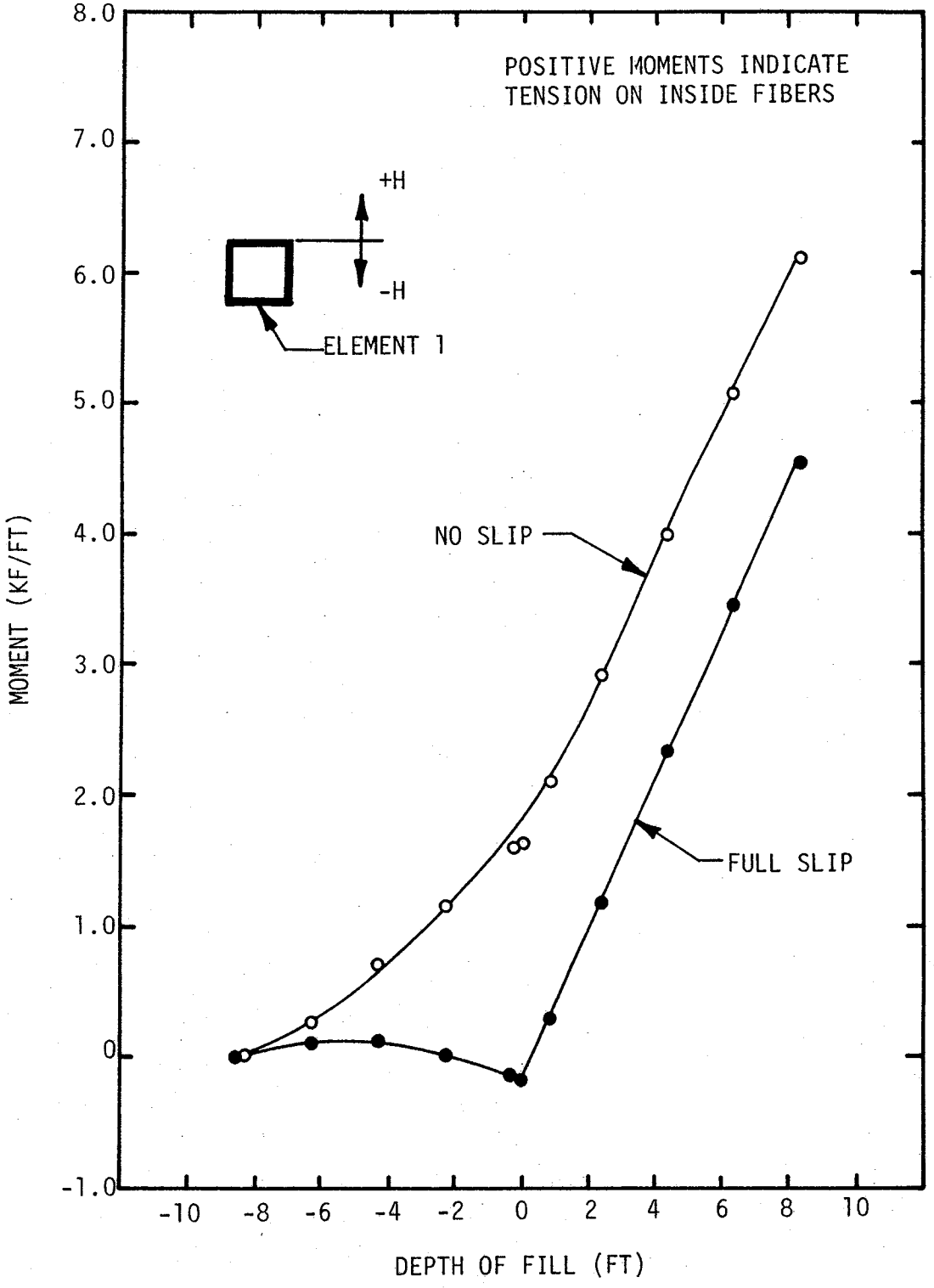

VARIATION OF MOMENT WITH DEPTH OF FILL FOR MIDSPAN OF BOTTOM SLAB

FIGURE 4.22

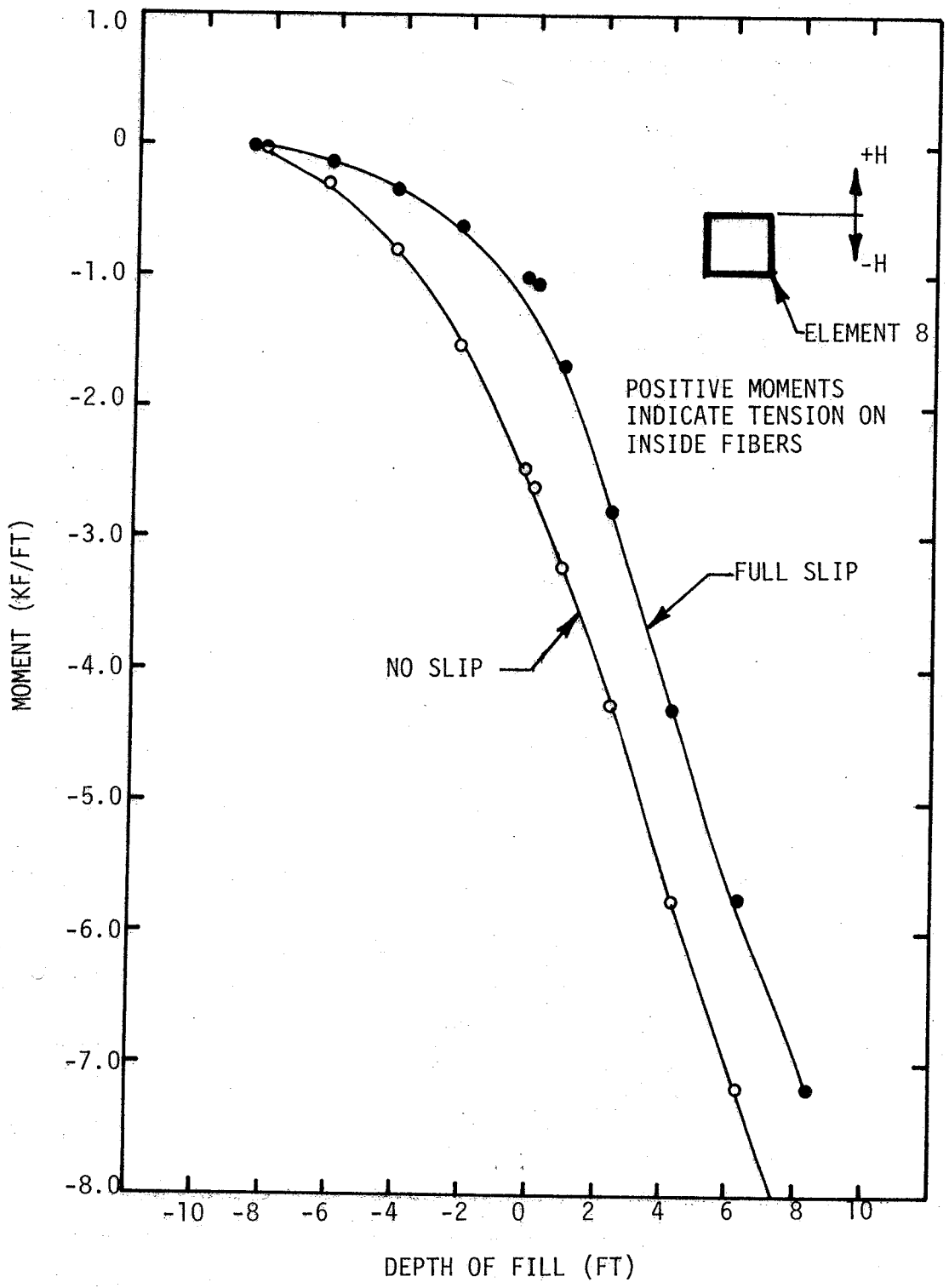

VARIATION OF MOMENT WITH DEPTH OF FILL FOR BOTTOM CORNER

FIGURE 4.23

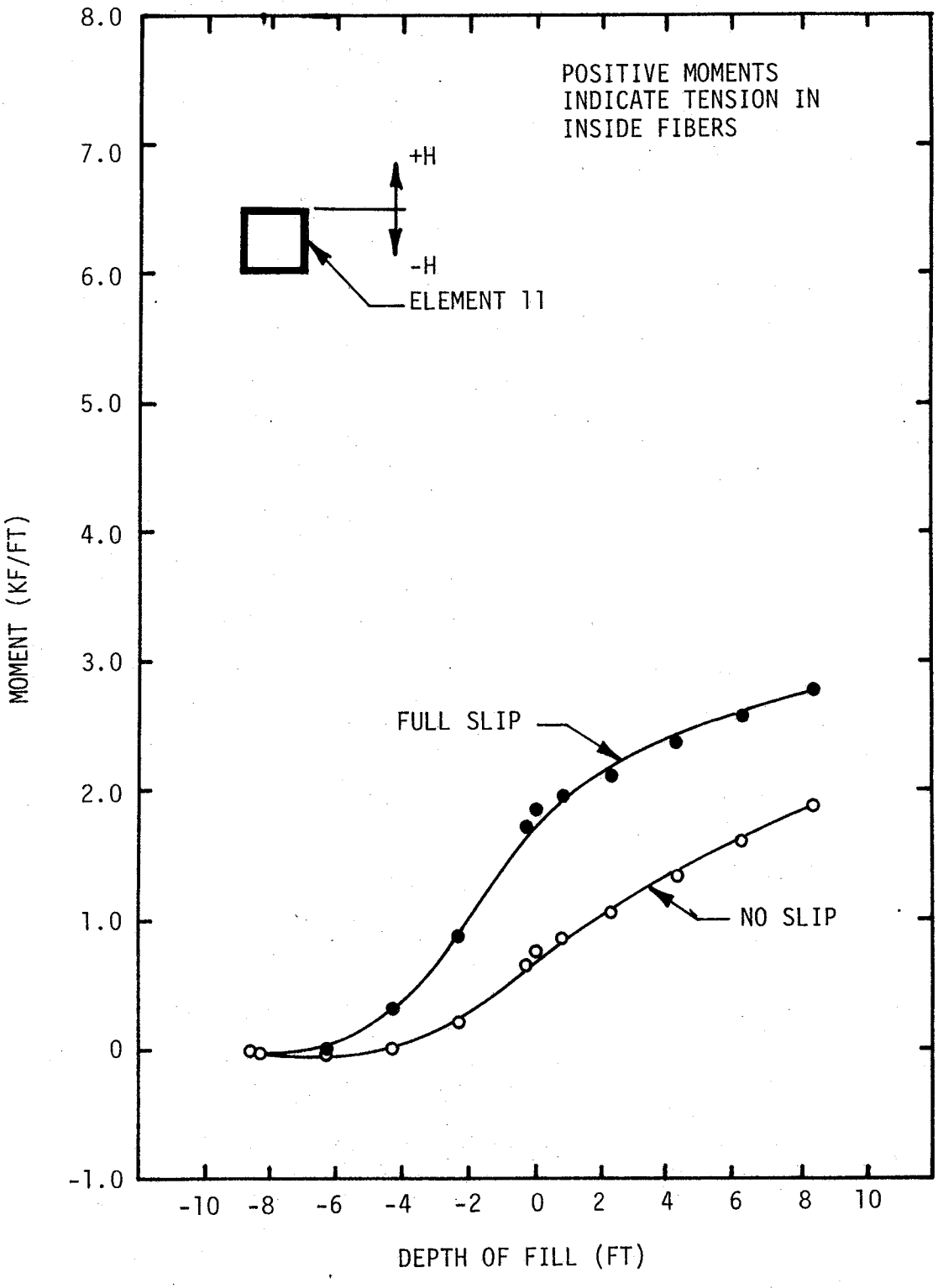

VARIATION IN MOMENT WITH DEPTH OF FILL FOR MIDSPAN OF WALL

FIGURE 4.24

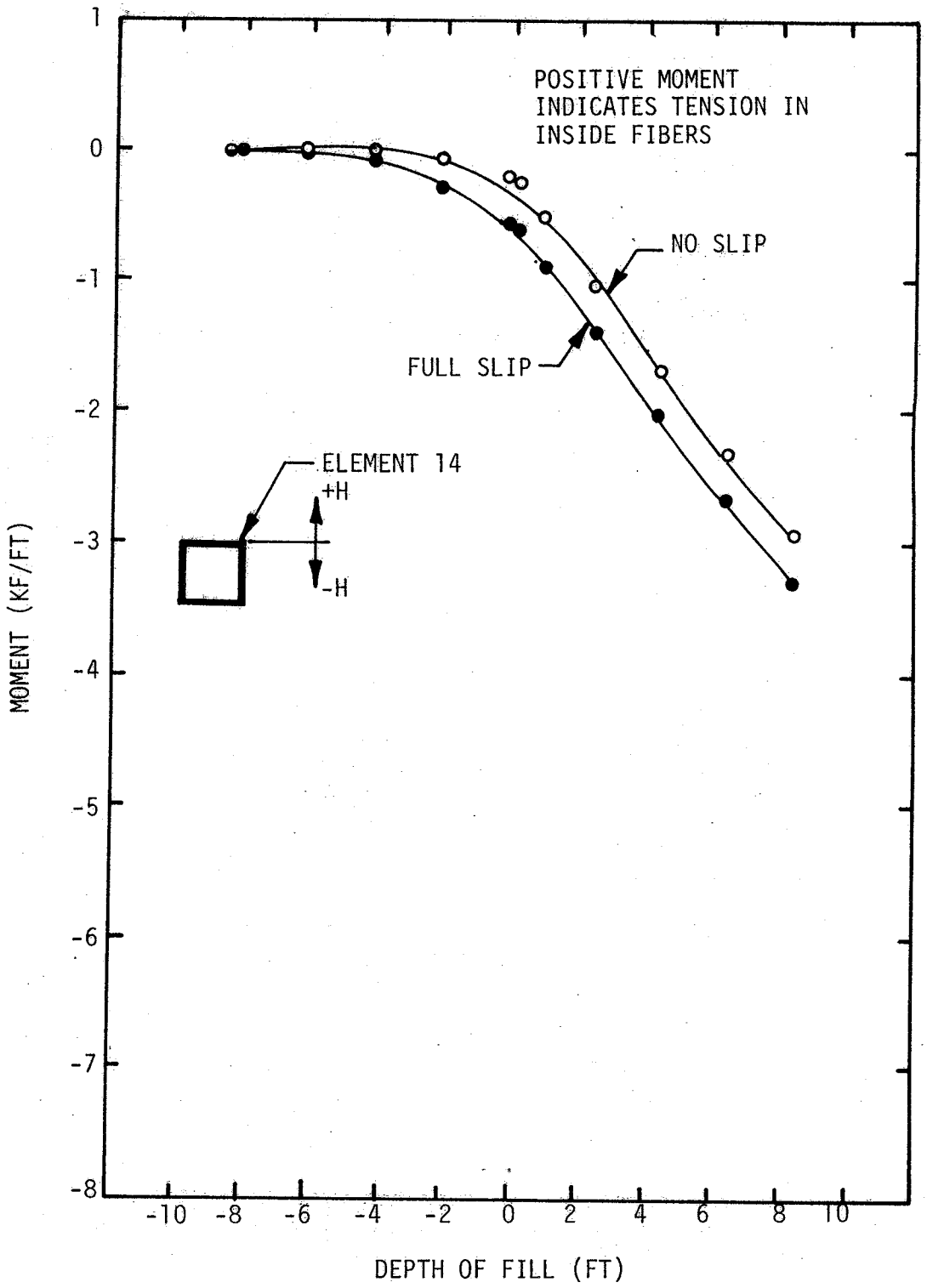

VARIATION OF MOMENT WITH DEPTH OF FILL FOR TOP CORNER

FIGURE 4.25

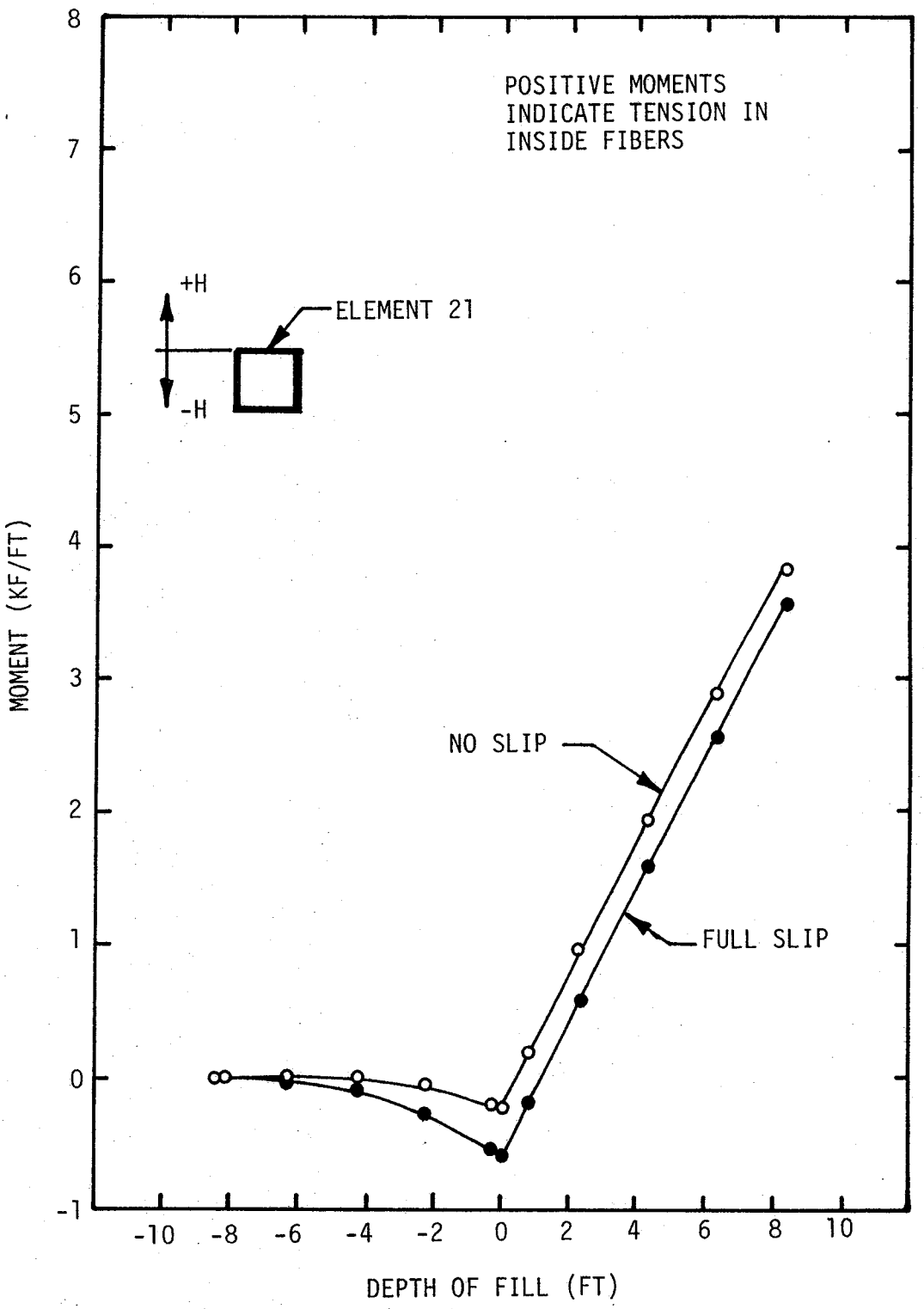

VARIATION OF MOMENT WITH DEPTH OF FILL FOR MIDSPAN OF TOP SLAB

FIGURE 4.26

force on the culvert from the soil while the depth of fill is below the crown height of the culvert. The only forces exerted on the vertical walls are normal pressures which cause an inward deflection of the vertical wall, inducing a negative moment in the bottom slab. This is overcome as soon as the first layer of soil is added above the crown of the culvert.

The variation of moment with depth of fill for the bottom corner of the culvert is given in Fig. 4.23. As expected, the moments are negative throughout the backfill process. Also, the no-slip condition is more critical due to the downward force applied to the sides of the culvert during the backfilling operations. For the midspan of the vertical wall, the variation in moments with backfill depth is given in Fig. 4.24. The moments are positive throughout the process as expected. Also, the full-slip condition is more critical here due to wedging of the soil along the sides of the culvert resulting in higher lateral earth pressures as the backfill level increases.

The variation of moments with depth of fill for the upper corner of the culvert is presented in Fig. 4.25. This section of the culvert exhibits negative moments throughout the process. There is very little difference between the full-slip and no-slip conditions for this section.

The variation in moments with depth of fill for the midspan of the top slab is given in Fig. 4.26. The moments are initially negative due to the inward forces on the sides of the culvert and the induced outward deflection of the top slab. The moments become positive as the depth of fill exceeds the crown of the culvert. There is very little difference between the full-slip and no-slip conditions. However, the full-slip condition produces somewhat larger negative moments due to larger lateral

pressures on the culvert.

The effects of backfill properties on calculated moments at critical sections of the box culvert are shown in Figs. 4.27-4.31. These analyses were done using the no-slip condition. As before, a positive moment produces tension on the inside of the culvert.

The variation of moments with depth of fill for the midspan section of the bottom slab is presented in Fig. 4.27. The results for the three soils are practically identical. As expected, moments are positive through the whole process.

The calculated moments in the bottom corner of the culvert are given in Fig. 4.28. The moments are negative throughout the process. Also, Soil 3 exhibits the most critical behavior, wheras Soil 1 is the least critical. This is due to the desirable properties of Soil 1 and undesirable strength and modulus properties of Soil 3.

The variation of moments with depth of fill for the midspan section of the vertical wall is given in Fig. 4.29. This section shows interesting results. The difference in moments predicted by the finite element analyses and shown in Fig. 4.29 is the product of primarily two parameters; the differences between soil properties, and the no-slip soil-structure interface condition used in the analyses.

First of all, the lateral pressures exerted on the sides of the culvert vary greatly with soil stiffness as shown in 4.20. Soil 1 is the stiffest of the three soils, and therefore exerts the least lateral earth pressure. Furthermore, the no-slip condition used for the analyses transmits the backfill weight to the culvert and this becomes significant as the level of backfill increases. This vertical component of the backfill load induces a small inward deflection of the bottom slab, and an outward

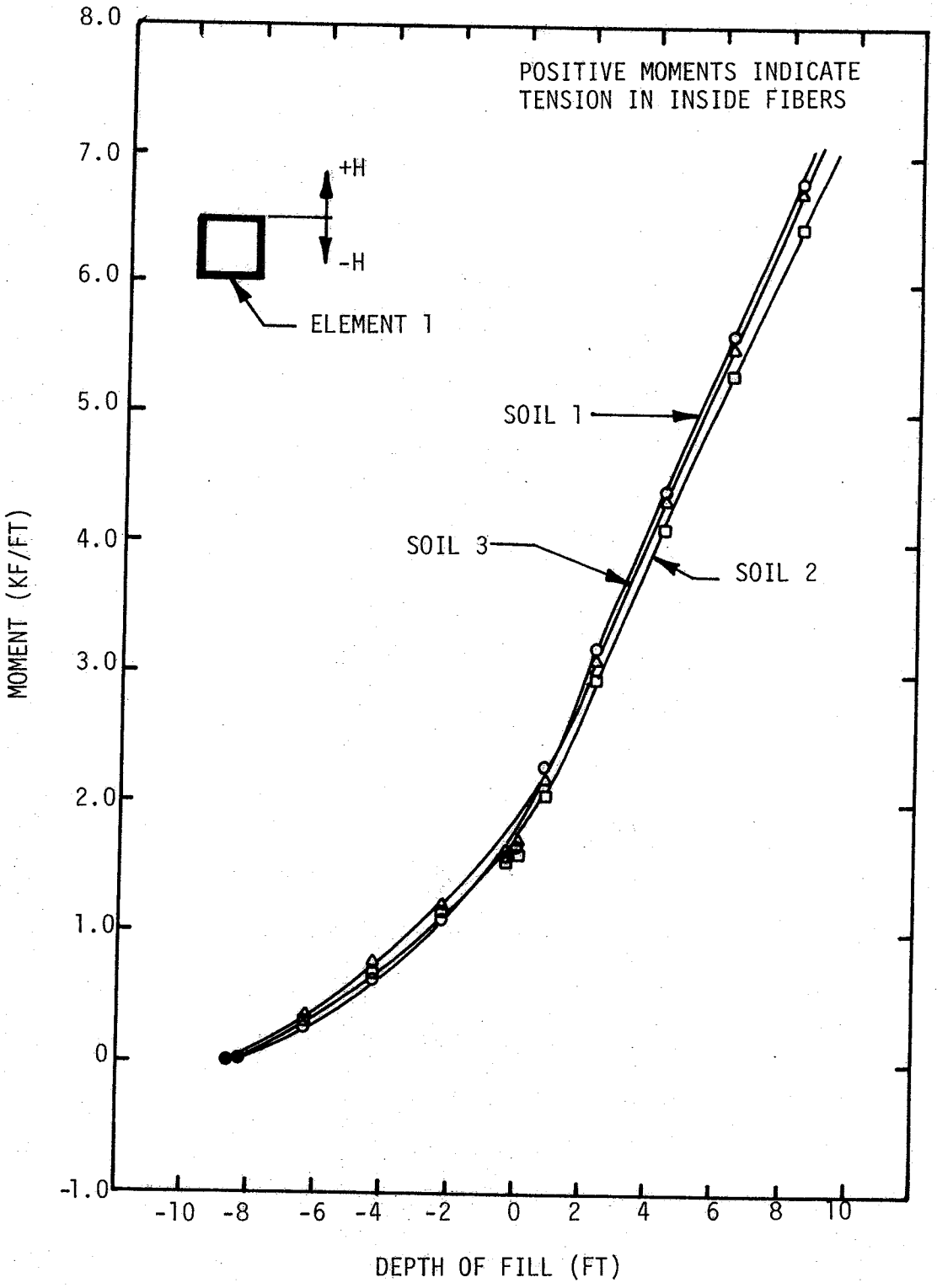

VARIATION OF MOMENT WITH DEPTH OF FILL FOR
MIDSPAN OF BOTTOM SLAB

FIGURE 4.27

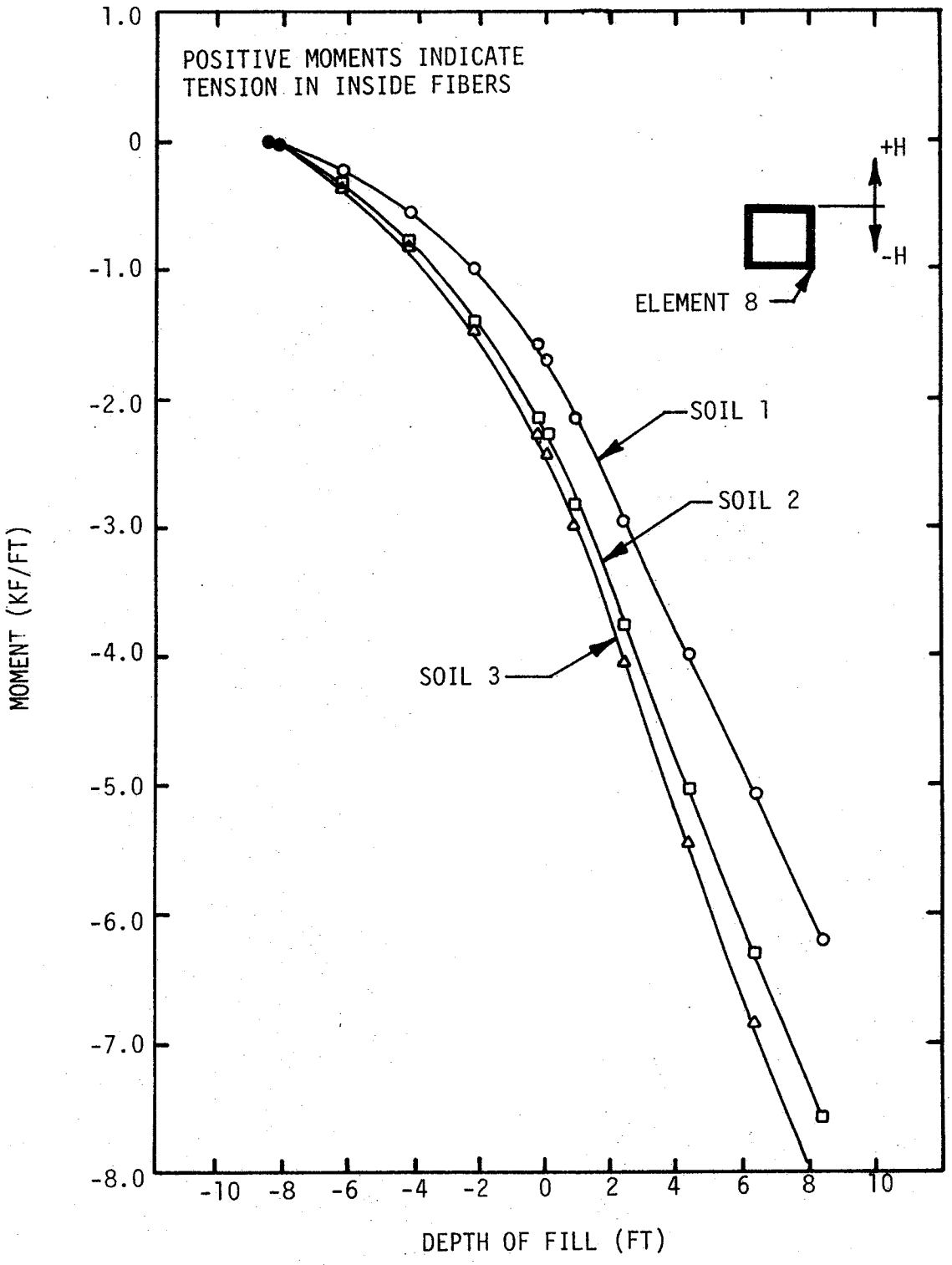

VARIATION OF MOMENT WITH DEPTH OF FILL FOR BOTTOM CORNER

FIGURE 4.28

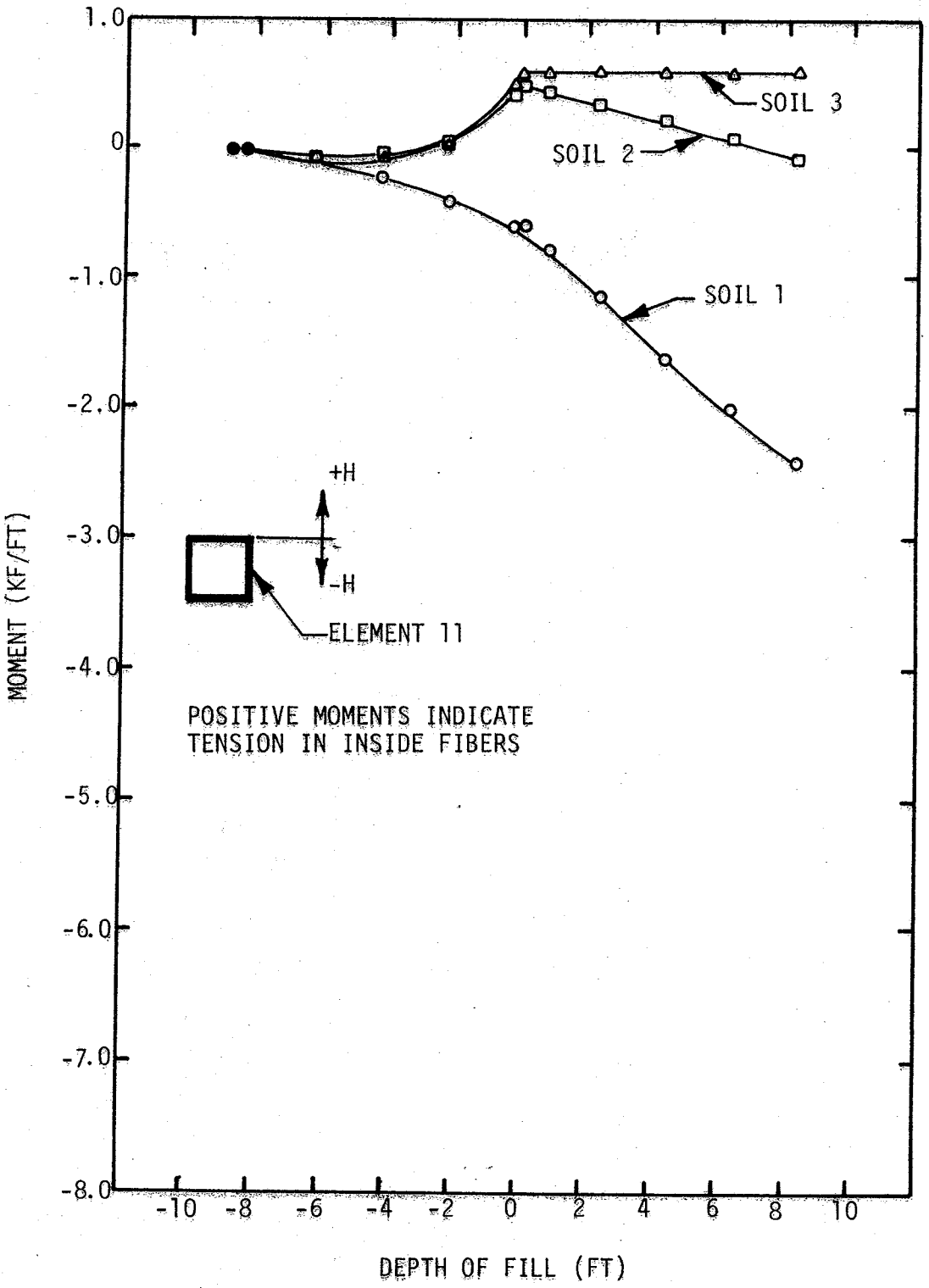

VARIATION OF MOMENT WITH DEPTH OF FILL FOR MIDSPAN OF WALL

FIGURE 4.29

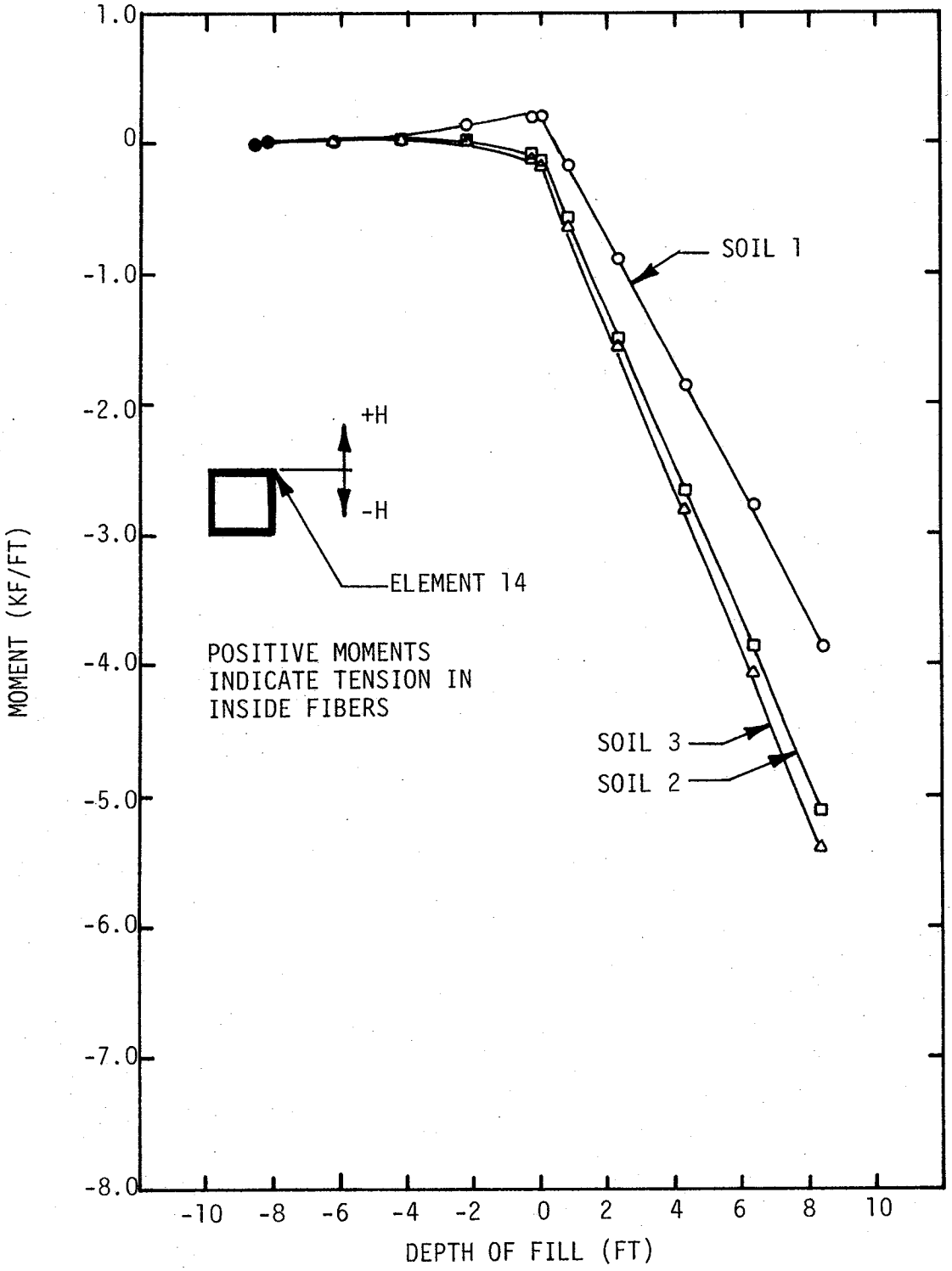

VARIATION OF MOMENT WITH DEPTH OF FILL FOR TOP CORNER

FIGURE 4.30

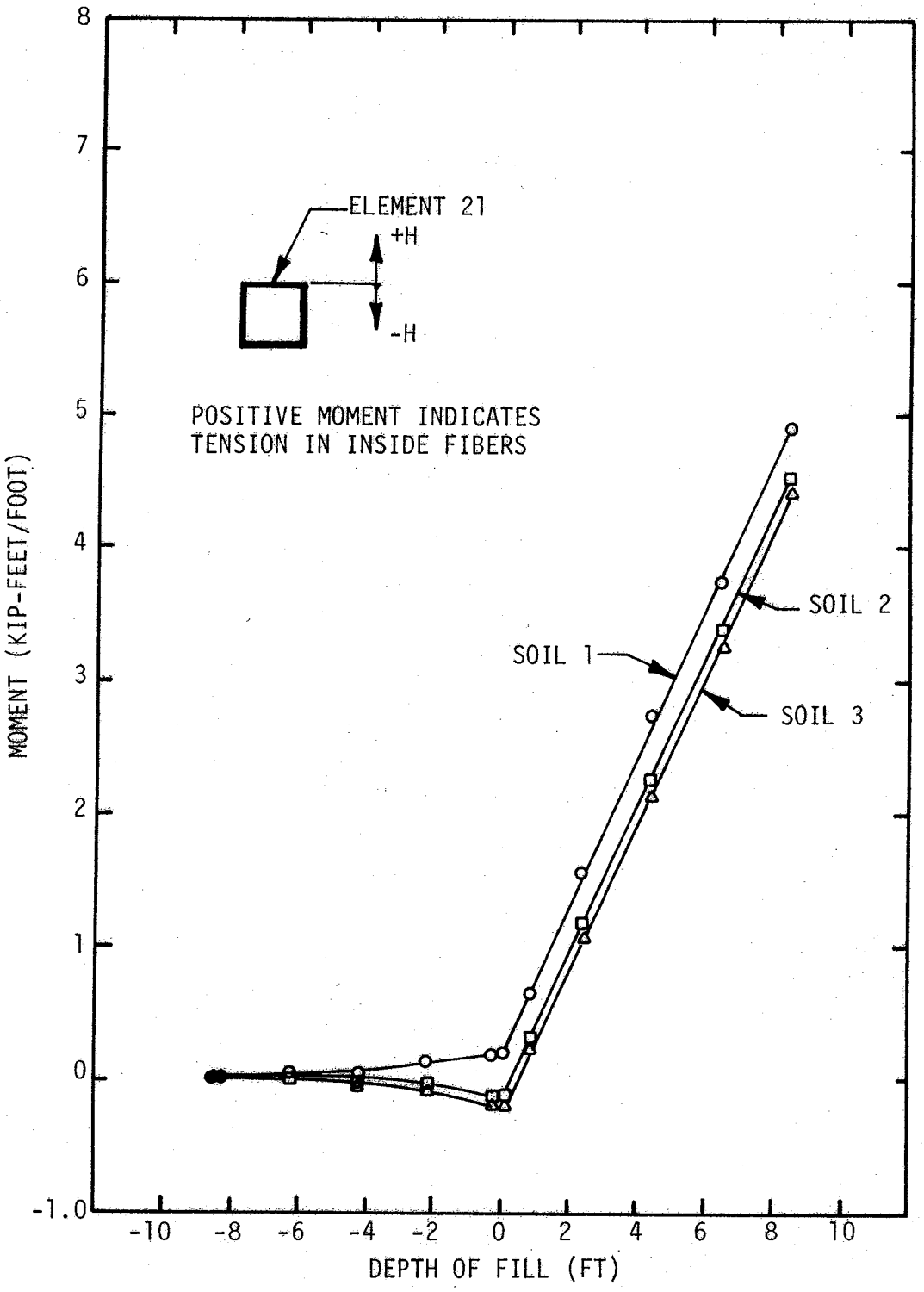

VARIATION OF MOMENT WITH DEPTH OF FILL FOR MIDSPAN OF TOP SLAB

FIGURE 4.31

deflection at the midspan of the vertical wall of the culvert, as shown in Fig. 4.32a. This outward deflection causes the negative moment shown in Fig. 4.29. As the height of fill becomes larger, the vertical force increases, causing a larger negative moment at the mid-section of the vertical wall.

This is not the case for Soils 2 and 3, however. These soils are not as stiff as Soil 1 and therefore the lateral pressures exerted by these soils are greater than that for Soil 1. Due to the larger lateral pressures, inflection points develop in the wall of the culvert, as shown in Fig. 4.32b, and in the moment distribution diagrams shown in Figs. 4.33 and 4.34. This would account for the negative moments at the corners and the positive moments at the midspan for the softer soils.

It should be noted that the deflections mentioned are very small. The illustrations of deflected shapes in Fig. 4.32 are somewhat exaggerated in magnitude.

The variation of moments with depth of fill for the upper corner of the culvert is shown in Fig. 4.30. The three soils show little difference, with Soil 1 being the least critical and Soil 3 the most critical.

For the midspan of the top slab, the moments are shown in Fig. 4.31. There is very little difference between the results of the three soils. All soils exhibit small moments until the depth of fill exceeds the crown level of the culvert. Here, all soils show positive moments increasing with depth of fill.

The moment distribution around the structure for a depth of fill equal to the crown height of the culvert is shown in Fig. 4.33. The comparison of the results obtained for the full-slip and no-slip conditions

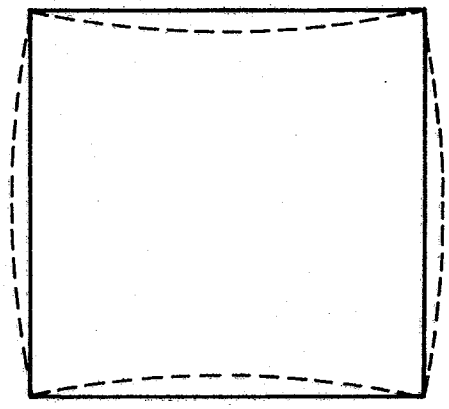

a. - DEFLECTIONS OF CULVERT DUE TO SOIL ONE LOADS

·NOT TO SCALE·

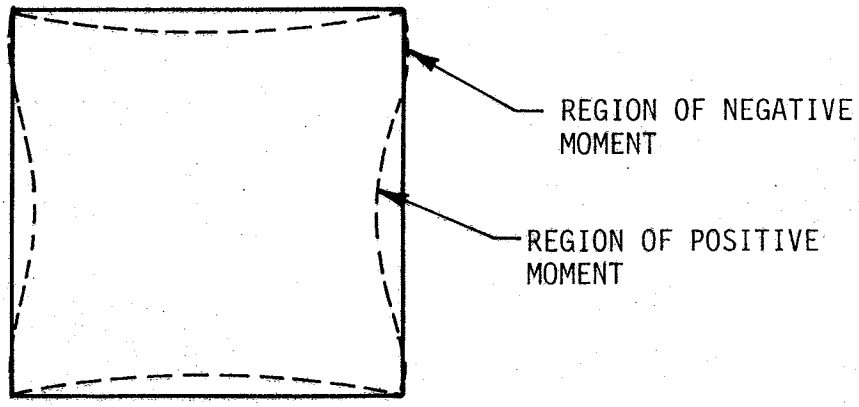

b. - DEFLECTIONS OF CULVERT DUE TO SOILS TWO AND THREE

·NOT TO SCALE·

IDEALIZED DEFLECTIONS OF CULVERT UNDER BACKFILL LOADS

FIGURE 4.32

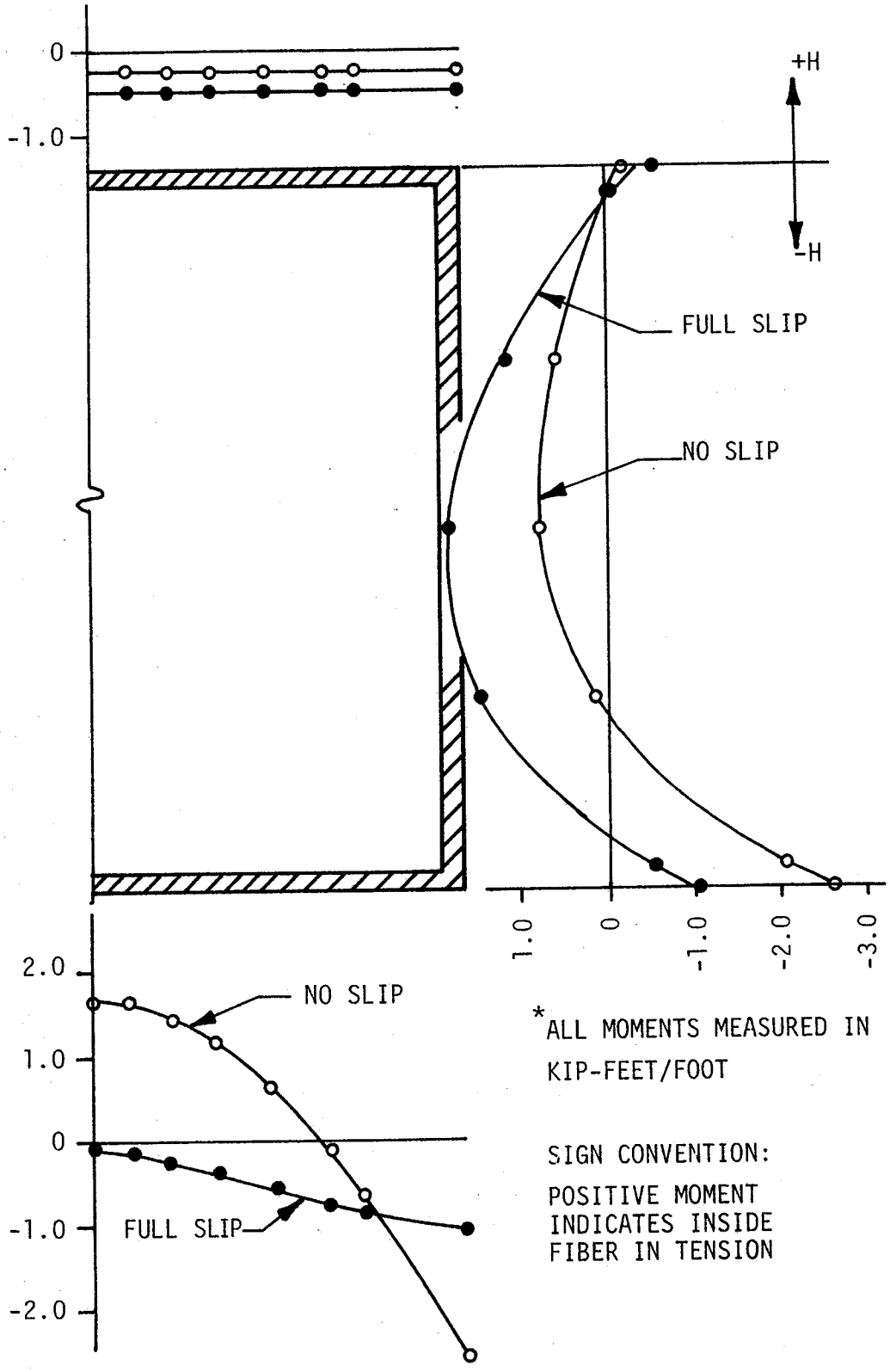

DISTRIBUTION OF MOMENTS AROUND STRUCTURE, H=0

FIGURE 4.33

indicates that the full-slip condition is much more critical on the sides of the box culvert, while the no-slip condition is much more critical on the bottom of the culvert. This is due to the large downward force exerted with the no-slip condition, and greater lateral pressures with the full-slip condition, respectively.

For a backfill height of 8 ft above the crown of the culvert, Fig. 4.34 shows the moment distribution around the structure. Along the bottom of the culvert the no-slip condition produces the larger moments, while along the side, the full-slip condition exhibits the larger moments. Along the top slab, the results are almost identical.

For the comparison of effects due to varying backfill properties, Fig. 4.35 shows the moment distribution with a depth of fill level with the crown of the culvert. Soils 2 and 3 show inflection points on the vertical walls indicating a change in the sign of the moment. This supports the results given in Fig. 4.29. Moments for Soil 1 are negative along the entire vertical wall.

The moment distribution for a backfill height of 8 ft above the crown of the culvert is shown in Fig. 4.36. Along the top and bottom slabs, results of the three soils are almost identical. The vertical wall shows the largest differences, with Soil 1 exhibiting negative moments all along the wall for the reasons explained in detail previously.

4.2.3 Stresses and Strains

Stresses on the inside and outside of the culvert were calculated for sections where strain measurements will become available from the field observations.

The predicted fiber stress on the inside of the culvert for the midspan of the top slab is shown in Fig. 4.37. As the backfill is added,

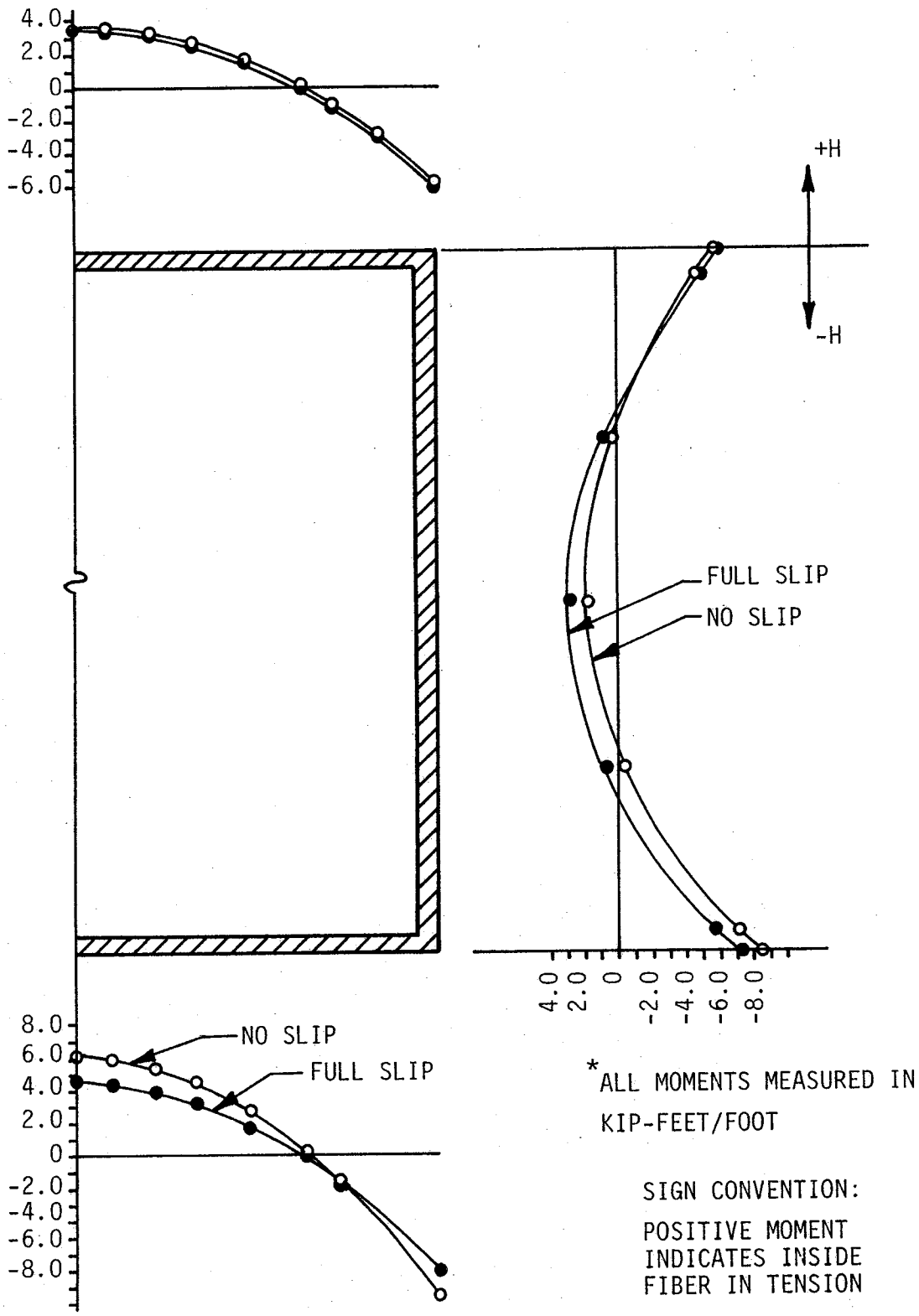

DISTRIBUTION OF MOMENTS AROUND STRUCTURE, H=8'

FIGURE 4.34

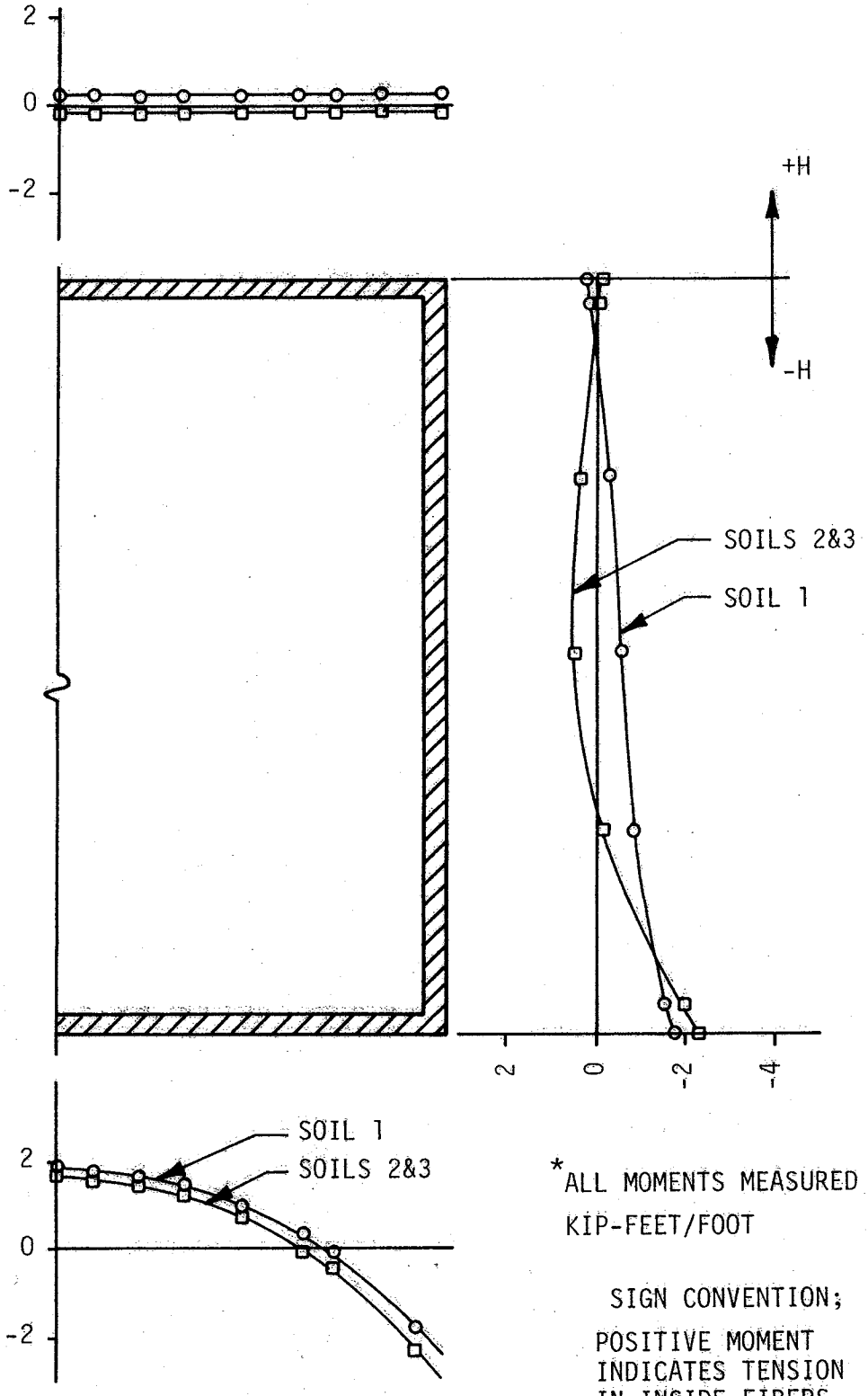

DISTRIBUTION OF MOMENTS AROUND STRUCTURE, H=0

FIGURE 4.35

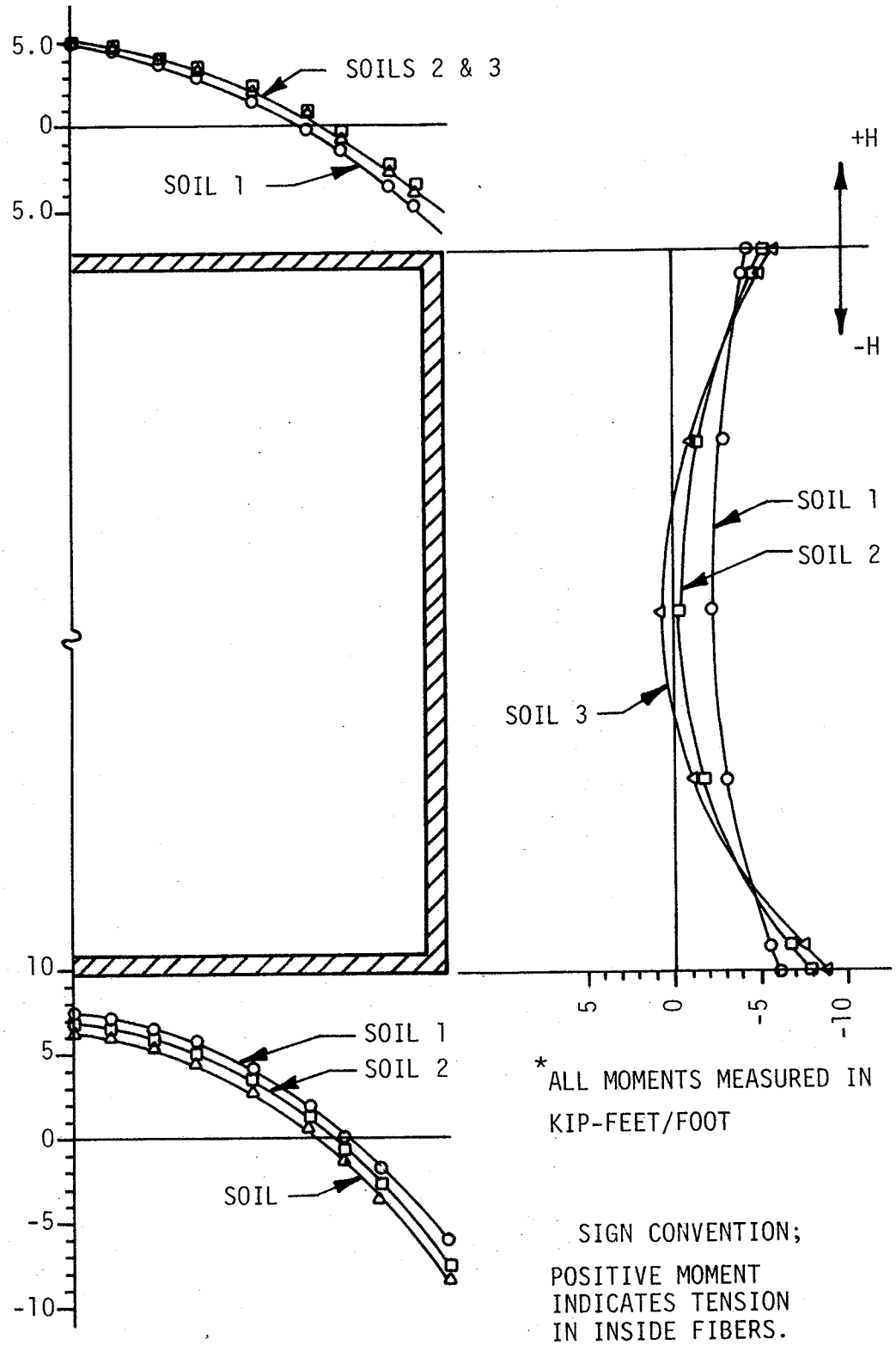

DISTRIBUTION OF MOMENTS AROUND STRUCTURE WITH H-8'

FIGURE 4.36

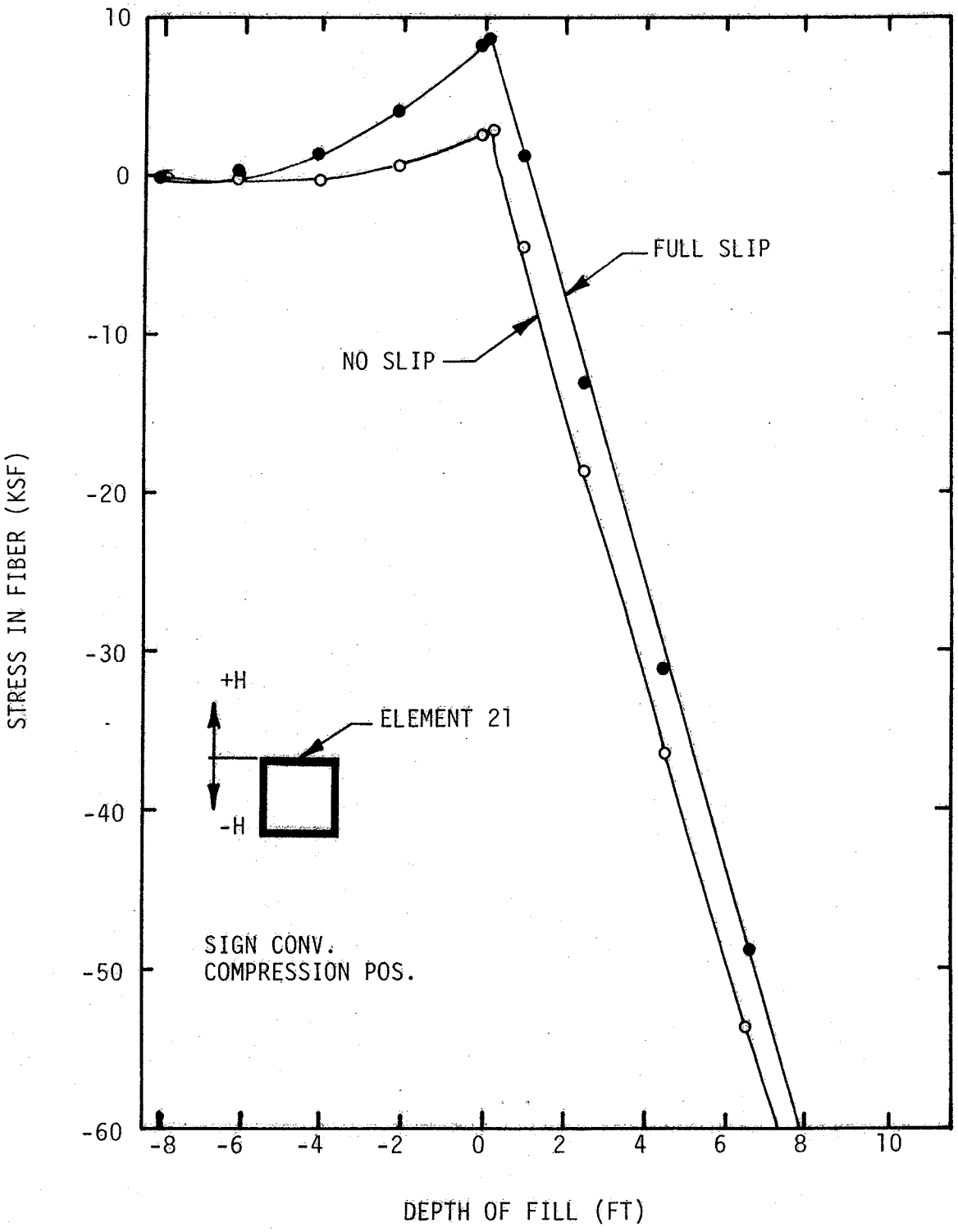

VARIATION OF FIBER STRESS WITH DEPTH OF FILL
INSIDE STRESSES, BEAM ELEMENT 21

FIGURE 4.37

the inside fibers are subjected to compressive [positive] stresses due to the deflections of the top slab. However, as the fill height exceeds the crown height of the culvert, the stresses become tensile [negative] and increase in magnitude almost linearly as further backfill is placed over the structure. The outside fiber stresses for this section of the culvert are shown in Fig. 4.38. The stresses are tensile during the initial stages and become compressive as the backfill rises above the crown of the culvert. In both cases shown in Figs. 4.37 and 4.38, the no-slip condition is more critical than the full-slip condition.

The variation of inside fiber stress with depth of fill for the upper corner of the box culvert is shown in Fig. 4.39. The stresses begin slightly tensile, but soon become compressive as further backfill is added. After the backfill height exceeds the crown height, the stresses increase linearly with the depth of fill.

The outside fiber stresses for the upper corner are shown in Fig. 4.40. The stresses start slightly compressive, but become tensile as the depth of fill increases.

In both cases shown in Figs. 4.39 and 4.40, the full-slip condition produces the most critical results. The deflections produced during backfilling for the full-slip condition are much more critical on the corners of the culvert. However, the no-slip condition produces more critical deflections at the midspan of the top slab, which explains the results shown previously in Figs. 4.37 and 4.38.

The effects of backfill properties on the fiber stresses are shown in Figs. 4.41-4.44. The variation of inside fiber stress of the midspan section of the top slab with depth of fill is shown in Fig. 4.41. The results are very similar after the backfill height exceeds the crown of

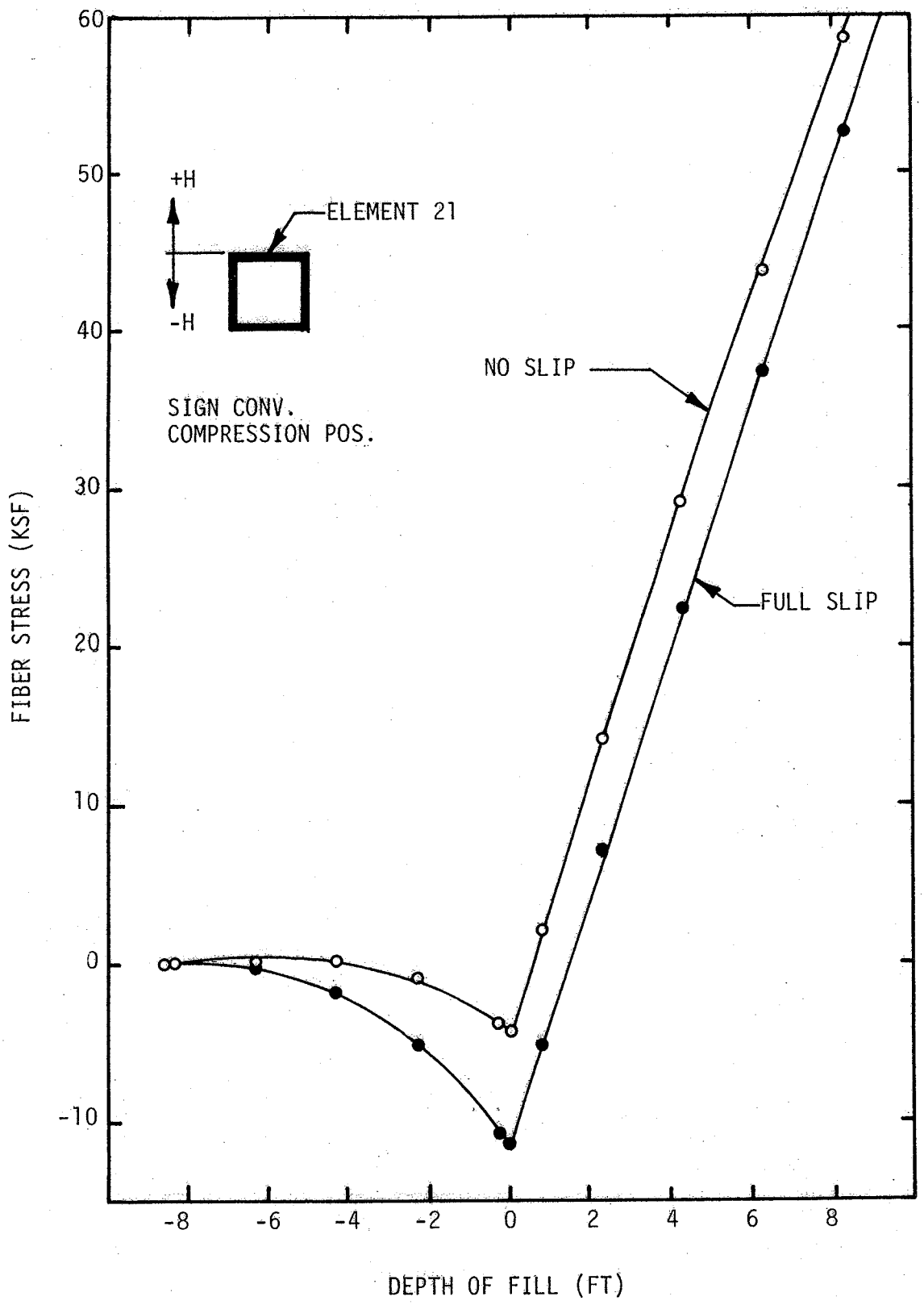

VARIATION OF FIBER STRESS WITH DEPTH OF FILL OUTSIDE STRESSES, ELEMENT 21

FIGURE 4.38

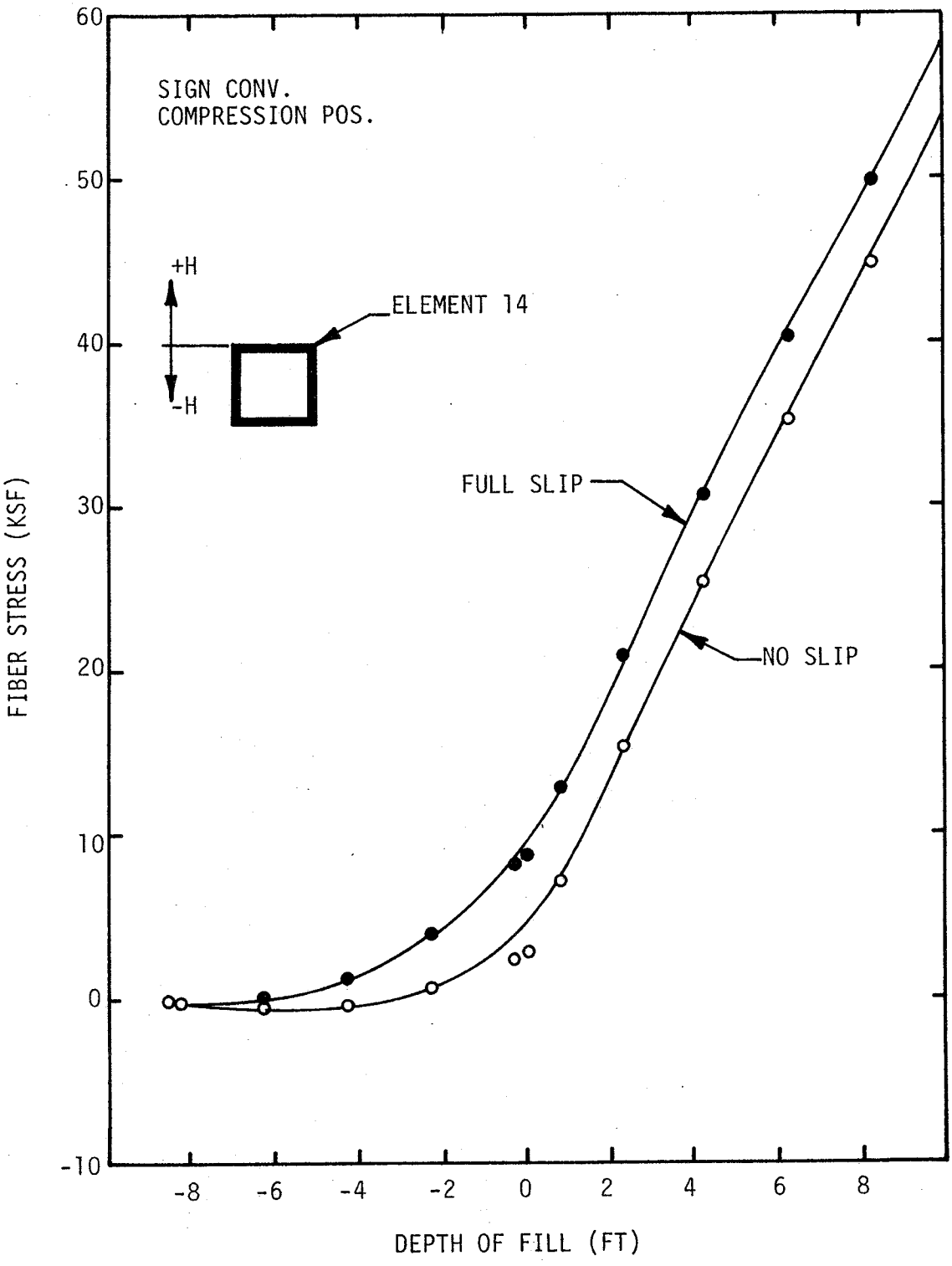

VARIATION OF FIBER STRESS WITH DEPTH OF FILL INSIDE STRESS, ELEMENT 14

FIGURE 4.39

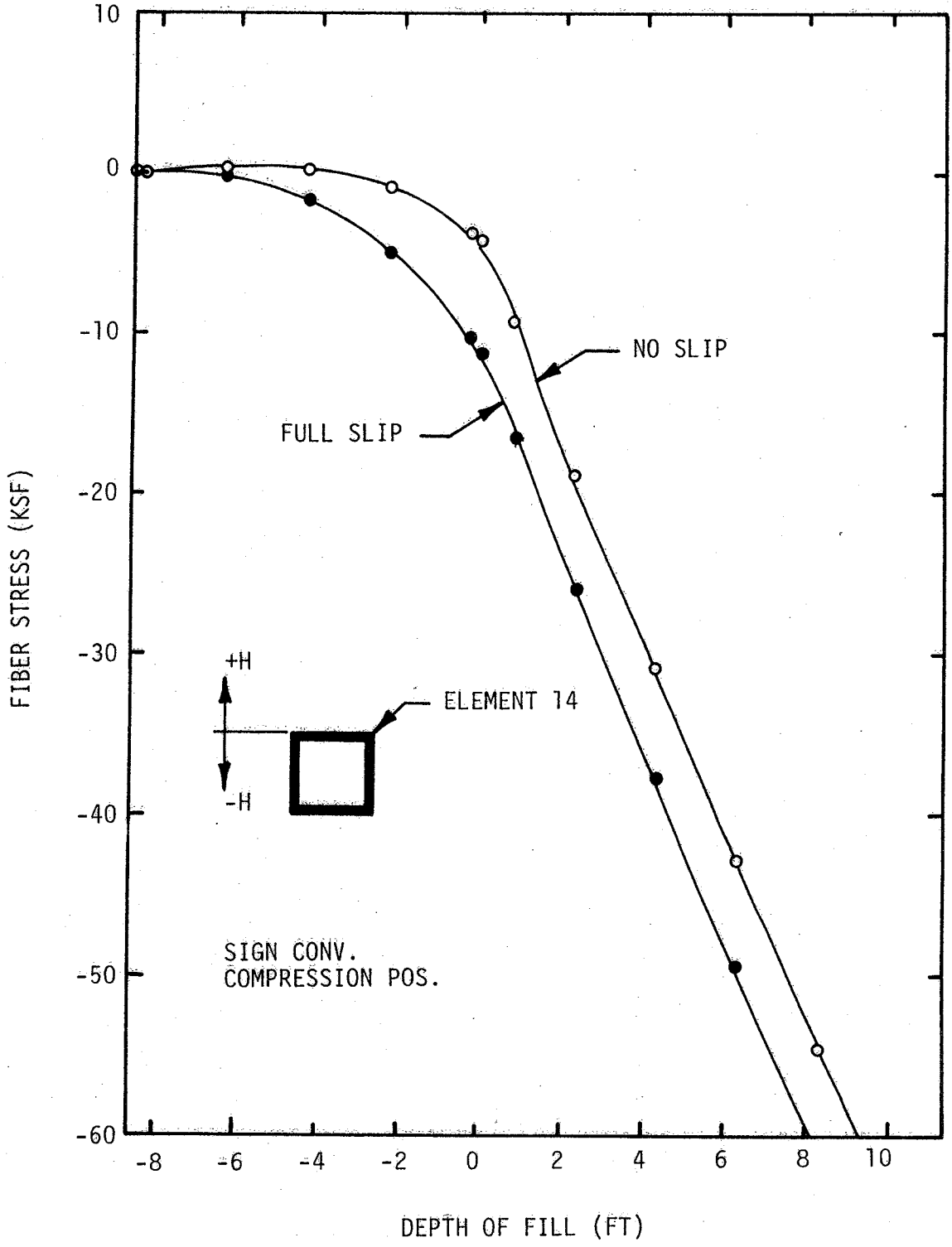

VARIATION OF FIBER STRESS WITH DEPTH OF FILL OUTSIDE STRESS, ELEMENT 14

FIGURE 4.40

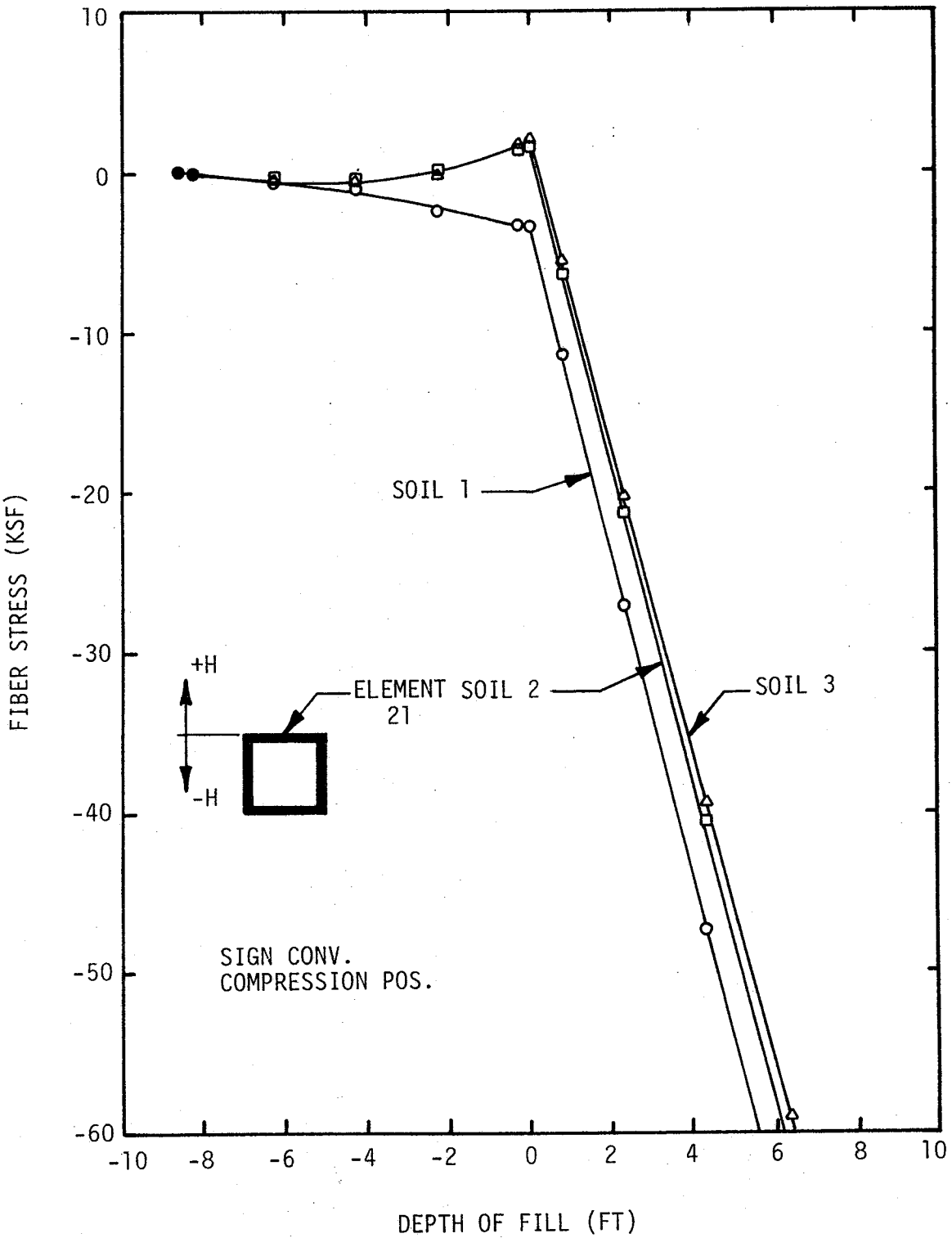

VARIATION OF FIBER STRESS WITH DEPTH OF FILL
INSIDE STRESS, ELEMENT 21

FIGURE 4.41

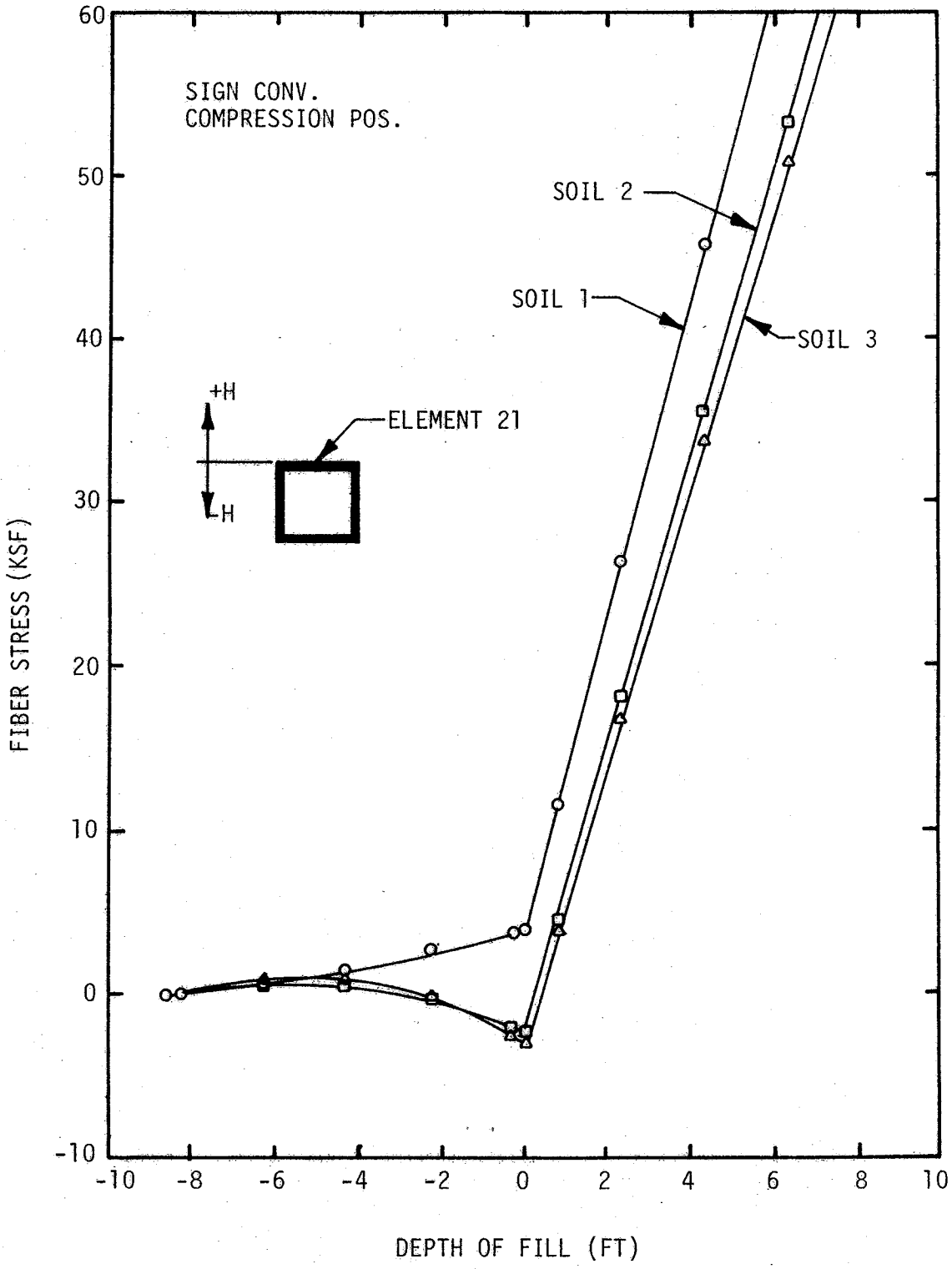

VARIATION OF FIBER STRESS WITH DEPTH OF FILL OUTSIDE STRESS, ELEMENT 21

FIGURE 4.42

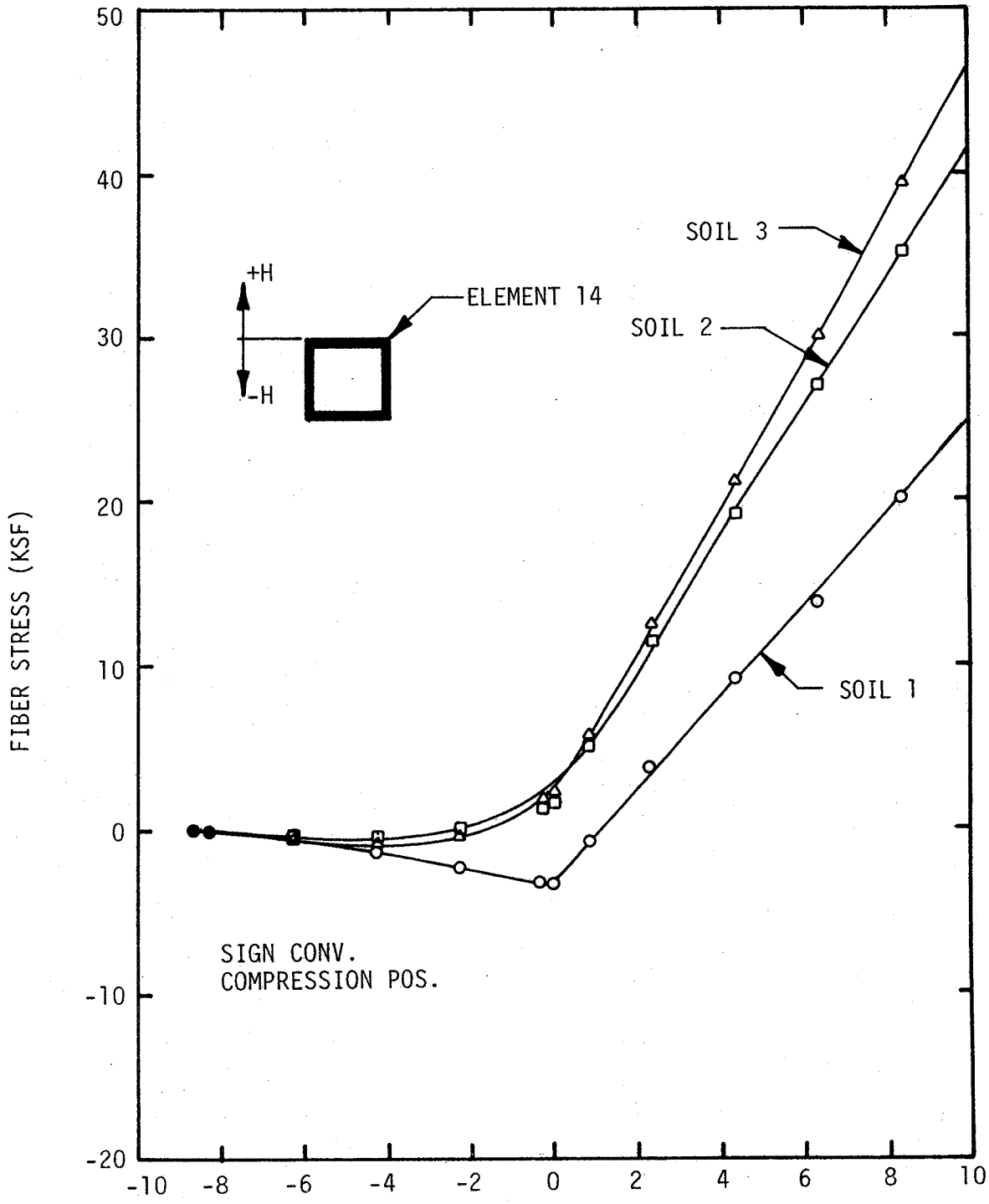

VARIATION OF FIBER STRESS WITH DEPTH OF FILL INSIDE STRESS, ELEMENT 14

FIGURE 4.43

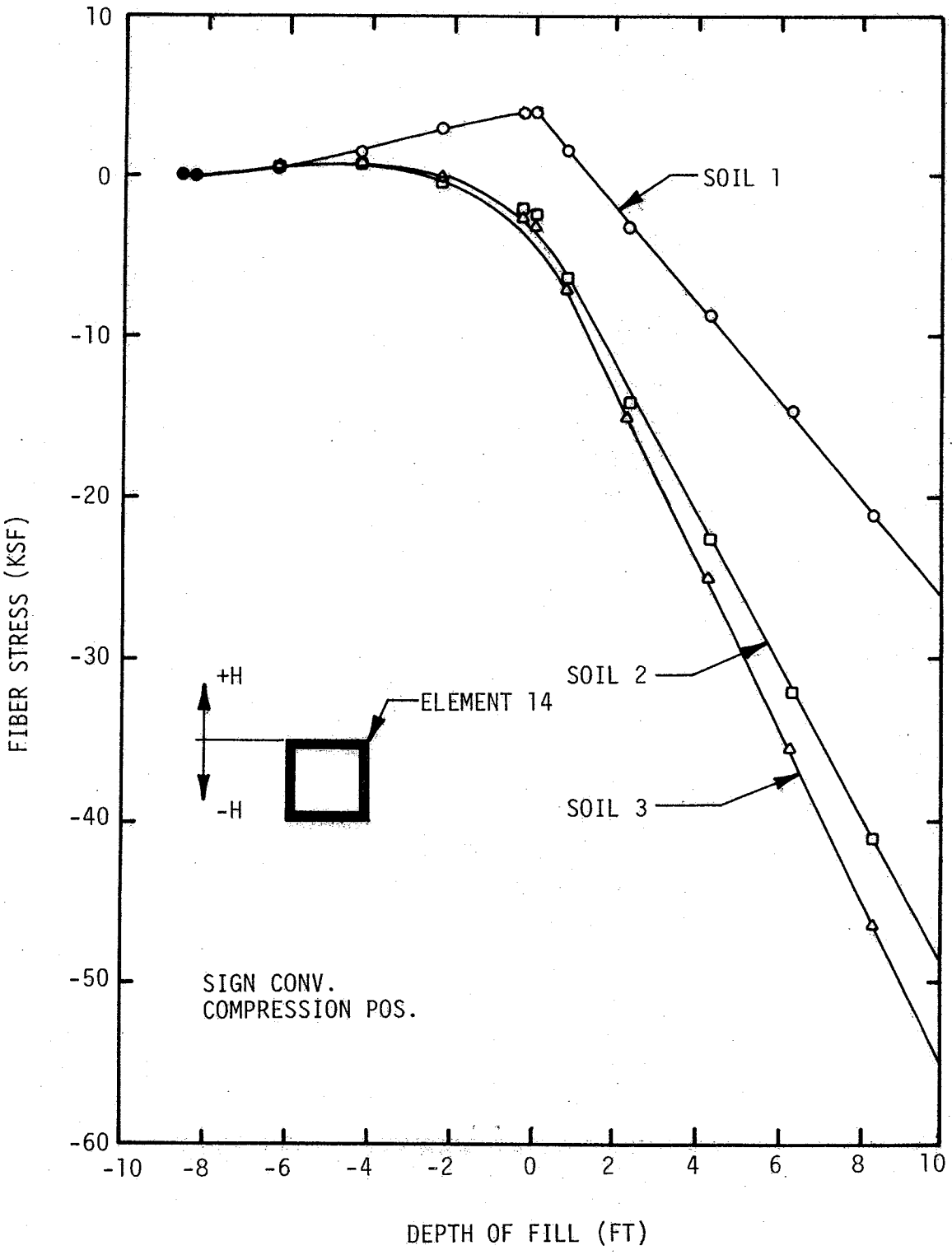

VARIATION OF FIBER STRESS WITH DEPTH OF FILL OUTSIDE STRESSES, ELEMENT 14

FIGURE 4.44

the culvert. However, due to different soil stiffnesses, there is a significant difference in fiber stress at a fill height equal to the crown height.

The variation of outside fiber stress at the same section is shown in Fig. 4.42. These results are very similar to those shown in Fig. 4.41, but compressive instead of tensile. Soil 1 shows a slightly more critical condition, with the results of Soils 2 and 3 being almost identical. All three soils exhibit a linear increase in stress after the backfill soil exceeds the crown height of the culvert.

The variation of inside fiber stress at the upper corner of the culvert with depth of fill is shown in Fig. 4.43. There is a significant difference between the results of Soil 1 and the results of Soils 2 and 3. Soil 1 produces the largest negative [tensile] stress, while Soils 2 and 3 produce large compressive stresses.

The outside fiber stresses at the same section are shown in Fig. 4.44. The results are very similar to those shown in Fig. 4.43.

By assuming a linear stress distribution in the reinforced concrete section, the fiber stresses at the inside and outside fibers were used to compute the stress in the reinforcing steel at the points where the strain gages are attached. Using the modulus of elasticity of the reinforcing steel, the strain was predicted for each of the two strain gages.

The variations of strain with depth of fill for the full-slip and no-slip conditions are given for each of the two strain gages in Figs. 4.45 and 4.46. These figures show very little difference as a result of variation in interface properties.

The strain predictions for the strain gage located at the midspan of the top slab are presented in Fig. 4.45. There is a slight compressive

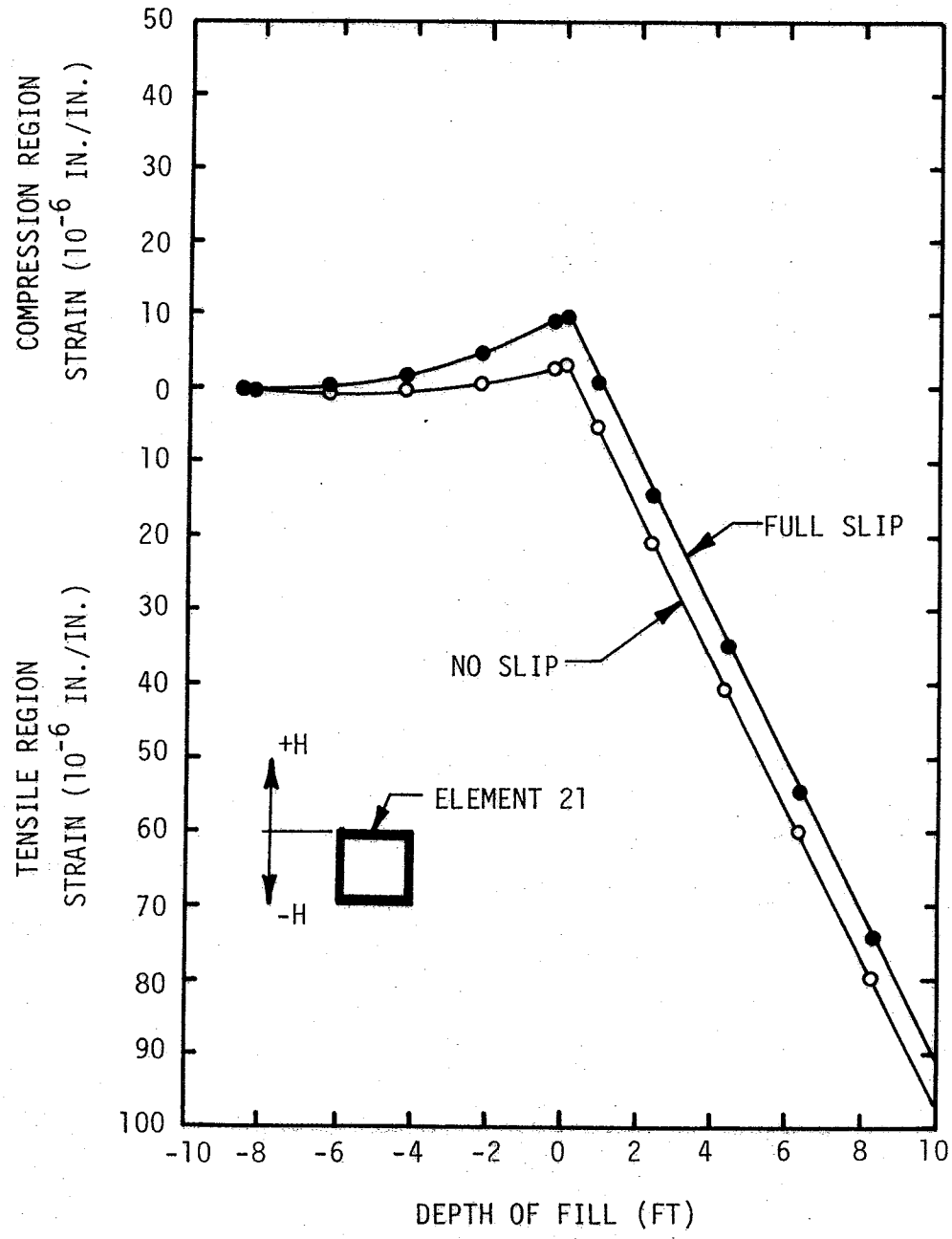

VARIATION OF STRAIN WITH DEPTH OF FILL STRAIN GAGE SG-1, ELEMENT 21

FIGURE 4.45

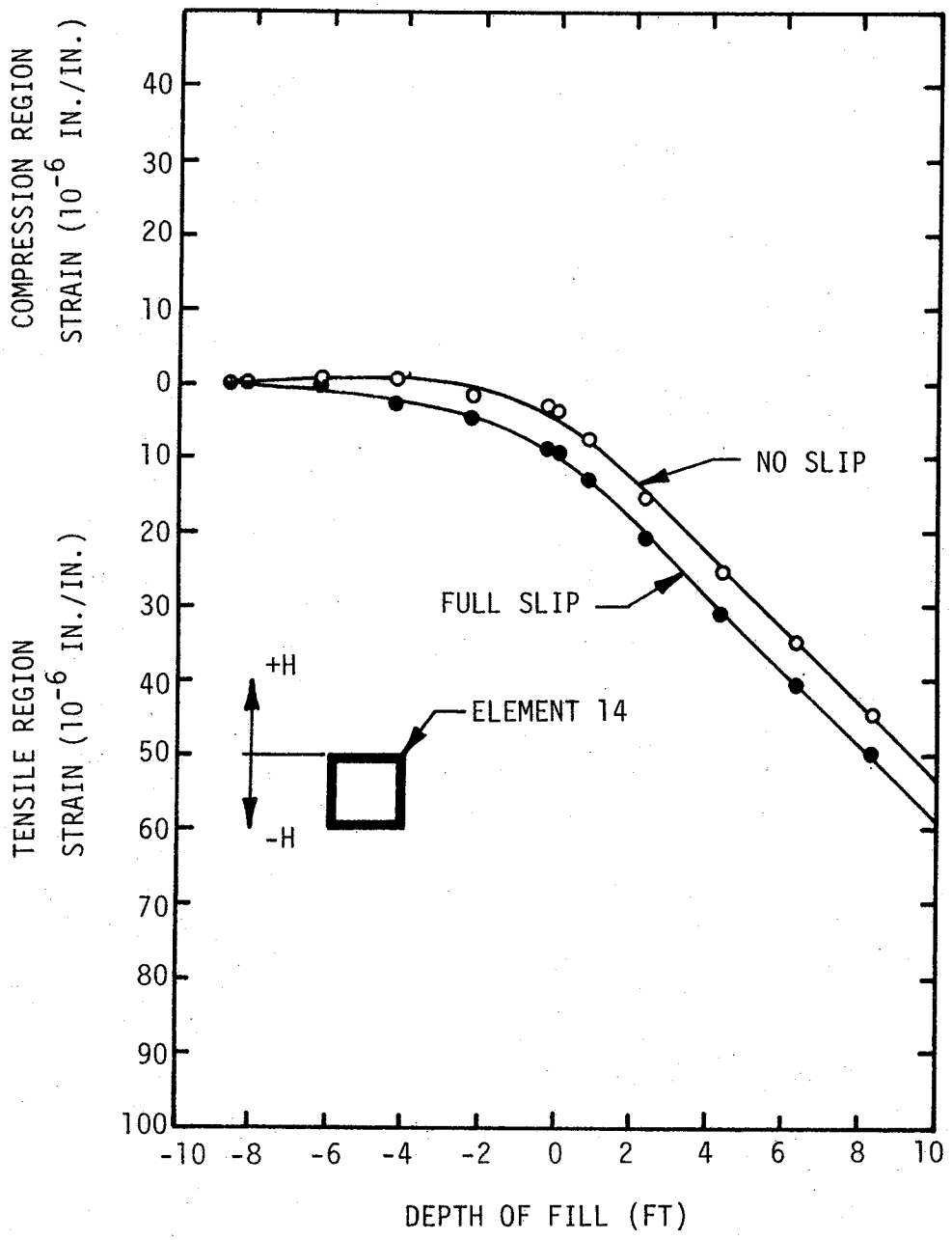

VARIATION OF STRAIN WITH DEPTH OF FILL STRAIN GAGE SG-2, ELEMENT 14

FIGURE 4.46

strain until the backfill reaches the crown height. Subsequent to this, the strains become tensile and increase in magnitude with depth of fill. The no-slip and full-slip results are very close, with the no-slip condition producing slightly higher tensile strains at maximum depth of fill.

The calculated strains for the strain gage located in the upper corner of the culvert are given in Fig. 4.46. The strains are primarily tensile, increasing linearly with depth of fill after the fill height exceeds the crown height. At this point, the full-slip condition exhibits the most critical condition.

The effects of varying soil conditions on calculated strains are shown in Figs. 4.47 and 4.48. For the midspan section of the top slab, Fig. 4.47 indicates that Soil 1 produces strains slightly higher than that for Soils 2 and 3, with the major difference between the soils occuring at fill heights less than the crown height. In this region Soil 1 exhibits tensile strains whereas Soils 2 and 3 indicate small compressive strains. These effects are produced by the varying stiffness of the soils and the associated relative deflections in the structural sections.

4.2.4 Deflections

Crown deflections were also computed as part of the finite element analyses. The variation in crown deflection with the depth of fill for the no-slip and full-slip conditions is given in Fig. 4.49. The no-slip condition shows larger values for deflection due to larger shear stresses on the sides of the culvert.

The effects of soil properties on crown deflection are shown in Fig. 4.50. Soil 3 is relatively wet and therefore exhibits larger deflections due to its lower modulus than the other two soils.

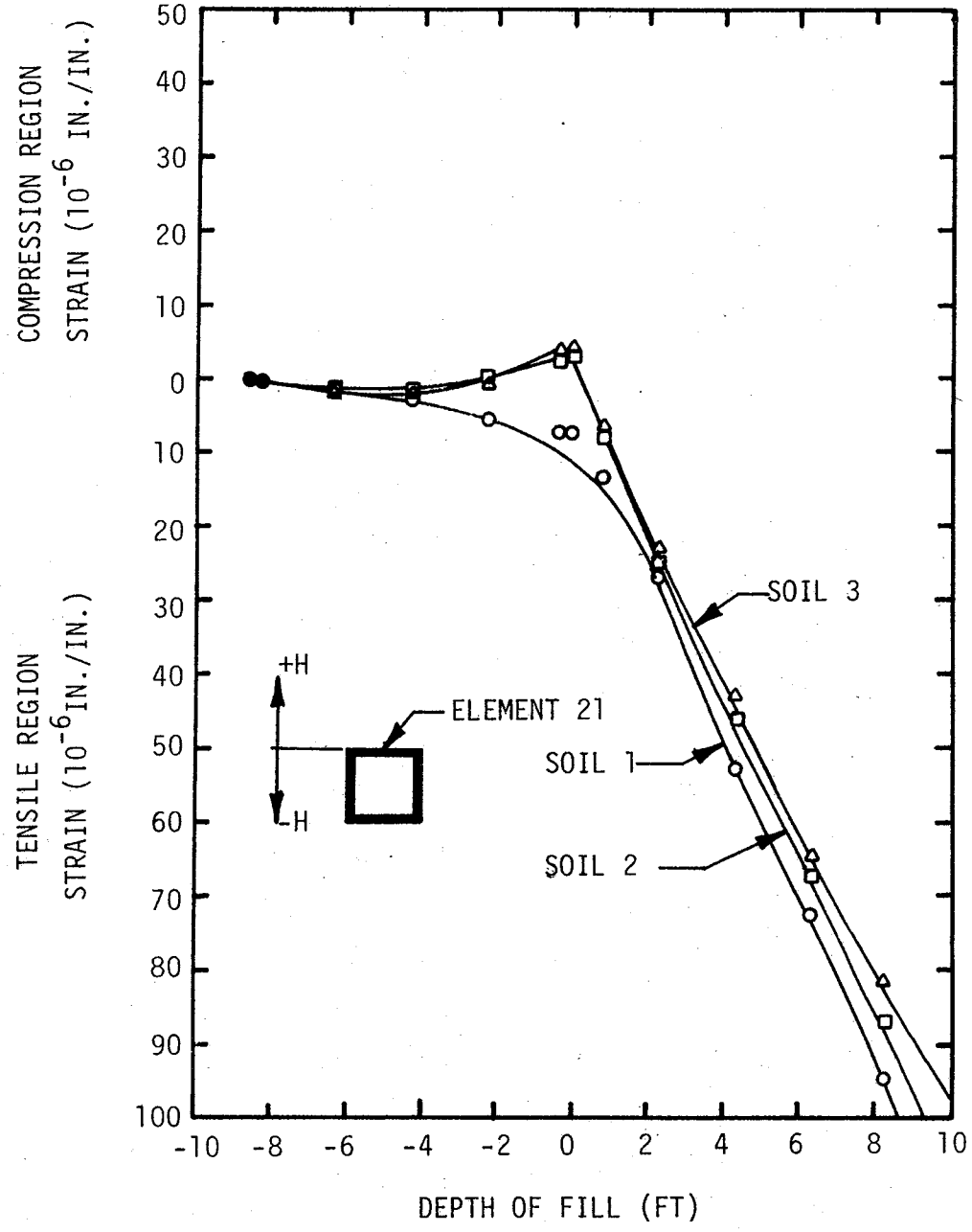

VARIATION OF STRAIN WITH DEPTH
OF FILL STRAIN GAGE SG-1, ELEMENT 21

FIGURE 4.47

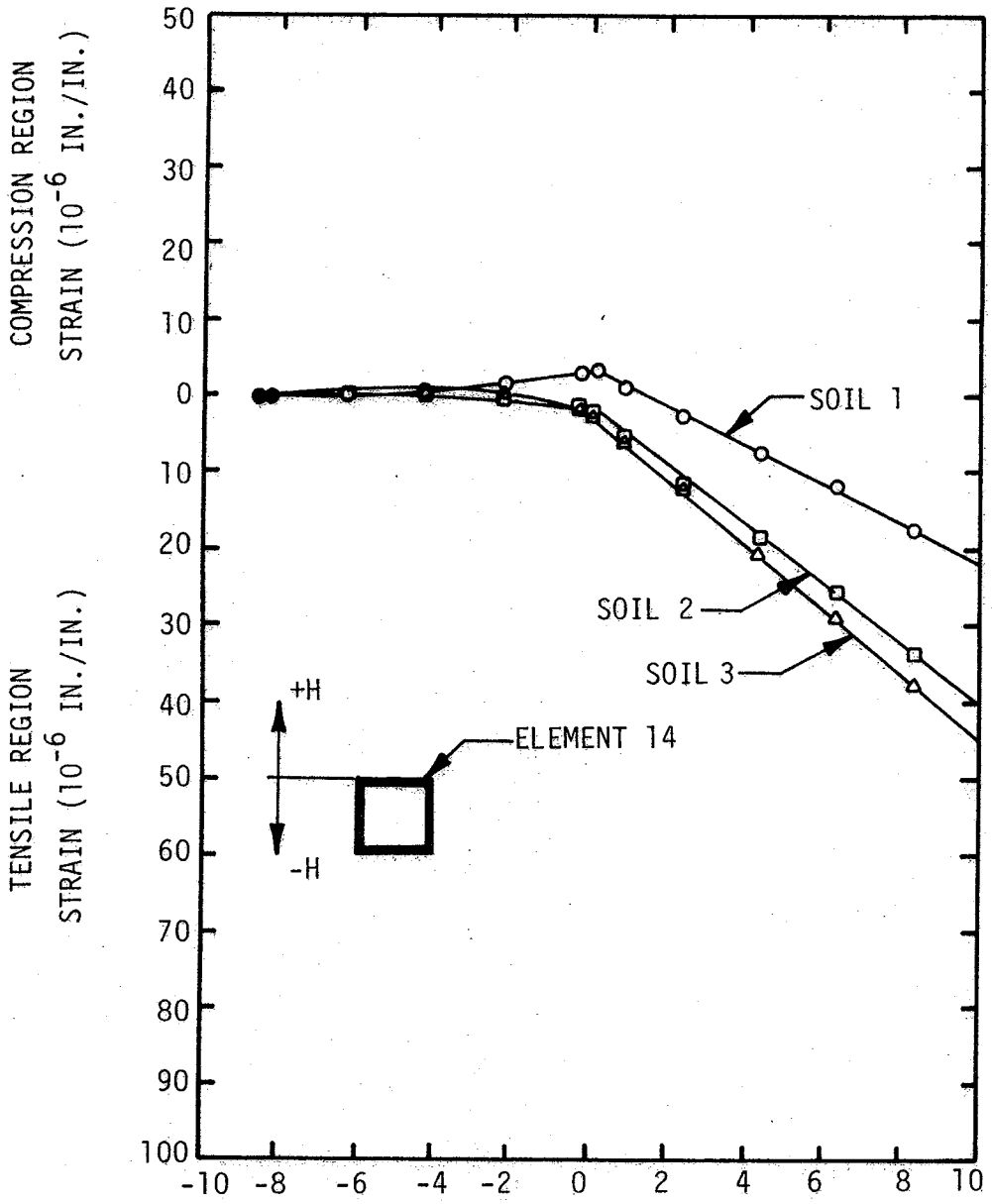

VARIATION OF STRAIN WITH DEPTH OF FILL STRAIN GAGE SG-2, ELEMENT 14

FIGURE 4.48

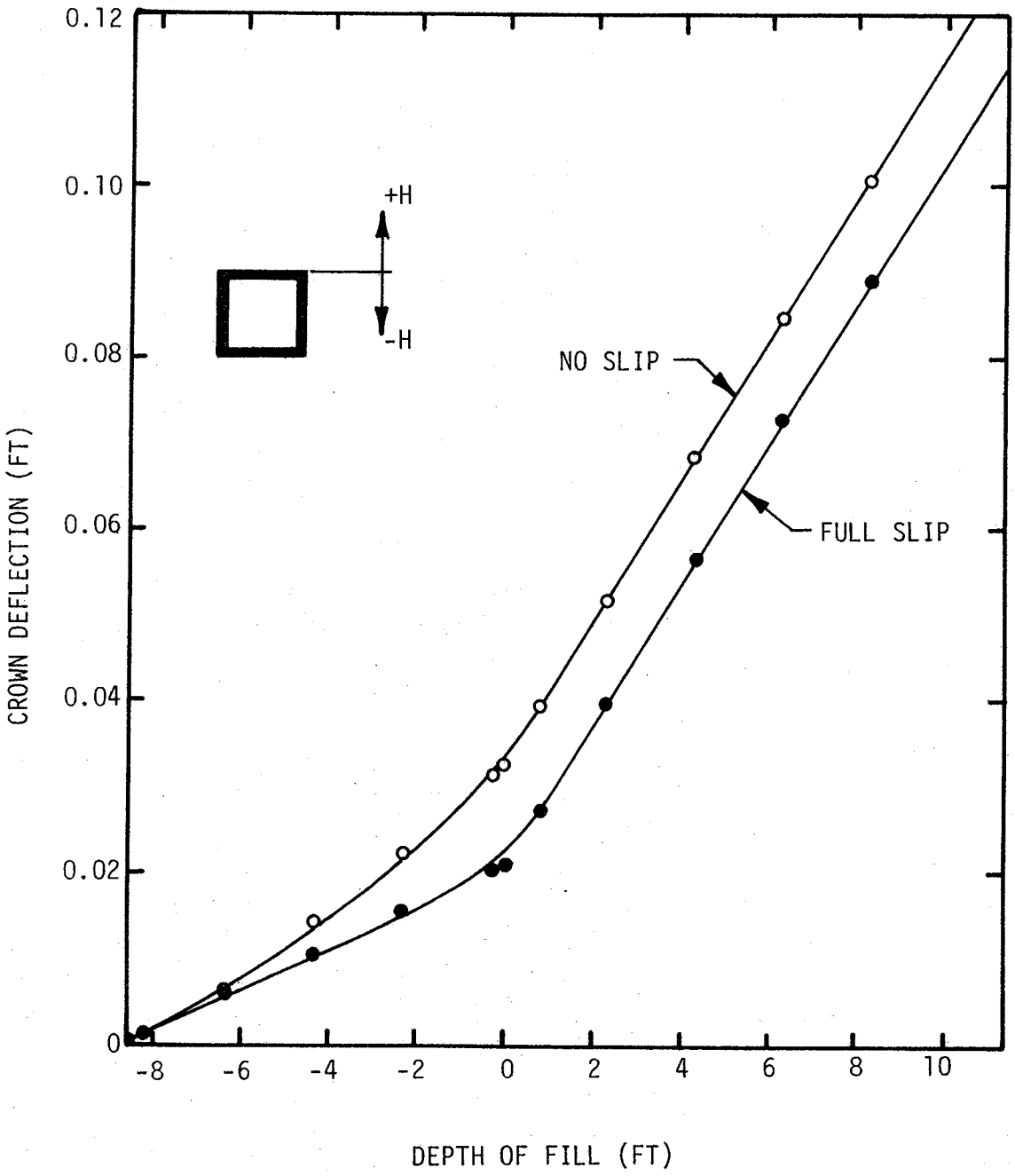

VARIATION OF CROWN DEFLECTION WITH DEPTH OF FILL

FIGURE 4.49